UNIVERSITY OF AMSTERDAM

UvA-DARE (Digital Academic Repository)

Search for pair production of third-generation scalar leptoquarks decaying into a top quark and a τ-lepton in pp collisions at √s = 13 TeV with the ATLAS detector

The ATLAS Collaboration

DOI
10.1007/JHEP06(2021)179

Publication date
2021

Document Version
Final published version

Published in
Journal of High Energy Physics

License
CC BY

Link to publication

Citation for published version (APA):
The ATLAS Collaboration (2021). Search for pair production of third-generation scalar leptoquarks decaying into a top quark and a *τ*-lepton in *pp* collisions at √s = 13 TeV with the ATLAS detector. *Journal of High Energy Physics*, *2021*(06), Article 179. https://doi.org/10.1007/JHEP06(2021)179

General rights
It is not permitted to download or to forward/distribute the text or part of it without the consent of the author(s) and/or copyright holder(s), other than for strictly personal, individual use, unless the work is under an open content license (like Creative Commons).

Disclaimer/Complaints regulations
If you believe that digital publication of certain material infringes any of your rights or (privacy) interests, please let the Library know, stating your reasons. In case of a legitimate complaint, the Library will make the material inaccessible and/or remove it from the website. Please Ask the Library: https://uba.uva.nl/en/contact, or a letter to: Library of the University of Amsterdam, Secretariat, P.O. Box 19185, 1000 GD Amsterdam, The Netherlands. You will be contacted as soon as possible.

UvA-DARE is a service provided by the library of the University of Amsterdam (https://dare.uva.nl)

Download date:13 Sep 2026

Published for SISSA by Springer

Received: *January 28, 2021*
Revised: *June 8, 2021*
Accepted: *June 8, 2021*
Published: *June 30, 2021*

Search for pair production of third-generation scalar leptoquarks decaying into a top quark and a τ-lepton in pp collisions at $\sqrt{s} = 13$ TeV with the ATLAS detector

The ATLAS collaboration

E-mail: atlas.publications@cern.ch

Abstract: A search for pair production of third-generation scalar leptoquarks decaying into a top quark and a τ-lepton is presented. The search is based on a dataset of pp collisions at $\sqrt{s} = 13$ TeV recorded with the ATLAS detector during Run 2 of the Large Hadron Collider, corresponding to an integrated luminosity of 139 fb^{-1}. Events are selected if they have one light lepton (electron or muon) and at least one hadronically decaying τ-lepton, or at least two light leptons. In addition, two or more jets, at least one of which must be identified as containing b-hadrons, are required. Six final states, defined by the multiplicity and flavour of lepton candidates, are considered in the analysis. Each of them is split into multiple event categories to simultaneously search for the signal and constrain several leading backgrounds. The signal-rich event categories require at least one hadronically decaying τ-lepton candidate and exploit the presence of energetic final-state objects, which is characteristic of signal events. No significant excess above the Standard Model expectation is observed in any of the considered event categories, and 95% CL upper limits are set on the production cross section as a function of the leptoquark mass, for different assumptions about the branching fractions into $t\tau$ and $b\nu$. Scalar leptoquarks decaying exclusively into $t\tau$ are excluded up to masses of 1.43 TeV while, for a branching fraction of 50% into $t\tau$, the lower mass limit is 1.22 TeV.

Keywords: Beyond Standard Model, Exotics, Hadron-Hadron scattering (experiments)

ArXiv ePrint: 2101.11582

Open Access, Copyright CERN,
for the benefit of the ATLAS Collaboration.
Article funded by SCOAP^3.

https://doi.org/10.1007/JHEP06(2021)179

Contents

1 Introduction 1

2 ATLAS detector 3

3 Data and simulated event samples 4

4 Event reconstruction 7

5 Search strategy 11
- 5.1 Event selection 12
- 5.2 Event categorisation 13

6 Background estimation 20
- 6.1 Irreducible backgrounds 20
  - 6.1.1 $t\bar{t}$ background 20
  - 6.1.2 $t\bar{t}W$ background 22
  - 6.1.3 Other irreducible backgrounds 22
- 6.2 Reducible backgrounds 22
  - 6.2.1 Fake τ_{had} candidates 22
  - 6.2.2 Non-prompt light leptons and charge misassignment 25

7 Analysis model and results 26

8 Conclusion 36

The ATLAS collaboration 45

JHEP06(2021)179

1 Introduction

The similarities between the quark and lepton sectors of the Standard Model (SM), which exhibit a similar structure, raise the possibility of an existing underlying symmetry connecting the two sectors. Consequently, many extensions of the Standard Model of particle physics contain leptoquarks (LQ) [1–7], hypothetical particles that carry non-zero baryon and lepton quantum numbers and are charged under all SM gauge groups. In particular, they are triplets with respect to the strong interaction, and have fractional electric charge. A LQ state can have either spin 0 (scalar LQ) or spin 1 (vector LQ), and only the former is considered in this paper. Because of their quantum numbers, LQs couple simultaneously to both quarks and leptons, enabling direct transitions between the two. Scalar LQs are assumed to couple to the quark-lepton pair via a Yukawa interaction,

with coupling constants that can vary across fermion generations, including the possibility of mixing between different quark and lepton generations. Consequently, scalar LQs can mediate processes that violate lepton flavour universality, and have been proposed as an explanation for measurements of B-meson decays that exhibit tantalising deviations from SM predictions [8–14]. The assumption that LQs can only interact with leptons and quarks of the same generation follows the minimal Buchmüller-Rückl-Wyler (BRW) model [15], which is adopted in this paper. The quark-lepton-LQ coupling is determined by two parameters: a model parameter β and the coupling parameter λ. Consequently, the coupling to the charged lepton is given by $\sqrt{\beta}\lambda$, while the coupling to the neutrino is given by $\sqrt{1-\beta}\lambda$.

In pp collisions, LQs are mainly produced in pairs ($\mathrm{LQ}\overline{\mathrm{LQ}}$) via gluon-gluon fusion and quark-antiquark annihilation, mediated by the strong interaction. There are also lepton-mediated t- and u-channel production processes that depend on the unknown strength of the Yukawa interaction. However, their contribution can usually be neglected for values of $\lambda \lesssim 1$, and particularly in the case of third-generation LQs (LQ_3), as they would require third-generation quarks in the initial state. The LQ pair-production cross section can therefore, to a very good approximation, be taken to depend only on the assumed value of the LQ mass (m_{LQ}) for a given LQ spin and centre-of-mass energy. Furthermore, it is assumed that the value of λ is such that LQs have narrow decay widths of about 0.2% of m_{LQ}, so that on-shell production dominates. Single LQ production in association with a lepton is also possible, but the cross section depends on the strength of the Yukawa interaction and it is not considered in this paper.

The most recent searches from the ATLAS and CMS experiments for pair production of LQs coupling to third-generation quarks and leptons were performed using 36.1 fb^{-1} of pp collisions at $\sqrt{s} = 13$ TeV at the Large Hadron Collider (LHC). The ATLAS results, many of which are reinterpretations of previously published searches for supersymmetric particles, are summarised in ref. [16]. The different ATLAS searches are not combined statistically and the results are presented as a function of the LQ mass and the branching ratio into charged leptons ($\mathcal{B}$) for two different classes of LQ signals: up-type LQs ($\mathrm{LQ}_3^{\mathrm{u}} \to b\tau/t\nu$) and down-type LQs ($\mathrm{LQ}_3^{\mathrm{d}} \to t\tau/b\nu$), which have different electric charges. Both types of LQs are excluded for masses below 800 GeV independently of $\mathcal{B}$. For the limiting cases of $\mathcal{B} = 1$ and $\mathcal{B} = 0$, masses below 1000 GeV and 1030 GeV (970 GeV and 920 GeV) are excluded for $\mathrm{LQ}_3^{\mathrm{u}}$ ($\mathrm{LQ}_3^{\mathrm{d}}$). Searches for LQs with off-diagonal couplings to third-generation quarks and first- or second-generation leptons have also been performed [17, 18]. The CMS experiment has performed searches for leptoquarks [19–23], obtaining similar mass exclusions.

This paper presents a dedicated search for the pair production of $\mathrm{LQ}_3^{\mathrm{d}}$ in the $t\tau t\tau$ decay mode. This search uses the full Run 2 dataset of pp collisions at $\sqrt{s} = 13$ TeV recorded with the ATLAS detector and corresponding to an integrated luminosity of 139 fb^{-1}. Events are selected if they have at least one light lepton (electron or muon, denoted by ℓ) and at least one hadronically decaying τ-lepton, or at least two light leptons. In addition, two or more jets, at least one of which must be identified as containing b-hadrons, are required. Six final states, defined by the multiplicity and flavour of lepton candidates, are considered in the analysis. Each of them is split into multiple event categories. The most sensitive event

JHEP06(2021)179

categories require at least one hadronically decaying τ-lepton candidate and exploit the presence of energetic final-state objects, which is characteristic of signal events. In those event categories the final discriminating variable used is the scalar sum of the transverse momenta of all selected leptons, the selected jets and the missing transverse momentum; this variable peaks at much higher values for the signal than for the background. The main background contributions arise from top-quark–antitop-quark ($t\bar{t}$) production with a jet or photon misidentified as a light lepton or with a jet misidentified as a hadronically decaying τ-lepton, and from SM processes yielding multiple leptons in the final state, such as $t\bar{t}$ production in association with a vector boson or a Higgs boson, and diboson production. The rest of the event categories are designed to be enriched in the most relevant backgrounds. A maximum-likelihood fit is performed across event categories to search for the signal and constrain several leading backgrounds simultaneously. Given the low background yields and good signal-to-background separation provided by the final discriminating variable used in the signal-rich event categories, the search sensitivity is determined by the limited number of data events rather than by the systematic uncertainties of the background estimation. This search is performed in the LQ mass range between 500 GeV and 1600 GeV as a function of $\mathcal{B}$. By considering LQ masses down to 500 GeV, the coverage of this search partly overlaps with that of ref. [16], for which masses below 800 GeV were excluded independently of $\mathcal{B}$. At the same time, this search significantly extends the reach to higher LQ masses.

2 ATLAS detector

The ATLAS detector [24] at the LHC covers almost the entire solid angle around the collision point,[1] and consists of an inner tracking detector surrounded by a thin superconducting solenoid producing a 2 T axial magnetic field, electromagnetic and hadronic calorimeters, and a muon spectrometer (MS) incorporating three large toroidal magnet assemblies. The inner detector contains a high-granularity silicon pixel detector, including the insertable B-layer [25, 26], and a silicon microstrip tracker, together providing a precise reconstruction of tracks of charged particles in the pseudorapidity range $|\eta| < 2.5$. The inner detector also includes a transition radiation tracker that provides tracking and electron identification information for $|\eta| < 2.0$. The calorimeter system covers the pseudorapidity range $|\eta| < 4.9$. Within the region $|\eta| < 3.2$, electromagnetic (EM) calorimetry is provided by barrel and endcap high-granularity lead/liquid-argon (LAr) electromagnetic calorimeters, with an additional thin LAr presampler covering $|\eta| < 1.8$ to correct for energy loss in material upstream of the calorimeters. Hadronic calorimetry is provided by a steel/scintillator-tile calorimeter, segmented into three barrel structures within $|\eta| < 1.7$, and two copper/LAr hadronic endcap calorimeters. The solid angle coverage is completed with forward copper/LAr and tungsten/LAr calorimeter modules optimised for electromagnetic and

[1] ATLAS uses a right-handed coordinate system with its origin at the nominal interaction point (IP) in the centre of the detector. The x-axis points from the IP to the centre of the LHC ring, the y-axis points upward, and the z-axis coincides with the axis of the beam pipe. Polar coordinates (r,ϕ) are used in the transverse plane, ϕ being the azimuthal angle around the beam pipe. The pseudorapidity is defined in terms of the polar angle θ as $\eta = -\ln\tan(\theta/2)$. Angular distance is measured in units of $\Delta R \equiv \sqrt{(\Delta\eta)^2 + (\Delta\phi)^2}$.

JHEP06(2021)179

hadronic measurements, respectively. The muon spectrometer measures the trajectories of muons with $|\eta| < 2.7$ using multiple layers of high-precision tracking chambers located in a toroidal field of approximately 0.5 T and 1 T in the central and endcap regions of ATLAS, respectively. The muon spectrometer is also instrumented with separate trigger chambers covering $|\eta| < 2.4$. A two-level trigger system [27], consisting of a hardware-based first-level trigger followed by a software-based high-level trigger (HLT), is used to reduce the event rate to a maximum of around 1 kHz for offline storage.

3 Data and simulated event samples

A dataset of pp collisions at $\sqrt{s} = 13\,\text{TeV}$ collected by the ATLAS experiment during 2015–2018 and corresponding to an integrated luminosity of 139 fb^{-1} is used. The uncertainty in the integrated luminosity is 1.7% [28], obtained using the LUCID-2 detector [29] for the primary luminosity measurements. The number of additional pp interactions per bunch crossing (pile-up) in this dataset ranges from about 8 to 70, with an average of 34. Only events recorded under stable beam conditions and for which all detector subsystems were known to be in a good operating condition are used. The trigger requirements are discussed in section 5.

Monte Carlo (MC) simulation samples were produced for the different signal and background processes using the configurations shown in table 1, with the samples used to estimate the systematic uncertainties in parentheses. All simulated samples, except those produced with the Sherpa 2.2.1 [30] event generator, utilised EvtGen 1.2.0 [31] to model the decays of heavy-flavour hadrons. Pile-up was modelled using events from minimum-bias interactions generated with Pythia 8.186 [32] with the A3 set of tuned parameters [33] (referred to as the 'tune'), and overlaid onto the simulated hard-scatter events according to the luminosity profile of the recorded data. The generated events were processed through a simulation [34] of the ATLAS detector geometry and response using Geant4 [35], and through the same reconstruction software as the dataset of pp collisions. Corrections were applied to the simulated events so that the particle candidates' selection efficiencies, energy scales and energy resolutions match those determined from data control samples. The simulated samples are normalised to their cross sections, and computed to the highest order available in perturbation theory.

Samples used to model the LQ_3^{d} signal were generated at next-to-leading order (NLO) in QCD with MadGraph5_aMC@NLO 2.6.0 [36], using the LQ model of ref. [37] that adds parton showers to previous fixed-order NLO QCD calculations [38, 39], and the NNPDF 3.0 NLO [40] parton distribution function (PDF) set. The parton shower (PS) and hadronisation were modelled using Pythia 8.230 [32] with the A14 tune [41]. MadSpin [42] was used for the decay of the scalar LQ_3^{d}. The coupling parameter λ was set to 0.3, resulting in the LQ_3^{d} width of about 0.2% of its mass [15, 43]. The charge of LQ_3^{d} is set to $1/3e$, implying that it decays into either a $t\tau$ or $b\nu$ pair. Most signal samples were produced for a model parameter of $\beta = 0.5$, which corresponds to identical amplitudes for the $\text{LQ}_3^{\text{d}} \to t\tau$ and $\text{LQ}_3^{\text{d}} \to b\nu$ processes and, therefore, similar branching ratios for the two decay modes. The signal samples had a mixture of final states so that desired branching ratios $\mathcal{B}$ were obtained

JHEP06(2021)179

by reweighting the samples based on generator information. These samples were produced for LQ_3^d mass values between 500 GeV and 800 GeV, in steps of 100 GeV, and between 800 GeV and 1.6 TeV, in steps of 50 GeV. Additional samples for $\beta = 1$ were generated for the same LQ_3^d mass values between 800 GeV and 1.5 TeV, to gain statistical precision in high-sensitivity signal regions. The leptoquark signal production cross sections were taken from calculations [44–47] of direct top-squark pair production, as both are massive, coloured, scalar particles with the same production modes. The calculations were at approximate next-to-next-to-leading order (NNLO) in QCD with resummation of next-to-next-to-leading logarithmic (NNLL) soft gluon terms, with uncertainties determined by variations of the factorisation and renormalisation scales, the strong coupling constant α_S, and the PDFs. The cross sections do not include lepton t-channel contributions, which are neglected in ref. [37] and may lead to corrections at the percent level [48]. Uncertainties affecting the modelling of the signal acceptance were estimated from the envelope of independent pairs of renormalisation and factorisation scale variations by a factor of 0.5 and 2, by propagating the PDF+α_S uncertainties following the PDF4LHC15 prescription [49], and by considering two alternative samples generated with settings that increase or decrease the amount of QCD radiation [50].

Samples used to model the $t\bar{t}$ and single-top-quark background were generated with the NLO generator Powheg-Box v2 [51–56] using the NNPDF3.0 NLO PDF set. In the $t\bar{t}$ sample, the Powheg-Box model parameter h_{damp}, which controls matrix element (ME) to PS matching and effectively regulates the high-p_T radiation, was set to 1.5 times the top-quark mass. Overlaps between the $t\bar{t}$ and tW final states were avoided by using the diagram removal scheme [57]. The parton shower, hadronisation, and underlying event were modelled by Pythia 8.210 with the NNPDF2.3 LO [58] PDF set in combination with the A14 tune. Uncertainties affecting the modelling of the acceptance and event kinematics of $t\bar{t}$ events due to the choice of PS and hadronisation model, the NLO ME-to-PS matching, and the effects of initial- and final-state QCD radiation [59] are estimated by comparing the nominal predictions with those obtained using the alternative simulated samples (see table 1). The $t\bar{t}$ and single-top-quark simulated samples are normalised to the cross sections calculated at NNLO in QCD including the resummation of NNLL soft gluon terms [60–63].

Samples for $t\bar{t}W$ and $t\bar{t}H$ production were generated using the NLO generators Sherpa 2.2.1 and Powheg-Box v2 [64], respectively, with the NNPDF3.0 NLO PDF set. In the case of the $t\bar{t}W$ sample, the ME was calculated for up to one additional parton at NLO and up to two partons at LO using Comix [65] and OpenLoops [66] and merged with the Sherpa parton shower [67] using the MePs@Nlo prescription [68]. The generated $t\bar{t}H$ events were interfaced to Pythia 8.2 and the A14 tune, and with Higgs decay branching ratios calculated using Hdecay [69, 70]. The cross section used to normalise the $t\bar{t}W$ ($t\bar{t}H$) sample is 601 (507) fb, which is computed at NLO in QCD with NLO electroweak corrections [36, 69, 71–77]. Uncertainties in the $t\bar{t}W$ ($t\bar{t}H$) cross section include $\pm 12\%$ ($^{+5.8\%}_{-9.2\%}$), estimated by varying the QCD factorisation and renormalisation scales, and $\pm 4\%$ ($\pm 3.6\%$) from PDF+α_S variations, estimated using the PDF4LHC15 prescription. Uncertainties affecting the modelling of the acceptance and event kinematics due to the choice of parton shower and hadronisation model are estimated by comparing the nominal

JHEP06(2021)179

Process	Generator	ME order	Parton shower	PDF	Tune
$LQ_3^d\overline{LQ}_3^d$	MG5_aMC	NLO	Pythia 8	NNPDF3.0 NLO	A14
$t\bar{t}$	Powheg-Box	NLO	Pythia 8	NNPDF3.0 NLO/ NNPDF2.3 LO	A14
	(Powheg-Box)	(NLO)	(Herwig 7)	(NNPDF3.0 NLO/ MMHT2014 LO)	(H7-UE-MMHT)
	(MG5_aMC)	(NLO)	(Pythia 8)	(NNPDF3.0 NLO/ NNPDF2.3 LO)	(A14)
	(Powheg-Box $h_{\text{damp}} = 3m_t$)	(NLO)	(Pythia 8)	(NNPDF3.0 NLO/ NNPDF2.3 LO)	(A14Var3CUp [41])
$t\bar{t}W$	Sherpa 2.2.1	MePs@Nlo	Sherpa	NNPDF3.0 NNLO	Sherpa default
	(MG5_aMC)	(NLO)	(Pythia 8)	(NNPDF3.0 NLO/ NNPDF2.3 LO)	(A14)
$t\bar{t}(Z/\gamma^* \to \ell^+\ell^-)$	MG5_aMC	NLO	Pythia 8	NNPDF3.0 NLO/ NNPDF2.3 LO	A14
	(Sherpa 2.2.0)	(LO multileg)	(Sherpa)	(NNPDF3.0 NLO)	(Sherpa default)
$t\bar{t} \to W^+bW^-\bar{b}\ell^+\ell^-$	MG5_aMC	LO	Pythia 8	NNPDF3.0 LO	A14
$t\bar{t}H$	Powheg-Box	NLO	Pythia 8	NNPDF3.0 NLO / NNPDF2.3 LO	A14
	(Powheg-Box)	(NLO)	(Herwig 7)	(NNPDF3.0 NLO/ MMHT2014 LO [82])	(H7-UE-MMHT)
Single top (t-, Wt-, s-channel)	Powheg-Box	NLO	Pythia 8	NNPDF3.0 NLO/ NNPDF2.3 LO	A14
$t(Z/\gamma^*)$	MG5_aMC	LO	Pythia 6	CTEQ6L1	Perugia2012 [83]
$tW(Z/\gamma^*)$	MG5_aMC	NLO	Pythia 8	NNPDF2.3 LO	A14
$t\bar{t}t$, $t\bar{t}t\bar{t}$	MG5_aMC	LO	Pythia 8	NNPDF2.3 LO	A14
$t\bar{t}W^+W^-$	MG5_aMC	LO	Pythia 8	NNPDF2.3 LO	A14
VV, $qqVV$, VVV	Sherpa 2.2.2	MePs@Nlo	Sherpa	NNPDF3.0 NNLO	Sherpa default
VH	Pythia 8	LO	Pythia 8	NNPDF2.3 LO	A14
W+jets	Sherpa 2.2.1	MePs@Nlo	Sherpa	NNPDF3.0 NLO	Sherpa default
Z+jets	Sherpa 2.2.1	MePs@Nlo	Sherpa	NNPDF3.0 NLO	Sherpa default

Table 1. The configurations used for event generation of signal and background processes. The samples used to estimate the systematic uncertainties are indicated in parentheses. V refers to production of an electroweak boson (W or Z/γ^*). The matrix element order refers to the order in the strong coupling constant of the perturbative calculation. If only one parton distribution function is shown, the same one is used for both the ME and parton shower generators; if two are shown, the first is used for the ME calculation and the second for the parton shower. Tune refers to the underlying-event tune of the parton shower generator. MG5_aMC refers to MadGraph5_aMC@NLO 2.2, 2.3, or 2.6; Pythia 6 refers to version 6.427 [78]; Pythia 8 refers to version 8.2; Herwig++ refers to version 2.7 [79]; Herwig 7 refers to version 7.0.4 [80]; MePs@Nlo refers to the method used in Sherpa to match the matrix element to the parton shower. All samples include leading-logarithm photon emission, either modelled by the parton shower generator or by Photos [81]. The mass of the top quark (m_t) and SM Higgs boson were set to 172.5 GeV and 125 GeV, respectively.

predictions with those obtained using the alternative simulated samples (see table 1). In the case of the $t\bar{t}W$ sample, an additional uncertainty on the modelling of the acceptance and event kinematics is considered from renormalisation and factorisation scale variations by a factor of 0.5 and 2, relative to the nominal scales.

The samples for $t\bar{t}(Z/\gamma^*)$ and diboson (VV) production follow refs. [50, 84]. For $t\bar{t}(Z/\gamma^*)$, the inclusive $t\bar{t}l^+l^-$ ME is computed, including off-shell Z and γ^* contributions

JHEP06(2021)179

with $m(\ell^+\ell^-) > 1\,\text{GeV}$. A dedicated $t\bar{t}$ sample, including rare $t \to Wb\gamma^*(\to \ell^+\ell^-)$ radiative decays and requiring $m(\ell^+\ell^-) > 1\,\text{GeV}$, referred to as the $t\bar{t} \to W^+bW^-\bar{b}\ell^+\ell^-$ sample, was added to the $t\bar{t}(Z/\gamma^*)$ sample and together these form the $t\bar{t}(Z/\gamma^*)$ (high mass) sample. The contribution from internal photon conversions ($\gamma^* \to \ell^+\ell^-$) with $m(\ell^+\ell^-) < 1\,\text{GeV}$ is modelled by QED multiphoton radiation in the inclusive $t\bar{t}$ sample and is referred to as $t\bar{t}\gamma^*$ (low mass). Care was taken to avoid both double-counting of contributions and uncovered regions of phase space when combining the different simulated samples. The cross section for $t\bar{t}(Z/\gamma^* \to \ell^+\ell^-)$ production is 167 fb, computed at NLO in QCD and electroweak couplings [36, 77]. The uncertainties from QCD scale and PDF+α_S variations are $\pm 12\%$ and $\pm 4\%$ respectively. The LO cross section from the $t\bar{t} \to W^+bW^-\bar{b}\ell^+\ell^-$ sample is scaled by a factor of 1.54, based on comparisons between the NNLO+NLL and LO cross sections for $t\bar{t}$ production [85–89], and assigned a 50% normalisation uncertainty, to cover possible residual effects in the predicted yield due to the simplified normalisation procedure used and/or the fact that the event kinematics were modelled using a LO simulation. Uncertainties affecting the modelling of the acceptance and event kinematics for the $t\bar{t}(Z/\gamma^*)$ sample include the same QCD scale and tune variations as considered for the $t\bar{t}H$ sample, PDF variations using the PDF4LHC15 prescription, and a comparison with an alternative LO multileg sample (see table 1). Diboson backgrounds are normalised using the cross sections computed by Sherpa 2.2.2. To cover possible mismodellings in the associated heavy-flavour production predicted by the parton shower, a 50% normalisation uncertainty is assigned and treated as correlated between the $WZ+{\geq}1c$ and $WZ+{\geq}1b$ subprocesses. The remaining rare background contributions listed in table 1 are normalised using their NLO theoretical cross sections, except for the $t\bar{t}t$ process, for which a LO cross section is used. To account for the fact that many of these processes are predicted using a LO simulation, and to cover possible mismodellings in the extreme kinematic regime probed by this search, a 50% normalisation uncertainty is assigned to all of them.

4 Event reconstruction

Interaction vertices from the pp collisions are reconstructed from at least two tracks with transverse momentum (p_T) larger than 500 MeV that are consistent with originating from the beam collision region in the x–y plane. If more than one primary vertex candidate is found, the candidate for which the associated tracks form the largest sum of squared p_T [90] is selected as the hard-scatter primary vertex.

Electron candidates are reconstructed from energy clusters in the electromagnetic calorimeter that are associated with inner-detector tracks [91]. They are required to satisfy $p_T > 10\,\text{GeV}$ and $|\eta_{\text{cluster}}| < 2.47$, excluding the transition region between the endcap and barrel calorimeters ($1.37 < |\eta_{\text{cluster}}| < 1.52$). Loose and tight electron identification working points are used [92], based on a likelihood discriminant employing calorimeter, tracking and combined variables that provide separation between electrons and jets. The associated track of an electron candidate is required to have at least two hits in the pixel detector and seven hits total in the pixel and silicon-strip detectors combined. For the tight identification working point, one of these pixel hits must be in the innermost layer (or the

JHEP06(2021)179

next-to-innermost layer if the module traversed in the innermost layer is non-operational), and there must be no association with a vertex from a reconstructed photon conversion [93] in the detector material (termed a 'material conversion' in this paper).

Muon candidates are reconstructed by matching tracks connecting track segments in different layers of the muon spectrometer to tracks found in the inner detector. The resulting muon candidates are re-fitted using the complete track information from both detector systems [94]. They are required to satisfy $p_{\mathrm{T}} > 10\,\mathrm{GeV}$ and $|\eta| < 2.5$. Loose and medium muon identification working points are used [94]. Medium muon candidates with $p_{\mathrm{T}} > 800\,\mathrm{GeV}$ are in addition required to have hits in at least three MS stations (referred to as the 'high-p_{T} working point'), in order to maximise the momentum resolution for the muon track and thus suppress backgrounds with high-p_{T} muons arising from momentum mismeasurements.

Electron (muon) candidates are matched to the primary vertex by requiring that the significance of their transverse impact parameter, d_0, satisfies $|d_0/\sigma(d_0)| < 5\,(3)$, where $\sigma(d_0)$ is the measured uncertainty in d_0, and by requiring that their longitudinal impact parameter, z_0, satisfies $|z_0 \sin\theta| < 0.5$ mm, where θ is the track's polar angle. To further suppress leptons from heavy-flavour hadron decays, misidentified jets, or photon conversions (collectively referred to as 'non-prompt leptons'), lepton candidates are also required to be isolated in the tracker and in the calorimeter. A track-based lepton isolation criterion is defined by calculating the quantity $I_R = \sum p_{\mathrm{T}}^{\mathrm{trk}}$, where the scalar sum includes all tracks (excluding the lepton candidate itself) within the cone defined by $\Delta R < R_{\mathrm{cut}}$ around the direction of the lepton. The value of R_{cut} is the smaller of r_{min} and $10\,\mathrm{GeV}/p_{\mathrm{T}}^{\ell}$, where r_{min} is set to 0.2 (0.3) for electron (muon) candidates and where p_{T}^{ℓ} is the lepton p_{T}. All lepton candidates must satisfy $I_R/p_{\mathrm{T}}^{\ell} < 0.15$. Additionally, electrons (muons) are required to satisfy a calorimeter-based isolation criterion: the sum of the transverse energy within a cone of size $\Delta R = 0.2$ around the lepton, after subtracting the contributions from pile-up and the energy deposit of the lepton itself, is required to be less than 20% (30%) of p_{T}^{ℓ}. Muons are required to be separated by $\Delta R > 0.2$ from any selected jets (defined below). If two electrons are closer than $\Delta R = 0.1$, only the one with the higher p_{T} is considered. An electron lying within $\Delta R = 0.1$ of a selected muon is rejected.

Light leptons of different qualities are used in the analysis, as summarised in table 2. 'Loose' light leptons simply satisfy the corresponding identification criteria, as well as the isolation and impact parameter requirements discussed above. They are used in the event preselection, and to define non-overlapping analysis channels (see section 5.1). 'Tight' and/or 'Very Tight' light leptons are then required, depending on the analysis channel, to improve the rejection of particular reducible backgrounds (see section 5.2). They are discussed further in the following. Uncertainties in light-lepton reconstruction, identification, isolation, and trigger efficiencies are taken into account, but have a negligible impact in the analysis.

Despite the fact that leptons in decays of hadrons that contain bottom- and charm-quarks are highly suppressed by the selection criteria described above, several analysis channels considered in this search (see section 5) require additional suppression of backgrounds containing non-prompt leptons, and other processes where the electron charge is incorrectly assigned. Non-prompt leptons are further rejected using a boosted decision

JHEP06(2021)179

tree (BDT) discriminant based on isolation and variables that are used in the calculation of the multivariate b-tagging discriminant (see description below) referred to as the non-prompt lepton BDT [95]. The efficiency at the chosen working point for muons (electrons) that satisfy the calorimeter- and track-based isolation criteria is about 80% (65%) for $p_{\mathrm{T}} \sim 20\,\mathrm{GeV}$ and reaches a plateau of 95% (90%) at $p_{\mathrm{T}} \sim 45\,\mathrm{GeV}$. The corresponding rejection factor[2] against leptons from the decay of b-hadrons is about 3.5 (10), after resolving ambiguities between overlapping reconstructed objects. Very Tight muon candidates are Tight muons that pass the non-prompt lepton BDT requirement (referred to as the 'non-prompt-lepton veto'). To further suppress material conversions, additional requirements on the associated track p_{T} and on the ratio of the electron's calorimeter energy to its track's momentum are applied to tight electrons. Tight electrons with incorrect charge assignment are rejected using a BDT discriminant based on calorimeter and tracking quantities [91]. An efficiency of 88% for isolated electrons with correct charge assignment is obtained, with a rejection factor of ∼3.3 for isolated electrons with incorrect charge assignment. The resulting electron candidates are further split into three classes: 'Material Conversion', 'Internal Conversion', and 'Very Tight'. Material conversion candidates have a reconstructed displaced vertex with radius $r > 20$ mm that includes the track associated with the electron.[3] The invariant mass of the associated track and the closest (in $\Delta\eta$) opposite-charge track reconstructed in the silicon detector, calculated at the conversion vertex, is required to be < 100 MeV. Internal conversion candidates, which correspond to the internal photon conversions (see section 3), are required to fail the requirements for material conversions, and the di-track invariant mass, this time calculated at the primary vertex, is also required to be < 100 MeV. Therefore, Very Tight electron candidates are Tight electrons that satisfy the non-prompt-lepton veto, the charge-misassignment veto, the internal-conversion veto, and the material-conversion veto requirements, and have $|\eta| < 2$. The last requirement rejects a small fraction of electrons with a large charge misassignment rate because of the limited number of hits used in the track reconstruction.

Hadronically decaying τ-lepton candidates (τ_{had}) are reconstructed from energy clusters in the calorimeters and associated inner-detector tracks [96, 97]. They are required to have either one or three associated tracks (referred to as 'one-prong' and 'three-prong' τ_{had} candidates, respectively), with a total charge of $\pm 1e$. The candidates are required to satisfy $p_{\mathrm{T}} > 25\,\mathrm{GeV}$ and $|\eta| < 2.5$, excluding the EM calorimeter's transition region, and to originate from the primary vertex. A recurrent neural network discriminant using calorimeter- and tracking-based variables is used to identify real τ_{had} candidates and reject jet backgrounds (referred to as 'fake τ_{had} candidates') [98]. Loose and medium identification working points are used, and the selected τ_{had} candidates are referred to as 'Loose' and 'Medium', respectively. The loose working point has a target efficiency of 85% (75%) for one-prong (three-prong) τ_{had} candidates, with an expected rejection factor against light-jets of 21 (90). The corresponding efficiencies and rejections for the medium working point are 75% (60%) and 35 (240) for one-prong (three-prong) τ_{had} candidates, respectively. Electrons

[2]The rejection factor is defined as the reciprocal of the efficiency.

[3]The beampipe and insertable B-layer inner radii are 23.5 mm and 33 mm, respectively.

JHEP06(2021)179

	e			μ		
	L	T	T*	L	T	T*
Identification	loose	tight	tight	loose	medium or high-p_{T}	medium or high-p_{T}
Isolation		Yes			Yes	
Non-prompt-lepton veto	No	No	Yes	No	No	Yes
Electron charge-misassignment veto	No	No	Yes		—	
Electron material-conversion veto	No	No	Yes		—	
Electron internal-conversion veto	No	No	Yes		—	
$\lvert d_0\rvert/\sigma_{d_0}$		< 5			< 3	
$\lvert z_0 \sin\theta\rvert$ [mm]		< 0.5			< 0.5	

Table 2. Summary of requirements applied to define Loose (L), Tight (T), and Very Tight (T*) light leptons. The quality cuts for tight muon identification depend on the transverse momentum of the muon candidates.

that are reconstructed as one-prong τ_{had} candidates are removed using a BDT with an efficiency (rejection factor) of 95% (30–100) for real (fake) τ_{had} candidates depending on the p_{T}. Additionally, τ_{had} candidates are required to be separated by $\Delta R > 0.2$ from any selected electron or muon candidates. The τ_{had} reconstruction and identification efficiencies and the τ_{had} energy scale in the simulation are calibrated to those measured in a data control sample of $Z \to \tau^+\tau^-$ events [99], and the associated uncertainties are considered in the analysis. The uncertainty in the τ_{had} identification efficiency is split into eight uncorrelated components, corresponding to different τ_{had} p_{T} ranges and separately for one-prong and three-prong candidates. It is approximately 2.5% (3.0%) for one-prong (three-prong) τ_{had} candidates with $p_{\mathrm{T}} < 300\,\mathrm{GeV}$, and 3.5% (6.5%) for $p_{\mathrm{T}} \geq 300\,\mathrm{GeV}$. The uncertainty in the τ_{had} energy scale is about 1.2% (3.0%) for one-prong (three-prong) τ_{had} candidates [99], and is split into eight independent components. An additional correction and associated uncertainties are estimated for the probability of misidentification of electrons as τ_{had} candidates using a data control sample of $Z \to e^+e^-$ events.

The inputs for jet reconstruction are built by combining measurements from both the tracker and the calorimeter using the particle flow (PFlow) algorithm [100, 101]. Jet candidates are reconstructed from such PFlow objects using the anti-k_t algorithm with a radius parameter $R = 0.4$ [102, 103]. After subtracting the expected energy contribution from pile-up following the jet area method [104], the jet energy scale (JES) and resolution (JER) are corrected to particle level using MC simulation, and then calibrated in situ using Z+jets, γ+jets and multijet events [101]. Jets are required to satisfy $p_{\mathrm{T}} > 25\,\mathrm{GeV}$ and $|\eta| < 2.5$. A jet-vertex tagger (JVT) is used to remove jets associated with pile-up vertices and having $p_{\mathrm{T}} < 60\,\mathrm{GeV}$ and $|\eta| < 2.4$ [105]. Any jets within $\Delta R = 0.2$ of a selected electron or a τ_{had} candidate are rejected. Uncertainties associated with jets arise from the JES and JER, and the efficiency to pass the JVT requirement. The largest contribution results from the JES, whose uncertainty dependence on jet p_{T} and η, jet flavour, and pile-up treatment is split into 27 uncorrelated components that are treated independently in the analysis [101].

JHEP06(2021)179

The total JES uncertainty varies from 1% to 4% depending on the jet p_{T}. A total of seven uncorrelated uncertainty components affecting the JER are also considered.

Jets containing b-hadrons are identified (b-tagged) via an algorithm [106, 107] that uses multivariate techniques to combine information about the impact parameters of displaced tracks and the topological properties of secondary and tertiary decay vertices reconstructed within the jet. For each jet, a value for the multivariate b-tagging discriminant is calculated. A jet is considered b-tagged if this value is above the threshold corresponding to an average 77% efficiency to tag a b-quark jet, with a light-jet[4] rejection factor of about 140, a charm-jet (c-jet) rejection factor of about 4, and a τ_{had}-jet rejection factor of about 17, as determined for jets with $p_{\mathrm{T}} > 20\,\mathrm{GeV}$ and $|\eta| < 2.5$ in simulated $t\bar{t}$ events. Correction factors derived from dedicated calibration samples enriched in b-jets, c-jets, or light jets, are applied to the simulated samples [106, 108, 109]. In the case of τ_{had}-jets, for which no dedicated calibration sample exists, the correction factors derived for c-jets are used. Uncertainties in these corrections include a total of nine independent sources affecting b-jets and five independent sources affecting c-jets. Six sources of uncertainty affecting light jets are also considered. An additional uncertainty is included for the extrapolation of these corrections to jets with p_{T} beyond the kinematic reach of the data calibration samples used ($p_{\mathrm{T}} > 300\,\mathrm{GeV}$ for b- and c-jets, and $p_{\mathrm{T}} > 750\,\mathrm{GeV}$ for light jets); it is taken to be correlated among the three jet flavours. Finally, an uncertainty related to the application of c-jet scale factors to τ_{had}-jets is considered. The approximate relative size of the b-tagging efficiency uncertainty is 2% for b-jets, 10% for c-jets and τ_{had}-jets, and 30% for light jets.

The missing transverse momentum $\vec{p}_{\mathrm{T}}^{\,\mathrm{miss}}$ (with magnitude $E_{\mathrm{T}}^{\mathrm{miss}}$) is defined as the negative vector sum of the p_{T} of all selected and calibrated objects in the event, including a term to account for momentum from soft particles in the event that are not associated with any of the selected objects [110]. This soft term is calculated from inner-detector tracks matched to the selected primary vertex, which makes it more resilient to contamination from pile-up interactions. Uncertainties associated with energy scales and resolutions of leptons and jets are propagated to $\vec{p}_{\mathrm{T}}^{\,\mathrm{miss}}$. Additional uncertainties originating from the modelling of the underlying event, in particular its impact on the p_{T} scale and resolution of unclustered energy, are negligible.

5 Search strategy

The search discussed in this paper targets $\mathrm{LQ}_3^{\mathrm{d}}$ pair production in the $t\tau t\tau$ final state, thus being particularly sensitive to high values of $\mathcal{B}$. In this decay mode, there is a high probability that the final state contains at least one light lepton from a semileptonic top-quark decay or a leptonic τ-lepton decay, which is used to trigger the event and to help suppress multijet backgrounds. The presence of additional τ_{had} candidates and/or additional light leptons is exploited to further reduce SM backgrounds and improve the search sensitivity. The final state of interest also contains two energetic b-jets, and may contain additional light jets from initial- or final-state radiation and/or from a hadronically decaying W boson in one of the top-quark decays. The multiple sources of leptons in the

[4]'Light jet' refers to a jet originating from the hadronisation of a light quark (u, d, s) or a gluon.

JHEP06(2021)179

event motivate the definition of different analysis channels depending on the multiplicity of light leptons, the multiplicity of τ_{had} candidates, and the electric charges of light leptons (see section 5.1). The analysis channels are subdivided into different event categories (see section 5.2) so that a maximum-likelihood fit is performed across event categories to search for the signal and constrain several leading backgrounds simultaneously. The requirement of multiple leptons in the event implies the presence of multiple neutrinos, which makes the kinematic reconstruction of the top quarks and consequently of the LQ invariant mass difficult. Nevertheless, the decay of a pair of massive LQs results in energetic final-state objects, which is exploited in the most sensitive analysis channels, both in optimising the event selection in the different categories considered and in defining a powerful event variable used in the statistical analysis to discriminate the signal from the background. Further details of the search strategy are provided in the following sections.

5.1 Event selection

The events used in the analysis are selected with high efficiency using single-lepton and dilepton triggers [27], which use electron and muon signatures. Single-lepton triggers with low p_{T} threshold and lepton isolation requirements are combined in a logical OR with higher-threshold triggers without isolation requirements to give maximum efficiency. Single-electron triggers with a p_{T} threshold of 24 (26) GeV in the 2015 (2016, 2017 and 2018) data-taking period(s) and isolation requirements are used along with triggers with a 60 GeV threshold and no isolation requirement, and with a 120 (140) GeV threshold with looser identification criteria. For single-muon triggers, the lowest p_{T} threshold is 20 (26) GeV in 2015 (2016–2018), while the higher p_{T} threshold is 50 GeV for all periods. The dielectron triggers require two electrons that satisfy loose identification criteria with different p_{T} thresholds: 12 GeV in 2015, 17 GeV in 2016, and 24 GeV in 2017–2018. Dimuon triggers utilise asymmetric p_{T} thresholds for leading (subleading) muons: 18 (8) GeV in 2015 and 22 (8) GeV in 2016–2018. An electron+muon trigger requires events to have an electron candidate satisfying loose identification with a 17 GeV threshold and a muon candidate with a 14 GeV threshold for all periods.

Events selected by the trigger are required to satisfy basic preselection requirements. They must have at least one primary vertex candidate. Events are required to contain either one light lepton and at least one τ_{had} candidate, or at least two light leptons. At this stage, the light leptons and τ_{had} candidates satisfy the Loose selection criteria (see section 4) and have $p_{\text{T}} > 10\,\text{GeV}$ and $p_{\text{T}} > 25\,\text{GeV}$, respectively. Furthermore, the leading light lepton in the event is required to have $p_{\text{T}} > 25\,\text{GeV}$. Events with one light lepton must have been selected by a single-lepton trigger, whereas events with at least two light leptons are required to be selected by a logical OR of the single-lepton and dilepton triggers. The selected light leptons are required to match, with $\Delta R < 0.15$, the corresponding leptons reconstructed by the trigger and to have a p_{T} exceeding the trigger p_{T} threshold by 1 GeV or 2 GeV (depending on the lepton trigger, lepton multiplicity criteria, and data-taking conditions), besides the 25 GeV requirement for the leading light leptons. These requirements are used to ensure operating in the trigger efficiency plateau, and to apply any corrections to the simulation in order to reproduce the per-lepton trigger efficiencies

JHEP06(2021)179

measured in data [111, 112]. In addition, two or more jets, at least one of which is b-tagged, are required. The trigger requirement has an efficiency of about 85% (98%) for signal events with one light lepton (at least two light leptons) satisfying the preselection requirements.

Six final states, termed 'channels', are analysed, defined by the multiplicity and flavour of Loose lepton candidates with the p_{T} requirements indicated above:

- $1\ell{+}{\geq}1\tau$: one light lepton and at least one τ_{had} candidate;
- $2\ell\mathrm{OS}{+}{\geq}1\tau$: two opposite-charge (denoted by OS, standing for opposite-sign) light leptons and at least one τ_{had} candidate;
- $2\ell\mathrm{SS}/3\ell{+}{\geq}1\tau$: two same-charge (denoted by SS, standing for same-sign) light leptons or three light leptons, and at least one τ_{had} candidate;
- $2\ell\mathrm{OS}{+}0\tau$: two OS light leptons and no τ_{had} candidates;
- $2\ell\mathrm{SS}{+}0\tau$: two SS light leptons and no τ_{had} candidates;
- $3\ell{+}0\tau$: three light leptons and no τ_{had} candidates.

The selection criteria are orthogonal to those of the other channels so that each event only contributes to a single analysis channel. Finally, in all analysis channels the minimum p_{T} requirement on light leptons is raised to 25 GeV. The analysis channels with no τ_{had} candidates are used for the determination of particular backgrounds, while those with at least one τ_{had} candidate are in addition used to search for the signal.

5.2 Event categorisation

The channels are subdivided into different event categories optimised either to search for the signal (referred to as 'signal regions', or SR), to obtain improved background estimates (referred to as 'control regions', or CR), or to validate the estimated backgrounds (referred to as 'validation regions', or VR). In the optimisation of the SRs, different features of the LQ signal are exploited, such as the multiplicity of τ_{had} candidates, the charge configuration of reconstructed leptons and, especially, the difference in kinematics of final-state objects between signal and background. In particular, the effective mass (m_{eff}), defined as the scalar sum of the transverse momenta of all selected leptons, the selected jets and the missing transverse momentum, is a powerful discriminating variable between signal and background. Additional kinematic variables exploited in the optimisation of the SRs include the p_{T} of τ_{had} candidates, and different invariant mass variables based on dilepton pair combinations (e.g. the invariant mass of the two leading τ_{had} candidates, $m_{\tau\tau}$). The CRs are defined by inverting particular selections in order to provide background-rich samples that do not overlap with the SRs. The VRs are defined to be kinematically closer to the SRs, and they do not overlap with the other CRs and SRs. A total of 7 SRs, 18 CRs, and 6 VRs are considered, with their definitions given below. For a $\mathrm{LQ}_3^{\mathrm{d}}$ signal with $\mathcal{B} = 1$, the acceptance times efficiency within the seven SRs is found to be about 10%, varying only slightly with the $\mathrm{LQ}_3^{\mathrm{d}}$ mass, with higher mass values resulting in higher acceptance times efficiency to pass the kinematic requirements.

JHEP06(2021)179

	1ℓ+1τOS			1ℓ+1τSS			1ℓ+$\geq 2\tau$		
	CR	VR	SR	CR	VR	SR	CR	VR	SR
e/μ selection	T			T			T		
$N_{\tau_{\text{had}}}$	1			1			≥ 2		
N_{jets}	≥ 4			≥ 3			≥ 2		
τ_{had} ID	Medium			Medium			Loose		
$\ell\tau_{\text{had}}$ charge	OS			SS			—		
$p_{\text{T},1}^{\tau}$ [GeV]	≥ 50	50–150	≥ 150	≥ 50	50–150	≥ 150	≥ 50	50–100	≥ 100
$p_{\text{T},2}^{\tau}$ [GeV]	—			—			≥ 25	25–50	≥ 50
$N_{b\text{-jets}}$	≥ 2	≥ 1		≥ 2	≥ 1		≥ 2	≥ 1	
$m_{\ell\tau}$ [GeV]	—	≥ 200		—	—	≥ 200	—		
$m_{\text{T}}(\ell, E_{\text{T}}^{\text{miss}})$ [GeV]	—			—	—	≥ 100	—		
$m_{\tau\tau}$ [GeV]	—			—			—	≥ 100	
$E_{\text{T}}^{\text{miss}}$ [GeV]	—	≥ 80		—	—	≥ 50	—		
m_{eff} [GeV]	< 800	≥ 800		< 800	≥ 800		< 800	≥ 800	

Table 3. Summary of event categories in the 1ℓ+$\geq 1\tau$ channel. All events are required to satisfy the preselection requirements. "T" denotes the Tight light-lepton selection criteria (see table 2). The p_{T} of the leading and subleading τ_{had} candidates are denoted by $p_{\text{T},1}^{\tau}$ and $p_{\text{T},2}^{\tau}$, respectively. The transverse mass of the system formed by the selected light lepton and the missing transverse momentum is denoted by $m_{\text{T}}(\ell, E_{\text{T}}^{\text{miss}})$.

In the 1ℓ+$\geq 1\tau$ channel, events are required to have one Tight light lepton and, either one Medium τ_{had} candidate and no additional Loose τ_{had} candidates, or at least two Loose τ_{had} candidates. A total of nine event categories are defined, which are summarised in table 3. They consist of two subcategories based on the multiplicity of τ_{had} candidates (1 or $\geq$2), with the former subcategory further split according to the charge configuration of the selected light lepton and τ_{had} candidate (OS or SS). The splitting between OS and SS events improves the sensitivity, since their background compositions and signal-to-background ratios are very different. For each of these subcategories, a CR, a VR, and a SR, are defined. All SRs require one or two high-p_{T} τ_{had} candidates, as appropriate, a requirement that provides significant background suppression, as illustrated in figure 1a. Further requirements are placed on additional kinematic variables, such as the invariant mass of the light lepton and the τ_{had} candidate ($m_{\ell\tau}$) (see figure 1b), used in the 1ℓ+1τOS and 1ℓ+1τSS SRs, or $m_{\tau\tau}$ (see figure 2a), used in the 1ℓ+$\geq 2\tau$ SR.

In the 2ℓOS+$\geq 1\tau$ channel, events are required to have two OS light leptons satisfying the Tight selection criteria, and at least one Loose or Medium τ_{had} candidate. A total of six event categories are defined, which are summarised in table 4. Separate SRs and VRs are defined for events with one Medium τ_{had} candidate (and no additional Loose τ_{had} candidates) and at least two Loose τ_{had} candidates. Backgrounds with resonant $\ell^+\ell^-$ pairs from quarkonia or Z-boson decays are suppressed by requiring that the dilepton invariant mass ($m_{\ell\ell}$) satisfies $m_{\ell\ell} > 12\,\text{GeV}$ and $|m_{\ell\ell} - m_Z| > 10\,\text{GeV}$, respectively, where m_Z represents the mass of the Z boson. The latter requirement is referred to as the 'Z-veto'. The event selections are further optimised based on the p_{T} of the leading τ_{had} candidate ($p_{\text{T},1}^{\tau}$) and the minimum invariant mass of a light lepton and a τ_{had} candidate ($m_{\ell\tau}^{\text{min}}$) (see

JHEP06(2021)179

	2ℓOS+1τ				2ℓOS+$\geq 2\tau$	
	CR^{Z}	$CR^{t\bar{t}}$	VR	SR	VR	SR
e/μ selection	T				T	
e/μ combinations	$ee/\mu\mu$	$e\mu$	$ee/\mu\mu$	$ee/\mu\mu/e\mu$	$ee/\mu\mu/e\mu$	
Z veto	Inverted	Yes	Yes	Yes	Yes	
$m_{\ell\ell}$ [GeV]	> 12				> 12	
$N_{\tau_{\text{had}}}$	1				≥ 2	
τ_{had} ID	Loose/Medium		Medium		Loose	
$p_{\text{T},1}^{\tau}$ [GeV]	≥ 25	≥ 25	25–150	≥ 150	≥ 25	≥ 75
$m_{\ell\tau}^{\text{min}}$ [GeV]	—	—	< 100	≥ 100	—	≥ 50
$m_{\tau\tau}$ [GeV]	—				<100	≥ 100
m_{eff} [GeV]	—	< 1000	—	—	—	—

Table 4. Summary of event categories in the 2ℓOS+$\geq 1\tau$ channel. All events are required to satisfy the preselection requirements. "T" denotes the Tight light-lepton selection criteria (see table 2).

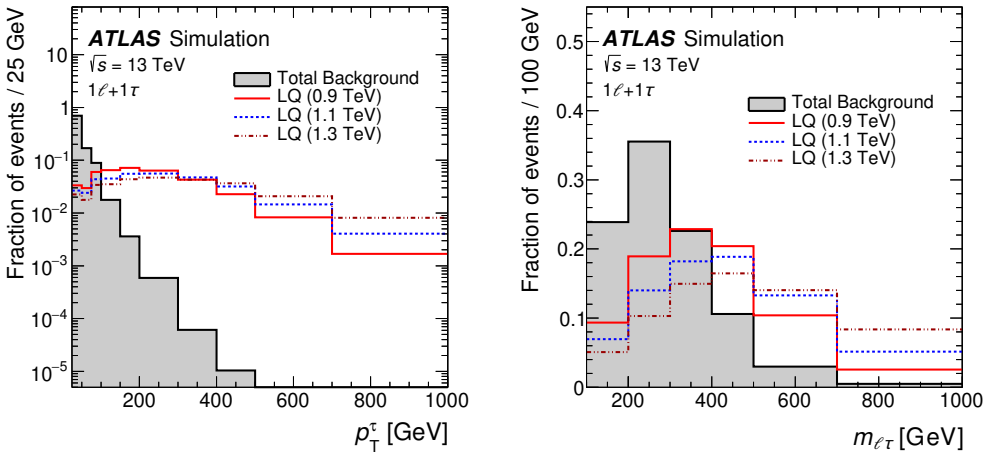

(a) **(b)**

Figure 1. Comparison of the distribution of (a) the p_{T} of the τ_{had} candidate (p_{T}^{τ}), and (b) the invariant mass of the light lepton and the τ_{had} candidate ($m_{\ell\tau}$), between the total background (shaded histogram) and the LQ signal for different mass values. The selection used corresponds to events in the 1ℓ+1τ event category (a) after the preselection requirements, and (b) after applying the additional requirement of $p_{\text{T}}^{\tau} > 150$ GeV. The last bin in each distribution contains the overflow.

figure 2b). In addition, two dedicated CRs are defined for events with one Loose or Medium τ_{had} candidate in order to estimate correction factors to apply to the jet misidentification (also referred to as 'fake') rate in the simulation for both sets of τ_{had} identification criteria. These CRs are enriched in Z+jets and dileptonic $t\bar{t}$ events, respectively, and do not take part of the final likelihood fit. Further details of the fake-τ_{had} background estimation can be found in section 6.2.1.

In the 2ℓSS/3ℓ+$\geq 1\tau$ channel, events are required to have either two light leptons with the same charge (2ℓSS) or three light leptons (3ℓ) with their charges adding up to ± 1. In

JHEP06(2021)179

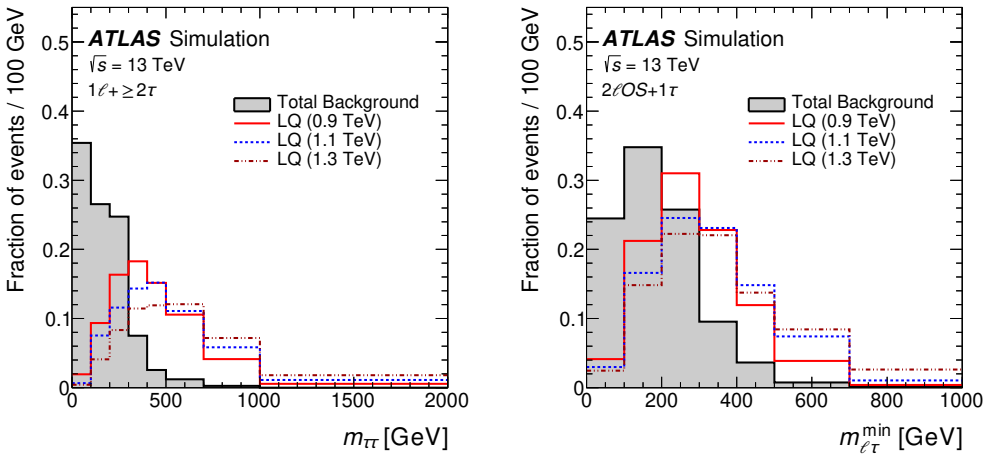

(a) **(b)**

Figure 2. Comparison of the distribution of (a) the invariant mass of the two leading τ_{had} candidates ($m_{\tau\tau}$), and (b) the minimum invariant mass of a light lepton and a τ_{had} candidate ($m_{\ell\tau}^{\text{min}}$), between the total background (shaded histogram) and the LQ signal for different mass values. The selection used in (a) corresponds to events in the $1\ell+\geq 2\tau$ category after the requirements of $p_{\text{T},1}^{\tau} > 100\,\text{GeV}$ and $p_{\text{T},2}^{\tau} > 50\,\text{GeV}$, whereas the selection used in (b) corresponds to events in the $2\ell\text{OS}+1\tau$ category after the requirement of $p_{\text{T}}^{\tau} > 150\,\text{GeV}$. The last bin in each distribution contains the overflow.

addition, at least one Loose τ_{had} candidate is required. Since two SS light leptons can originate from backgrounds with non-prompt leptons, photon conversions, and electron charge misassignment (QMisID), the two SS light leptons in the event are required to satisfy the Very Tight selection criteria. In the case of 3ℓ events, the light lepton that has opposite charge to the SS lepton pair is required to satisfy the Tight selection criteria. In addition, it is required that any $e^{\pm}e^{\pm}$, $e^{+}e^{-}$ or $\mu^{+}\mu^{-}$ pair in the event satisfies $m_{\ell\ell} > 12\,\text{GeV}$ and $|m_{\ell\ell} - m_Z| > 10\,\text{GeV}$. Similarly, 3ℓ events are required to satisfy $|m_{3\ell} - m_Z| > 10\,\text{GeV}$ to eliminate potential backgrounds with $Z \to 2\ell\gamma^{*} \to 4\ell$ where one lepton has very low momentum and is not reconstructed. Selected events fall into one of three event categories, two SRs and one VR, simply defined using $p_{\text{T},1}^{\tau}$ (see table 5). Events with $p_{\text{T},1}^{\tau} > 225\,\text{GeV}$ are assigned to the main signal region, SR-H (with the symbol "H" representing "High"), which is optimal for high LQ masses, while events with $125 \leq p_{\text{T},1}^{\tau} < 225\,\text{GeV}$ fall into SR-L (with the symbol "L" standing for "Low") and extend the sensitivity to lower LQ masses. The VR contains the events with $25 \leq p_{\text{T},1}^{\tau} < 125\,\text{GeV}$.

Finally, the $2\ell\text{OS}+0\tau$, $2\ell\text{SS}+0\tau$, and $3\ell+0\tau$ channels require there be no τ_{had} candidates and are primarily used to improve the background modelling, as discussed in section 6. Events in the $2\ell\text{OS}+0\tau$ channel are selected by requiring an OS $e\mu$ pair with both light leptons satisfying the Tight selection criteria and no additional Loose light leptons, at least two jets, at least one b-tagged jet, and no Loose τ_{had} candidates. This selection provides a $t\bar{t}$-rich control sample (denoted $t\bar{t}0\tau$ CR) that does not take part of the final likelihood fit, but that is used to derive corrections to improve the $t\bar{t}$ background modelling (see section 6.1.1). Events in the $2\ell\text{SS}+0\tau$ channel are selected by requiring two SS light

JHEP06(2021)179

	2ℓSS/3ℓ+$\geq$1τ		
	VR	SR-L	SR-H
e/μ selection	T* (2ℓSS) T*/T (3ℓ)		
Z veto	Yes		
$m_{\ell\ell}$ [GeV]	> 12		
$N_{\tau_{\text{had}}}$	≥ 1		
τ_{had} ID	Loose		
$p_{\text{T},1}^{\tau}$ [GeV]	25–125	125–225	≥ 225

Table 5. Summary of event categories in the 2ℓSS/3ℓ+$\geq$1τ channel. All events are required to satisfy the preselection requirements. "T" and "T*" denote the Tight and Very Tight light-lepton selection criteria (see table 2).

leptons satisfying the Very Tight selection criteria, except for some event categories where the internal conversion (IntC) or material conversion (MatC or Mat Conv) vetoes are inverted. A total of eight event categories, all of which are CRs, are defined so as to be enriched in different backgrounds: $t\bar{t}$ with non-prompt electrons or muons, $t\bar{t}W$, internal conversions, and material conversions, (denoted by 2ℓtt(e) or 2ℓtt(μ), 2ℓttW, 2ℓIntC, and 2ℓMatC, respectively), which are summarised in table 6. The last two CRs select events with two SS light leptons containing at least one electron that satisfies the corresponding inverted conversion veto requirement. The 2ℓtt(e) and 2ℓtt(μ) CRs select events with a SS $ee/\mu e$ pair and a SS $\mu\mu/e\mu$ pair, respectively, where the first (second) lepton denotes the leading (subleading) lepton in p_{T}. The definition of these CRs exploits the fact that in SS dilepton events from $t\bar{t}$ production the subleading lepton in p_{T} is typically a non-prompt lepton. In addition, the events are restricted to have two or three jets in order to suppress the contribution from $t\bar{t}W$ production. In the case of the 2ℓttW CR, no restriction is imposed on the light-lepton flavours, and the events are required to have at least four jets. The 2ℓtt(e), 2ℓtt(μ), and 2ℓttW CRs are further split according to the charge of the light leptons ($++$ or $--$) in order to improve the discrimination between charge asymmetric and charge symmetric backgrounds (dominated by $t\bar{t}W$ and $t\bar{t}$, respectively). Events in the 3ℓ+0τ channel are selected by requiring three light leptons satisfying the Tight or Very Tight selection criteria, with their charges adding up to ± 1. A total of four CRs are defined, which are summarised in table 7. Two CRs select events compatible with having a Z-boson candidate, but differing in their jet multiplicity requirements, in order to provide samples enriched in diboson (denoted by 3ℓVV) and $t\bar{t}Z$ backgrounds (denoted by 3ℓttZ), respectively. Similarly to the 2ℓSS+0τ channel, two additional CRs are defined so as to be enriched in internal- and material-conversion backgrounds, respectively, by inverting the corresponding conversion veto requirement on one of the electrons belonging to the SS lepton pair.

The m_{eff} distribution is used as the final discriminating variable in all SRs. It peaks at approximately $2m_{\text{LQ}}$ for signal events, and at lower values for the backgrounds, as illustrated in figure 3. The overall rate and composition of the background varies across the

JHEP06(2021)179

	2ℓSS+0τ				
	2ℓtt(e)$\pm$	2ℓtt(μ)$\pm$	2ℓttW$\pm$	2ℓIntC	2ℓMatC
e/μ selection			T*		
e/μ combination	$ee/\mu e$	$\mu\mu/e\mu$	$ee/\mu\mu/e\mu/\mu e$	$ee/e\mu/\mu e$	$ee/e\mu/\mu e$
Electron internal conversion veto	Yes	Yes	Yes	Inverted	Yes
Electron material conversion veto	Yes	Yes	Yes	Yes	Inverted
N_{jets}	2–3	2–3	≥ 4	≥ 2	≥ 2
Z veto			Yes		
m_{ee} [GeV]			≥ 12		

Table 6. Summary of event categories in the 2ℓSS+0τ channel. All events are required to satisfy the preselection requirements. "T*" denotes the Very Tight light-lepton selection criteria (see table 2). Events that belong to the tt(e), tt(μ), and ttW categories are further split into two CRs for ++ and $--$ charge events. IntC and MatC stand for internal and material conversions, respectively. The first (second) light lepton quoted in a pair denotes the leading (subleading) lepton in p_{T}. Backgrounds with resonant e^+e^- pairs from quarkonia or Z-boson decays due to electron charge misassignment are suppressed by requirements on the dielectron invariant mass (m_{ee}).

	3ℓ+0τ			
	3ℓVV	3ℓttZ	3ℓIntC	3ℓMatC
e/μ selection	T	T	T(ℓ_0), T*(ℓ_1 and ℓ_2)	T(ℓ_0), T*(ℓ_1 and ℓ_2)
Electron internal conversion veto	Yes	Yes	Inverted(ℓ_1 or ℓ_2)	Yes(ℓ_1 and ℓ_2)
Electron material conversion veto	Yes	Yes	Yes(ℓ_1 and ℓ_2)	Inverted(ℓ_1 or ℓ_2)
N_{jets}	2–3	≥ 4	≥ 2	≥ 2
Z veto	Inverted	Inverted	Yes	Yes
$m_{\ell\ell}$ [GeV]			≥ 12	

Table 7. Summary of four CR categories in the 3ℓ+0τ channel. All events are required to satisfy the preselection requirements. "T" and "T*" denote the Tight and Very Tight light-lepton selection criteria (see table 2). IntC and MatC stand for internal and material conversions, respectively. Same-charge (opposite-charge) lepton pairs are also referred to as same-sign (opposite-sign) with abbreviation SS (OS). The OS lepton (relative to the SS pair) is denoted ℓ_0, but is not necessarily the one with highest p_{T}; the remaining SS leptons are denoted ℓ_1 (closest in ΔR to ℓ_0) and ℓ_2 (the remaining one).

different SRs, as illustrated in figure 4. The dominant background in the 1ℓ+1τOS SR is $t\bar{t}$ production with both the light lepton and τ_{had} candidate originating from the W boson decays. In contrast, the main background in the 1ℓ+1τSS SR is also $t\bar{t}$ production, but with one jet misidentified as a τ_{had} candidate (fake τ_{had}), one non-prompt light lepton, or an electron with misassigned charge, followed by $t\bar{t}W$ and VV production. In the 1ℓ+$\geq 2\tau$, 2ℓOS+1τ, and 2ℓOS+$\geq 2\tau$ SRs, about half of the background is also $t\bar{t}$ with one fake τ_{had} candidate, while the remaining contributions arise from $t\bar{t}W$, $t\bar{t}Z/\gamma^*$, and $t\bar{t}H$ production, with varying fractions across the SRs. Finally, the 2ℓSS/3ℓ+$\geq 1\tau$ SRs are dominated by backgrounds with real leptons, with comparable contributions from $t\bar{t}W$, $t\bar{t}Z/\gamma^*$, $t\bar{t}H$, and VV production. Despite their limited purity, the CRs defined above are useful for checking

JHEP06(2021)179

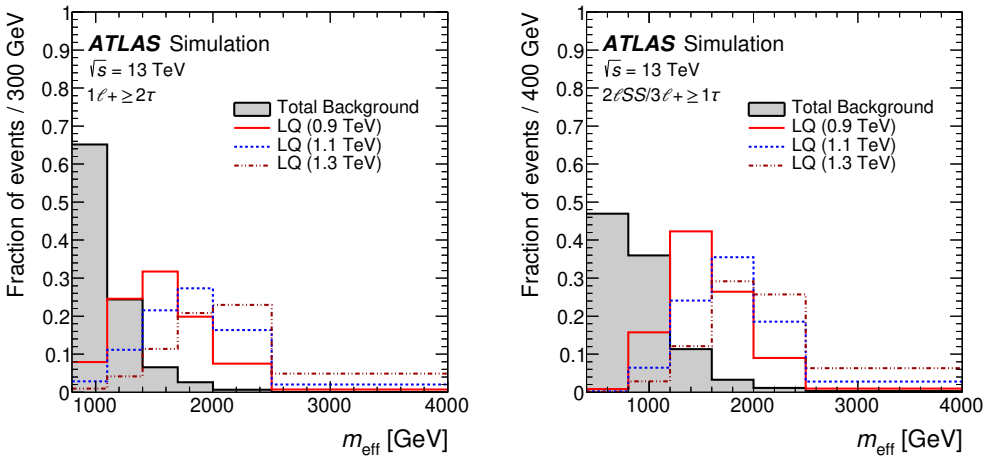

(a) **(b)**

Figure 3. Comparison of the m_{eff} distribution in (a) the $1\ell+\geq 2\tau$ SR, and (b) the $2\ell\text{SS}/3\ell+\geq 1\tau$ SR-H, between the total background (shaded histogram) and the LQ signal for different mass values. The last bin in each distribution contains the overflow.

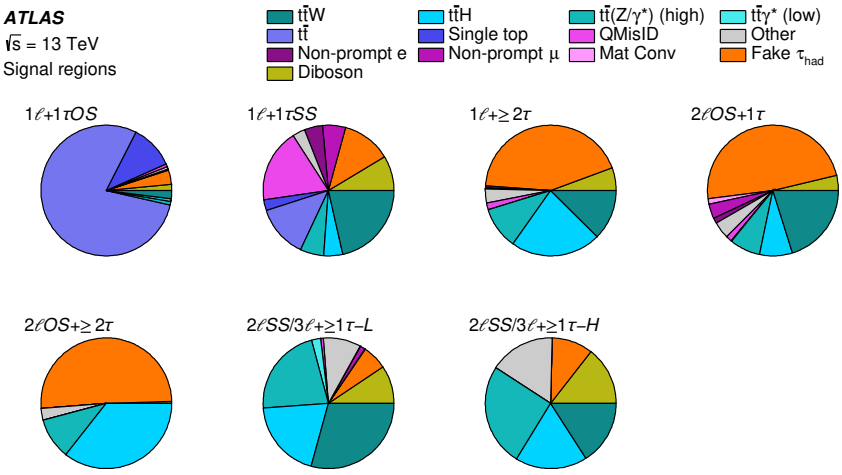

Figure 4. The fractional contributions of the various backgrounds to the total predicted background in each of the seven signal region categories (see section 5). The background estimation methods are described in section 6. The background contributions after the likelihood fit to data under the background-only hypothesis are shown (see section 7).

and correcting the background prediction (see section 6) and constraining the related systematic uncertainties through the likelihood fit to data that also includes the SRs. The VRs are meant to provide an independent validation of the background prediction, and thus are not included in the fit.

JHEP06(2021)179

6 Background estimation

Backgrounds are categorised into irreducible and reducible backgrounds. Irreducible backgrounds (section 6.1) have only prompt selected leptons, i.e. produced in W/Z boson decays, in leptonic τ-lepton decays, or internal conversions. Reducible backgrounds (section 6.2) have prompt leptons with misassigned charge, at least one non-prompt light lepton, or fake τ_{had} candidates. All backgrounds are estimated using the simulated samples described in section 3, which also discusses the systematic uncertainties in the modelling of these processes, so this is not repeated below. In some cases, the simulation is improved using additional corrections derived in data control samples. In particular, the event kinematics of the simulated $t\bar{t}$ background, or the τ_{had} fake rate predicted by the simulation, require dedicated corrections to better describe the data. In addition, the yields of some simulated backgrounds, in particular $t\bar{t}W$ and non-prompt-lepton backgrounds, are adjusted via normalisation factors that are determined by performing a likelihood fit to data across all event categories as discussed in section 7.

6.1 Irreducible backgrounds

Background contributions with prompt leptons originate from a wide range of physics processes with their relative importance varying by channel. In the $1\ell{+}1\tau$OS category the main irreducible background is $t\bar{t}$ production, followed by tW production, whereas in the rest of analysis channels the main irreducible backgrounds originate from $t\bar{t}W$ and $t\bar{t}(Z/\gamma^*)$ production, followed by VV (in particular WZ) production. Smaller contributions originate from the following rare processes: tZ, WtZ, $t\bar{t}WW$, VVV, $t\bar{t}t$, and $t\bar{t}t\bar{t}$ production.

6.1.1 $t\bar{t}$ background

Detailed measurements of differential cross sections have shown that the $t\bar{t}$ simulation does not model the top-quark p_{T} spectrum with sufficient accuracy, overestimating it in the high-p_{T} tail [113, 114]. In addition, the simulation underestimates the production of $t\bar{t}$ events with high jet multiplicity [114]. This leads to discrepancies between data and simulation in the distributions of several kinematic quantities of interest in this search, in particular the m_{eff} variable. In order to improve the description, dedicated corrections as a function of jet multiplicity and m_{eff} (referred to as 'kinematic reweighting') are derived in the $t\bar{t}0\tau$ CR. The corrections are derived by comparing the data, after subtracting small background contributions estimated from the simulation, with the predicted sum of $t\bar{t}$ and tW processes.[5] The correction factors as a function of jet multiplicity vary from 1.05 for exactly two jets, to 1.1 for at least six jets. After correcting the jet multiplicity spectrum, a further correction as a function of m_{eff} is derived for each jet multiplicity, and parameterised as a first-degree polynomial. For example, for exactly four jets, the resulting correction factor varies from ∼1.1 for $m_{\text{eff}} = 200\,\text{GeV}$ to ∼0.4 for $m_{\text{eff}} = 3\,\text{TeV}$, as shown in figure 5a. This kinematic reweighting is applied to all (nominal and alternative) $t\bar{t}$ and tW simulated events, and prior to the derivation of any further corrections to improve the modelling of fake τ_{had} candidates or non-prompt leptons (see sections 6.2.1 and 6.2.2). The comparison

[5] The sum of $t\bar{t}$ and tW backgrounds is considered since they interfere at NLO.

JHEP06(2021)179

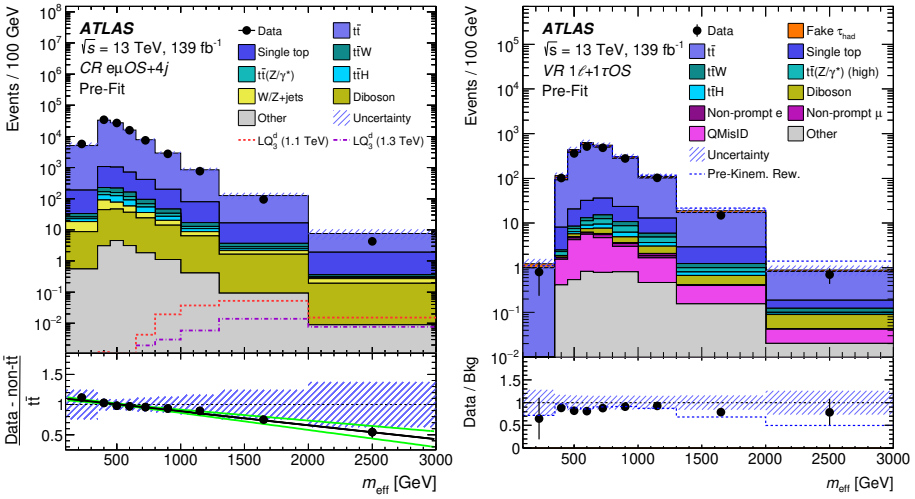

(a) **(b)**

Figure 5. (a) Comparison between data and the background prediction for the m_{eff} distribution in events selected by requiring an opposite-charge (OS) $e\mu$ pair, exactly four jets, and at least one b-tagged jet. The background contributions shown are before the likelihood fit to data ("Pre-Fit"). The lower panel displays the ratio of the data, after subtracting the small background contributions estimated from the simulation, to the predicted sum of $t\bar{t}$ and tW processes, along with the corresponding fit using a first-degree polynomial (black solid line). The associated green lines represent the estimated uncertainty in the reweighting function. (b) Comparison of the m_{eff} distribution between data and the pre-fit background prediction after the kinematic reweighting in the 1ℓ+1τOS VR. The total background prediction before the kinematic reweighting ("Pre-Kinem. Rew.") is shown as a dashed blue histogram. The ratio of the data to the total pre-fit background prediction ("Bkg") is shown in the lower panel. The size of the combined statistical and systematic uncertainty in the background prediction is indicated by the blue hatched band. The ratios of the data to the total pre-fit predictions before and after kinematic reweighting are shown in the lower panel. The last bin in each figure contains the overflow.

between the data and the background prediction after the kinematic reweighting, and before the likelihood fit (denoted "pre-fit"), is illustrated in figure 5b for the m_{eff} distribution in the 1ℓ+1τOS VR, which is dominated by $t\bar{t}$ background with a real τ_{had} candidate. Good agreement is observed within the estimated pre-fit uncertainties. The agreement in normalisation is further improved after the likelihood fit (denoted "post-fit"), as shown in figure 11. The modelling of several other kinematic quantifies such as the lepton p_{T}, $E_{\text{T}}^{\text{miss}}$, and the scalar sum of jet p_{T}, is also improved by the kinematic reweighting. Although this kinematic reweighting is derived using $t\bar{t}$ dileptonic events, it is also applied to $t\bar{t}$ semileptonic events selected in the 1ℓ+1τ channel. A systematic uncertainty from the slight difference between the slope of the nominal m_{eff} correction factor and that derived in the 1ℓ+1τOS CR is also considered, with negligible impact on the final result.

JHEP06(2021)179

6.1.2 $t\bar{t}W$ background

The $t\bar{t}W$ background represents a non-negligible background in several event categories. Despite the use of state-of-the-art simulations, accurate modelling of additional QCD radiation in $t\bar{t}W$ production remains challenging. Event categories sensitive to the $t\bar{t}W$ background were defined in the analysis in order to study and constrain this background. These event categories are split by the sign of the sum of lepton charges (referred to as 'total charge') to better discriminate the $t\bar{t}W$ process, which has a large charge asymmetry, from other SM backgrounds that are charge symmetric. To illustrate this point, the distribution of the scalar sum of the lepton p_{T} (denoted by $H_{\mathrm{T,\,lep}}$) in the $2\ell\mathrm{SS}{+}0\tau$ channel, obtained by subtracting the distributions for events with positive total charge and with negative total charge, is shown in figure 6a. In this subtraction, only the charge asymmetric processes remain visible, allowing a better assessment of the modelling of the $t\bar{t}W$ process by the simulation. Disagreement between the data and the prefit prediction from the simulation is observed, corresponding to an overall normalisation factor that is assigned to the $t\bar{t}W$ background, and which is determined during the likelihood fit. The measured normalisation factor is $\hat{\lambda}_{t\bar{t}W} = 1.78 \pm 0.15$, which is compatible with that determined in the SM $t\bar{t}t\bar{t}$ analysis [115], and with a previous measurement of the $t\bar{t}W$ production cross section [116]. Agreement is improved after the application of the background corrections resulting from the likelihood fit, in particular the above $t\bar{t}W$ normalisation factor, as shown in figure 6b for the m_{eff} distribution.

6.1.3 Other irreducible backgrounds

The total yields in the 3ℓVV and 3ℓttZ CRs are used in the likelihood fit to improve the prediction of the background contribution from the VV and $t\bar{t}(Z/\gamma^*)$ processes, respectively. A comparison of the m_{eff} distribution between the data and the total prediction in these two CRs exhibits adequate modelling by the simulation even before the likelihood fit to data, as shown in figure 7. The rate of the background from internal conversions with $m(e^+e^-) < 1\,\mathrm{GeV}$ is estimated using the two dedicated CRs (2ℓIntC and 3ℓIntC). The total yield in each category is used in the likelihood fit to determine the following normalisation factor: $\hat{\lambda}_e^{\mathrm{IntC}} = 1.77 \pm 0.32$, where the uncertainty is dominated by the statistical uncertainty. The normalisation of the internal-conversion background is validated by comparing data and scaled simulation in a dedicated control sample enhanced in $Z \to \mu^+\mu^-\gamma^*(\to e^+e^-)$ candidate events, defined by requiring two OS Tight muons and one electron satisfying the Very Tight requirements, except for the internal conversion veto. The level of agreement found between observed and predicted yields is within 25%, which is assigned as a systematic uncertainty associated with the extrapolation of the estimate from the 2ℓIntC and 3ℓIntC CRs to the other event categories.

6.2 Reducible backgrounds

6.2.1 Fake τ_{had} candidates

In most event categories requiring at least one τ_{had}, the dominant background originates from $t\bar{t}$ production with at least one fake τ_{had} candidate. Consequently, the estimation

JHEP06(2021)179

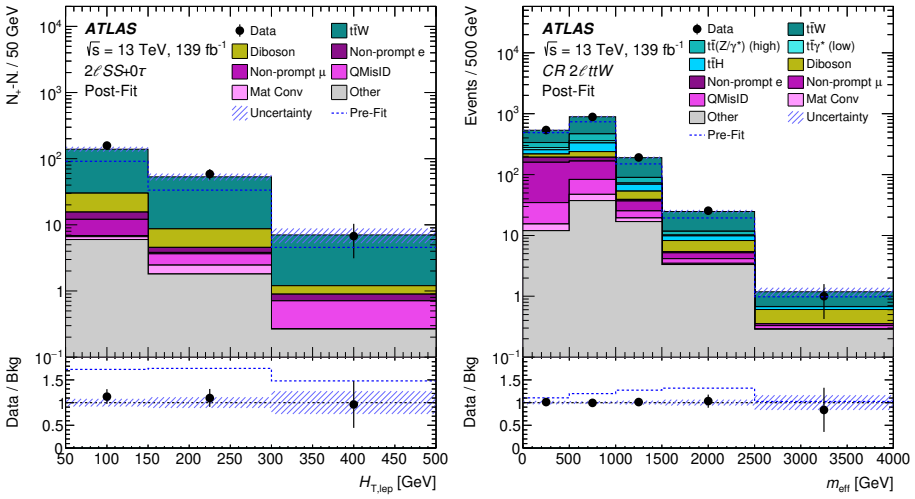

(a) **(b)**

Figure 6. (a) Comparison between data and the background prediction for the distribution of the scalar sum of the lepton p_{T} ($H_{\mathrm{T,\,lep}}$) in the 2ℓSS+0τ channel, obtained by subtracting the corresponding distributions for events with positive and negative total charge. In (b) the comparison is performed for the m_{eff} distribution in the 2ℓttW CR without splitting according to total charge. The background contributions after the likelihood fit to data ("Post-Fit") under the background-only hypothesis are shown as filled histograms. The total background prediction before the likelihood fit to data ("Pre-Fit") is shown as a dashed blue histogram in the upper panel. The ratio of the data to the background ("Bkg") prediction is shown in the lower panel, separately for post-fit background (black points) and pre-fit background (dashed blue line). The size of the combined statistical and systematic uncertainty in the background prediction is indicated by the blue hatched band. The last bin in each figure contains the overflow.

of fake-τ_{had} background relies heavily on the simulation accurately modelling the $t\bar{t}$ event kinematics and the τ_{had} misidentification rate from jets. As discussed in section 6.1.1, a kinematic reweighting is applied to $t\bar{t}$ simulated events in order to improve the description of the event kinematics. In order to evaluate such a correction factor, which depends on the jet multiplicity of the events, fake τ_{had} candidates in $t\bar{t}$ simulated events are considered as additional jets. After the kinematic reweighting is applied, a suitable correction to the fake-τ_{had} rate in the simulation is measured. A CR is defined by requiring an OS $e\mu$ pair, at least two jets, at least one b-tagged jet, at least one Loose or Medium τ_{had} candidate, and $m_{\mathrm{eff}} < 1\,\mathrm{TeV}$ (denoted by $\mathrm{CR}^{t\bar{t}}$ in table 4). The upper bound on m_{eff} ensures that any potential $\mathrm{LQ}_3^{\mathrm{d}}$ signal contamination would be negligible. This CR is enriched in dileptonic $t\bar{t}$ events, such that the selected τ_{had} candidates primarily originate from jets, and are used to determine a normalisation factor to correct for possible mismodelling of the fake-τ_{had} rate in the simulation per τ_{had} candidate. According to the simulation, the flavour composition of the jets giving a fake τ_{had} candidate in this CR is similar to that in the SRs considered. This normalisation factor is measured as a function of $p_{\mathrm{T}}^{\tau_{\mathrm{had}}}$, and for one-prong and three-prong τ_{had} candidates separately. In the case of one-prong

JHEP06(2021)179

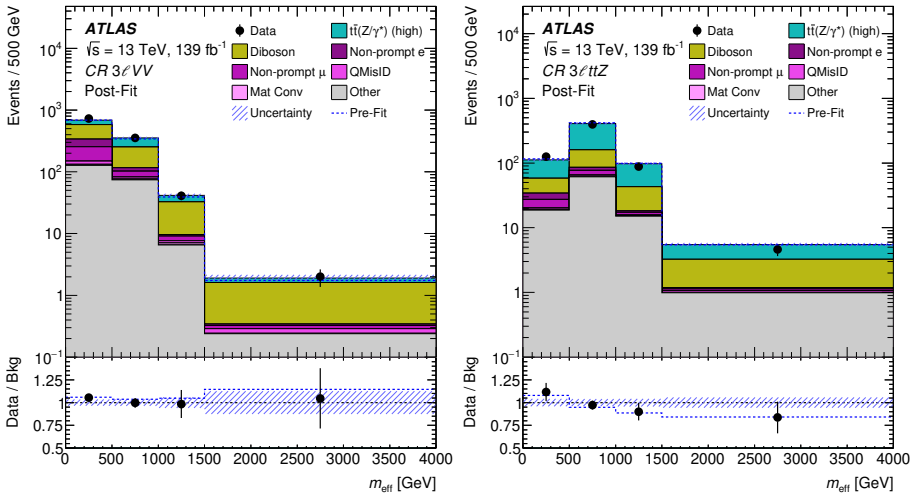

(a) **(b)**

Figure 7. Comparison between data and the background prediction for the m_{eff} distribution in (a) the 3ℓVV CR and (b) the 3ℓttZ CR. The background contributions after the likelihood fit to data ("Post-Fit") under the background-only hypothesis are shown as filled histograms. The total background prediction before the likelihood fit to data ("Pre-Fit") is shown as a dashed blue histogram in the upper panel. The ratio of the data to the background ("Bkg") prediction is shown in the lower panel, separately for post-fit background (black points) and pre-fit background (dashed blue line). The size of the combined statistical and systematic uncertainty in the background prediction is indicated by the blue hatched band. The last bin in each figure contains the overflow.

(three-prong) τ_{had} candidates satisfying the Loose requirement, the normalisation factors range from 1.07 ± 0.06 (1.10 ± 0.31) for $p_{\text{T}}^{\tau_{\text{had}}}$ in the range of 25–45 GeV (25–50 GeV), to 0.57 ± 0.19 (0.80 ± 0.30) for $p_{\text{T}}^{\tau_{\text{had}}} \geq 100$ GeV (75 GeV). The quoted uncertainty includes the statistical uncertainty in the CR, the uncertainty in the contribution from real τ_{had} candidates that is subtracted in the CR, and the difference between this normalisation factor and one measured in a separate CR enhanced in Z+jets events (denoted by CR^{Z} in table 4), which has a different jet-flavour composition of fake τ_{had} candidates than CR$^{t\bar{t}}$. No statistically significant differences are found between the normalisation factors for Loose and Medium τ_{had} candidates; therefore, the above normalisation factors are applied to all channels requiring at least one τ_{had} candidate. All simulated background events with at least one fake τ_{had} candidate[6] are scaled by the product of the corresponding per-candidate normalisation factors calculated according to the multiplicity of fake τ_{had} and non-prompt light leptons (see section 6.2.2) before the likelihood fit to data. After applying the kinematic reweighting and the p_{T}-dependent fake-τ_{had} normalisation factors discussed above, the simulation is found to provide good modelling of relevant kinematic distributions for the fake-τ_{had} background before the likelihood fit to data, as shown in figures 8a and 8b. The uncertainties associated with the normalisation factors are accounted for as nuisance parameters in the likelihood fit (see section 7). To account for the approximation of treating

[6]This includes $t\bar{t}$ as well as other subleading processes such as single top, V+jets, etc.

JHEP06(2021)179

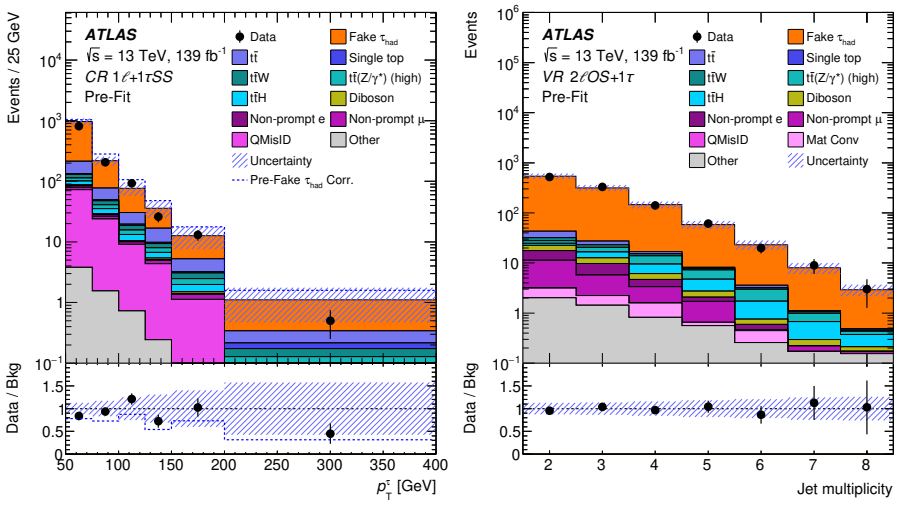

(a) **(b)**

Figure 8. Comparison between data and the background prediction for (a) the τ_{had} p_{T} (p_{T}^{τ}) distribution in the 1ℓ+1τSS CR, and (b) the jet multiplicity distribution in the 2ℓOS+1τ VR. The background contributions before the likelihood fit to data ("Pre-Fit") are shown as filled histograms. The ratio of the data to the background ("Bkg") prediction is shown in the lower panel. In (a), the total background prediction before the correction with the per-candidate normalisation factors ("Pre-Fake τ_{had} Corr.") is shown as a dashed blue histogram (line) in the upper (lower) panel. The size of the combined statistical and systematic uncertainty in the background prediction is indicated by the blue hatched band. The last bin in each figure contains the overflow.

fake τ_{had} candidates as jets in the $t\bar{t}$ kinematic reweighting, in the statistical analysis, the uncertainties associated with the PS and hadronisation model, the ME-to-PS matching, and the modelling of QCD radiation, are treated as uncorrelated between $t\bar{t}$ events with at least one fake τ_{had} candidate and the rest of the $t\bar{t}$ events.

6.2.2 Non-prompt light leptons and charge misassignment

Non-prompt leptons originate from material conversions, heavy-flavour hadron decays, or the improper reconstruction of other particles, with an admixture strongly depending on the lepton quality requirements and varying across event categories. These backgrounds are in general very small in all SRs and thus are estimated from simulation, with the normalisation determined by the likelihood fit. The main contribution to the non-prompt-lepton background is from $t\bar{t}$ production, followed by much smaller contributions from V+jets and single-top-quark processes. The non-prompt light leptons in the simulated samples are labelled according to whether they originate from heavy-flavour (HF) or light-flavour (LF) hadron decays, or from a material conversion candidate. The HF category includes leptons from both bottom and charm decays. QMisID backgrounds arise mainly from $t\bar{t}$ production, with one electron having a hard bremsstrahlung emission followed by an asymmetric conversion ($e^{\pm} \to e^{\pm}\gamma^{*} \to e^{\pm}e^{+}e^{-}$) or a mismeasured track curvature. The muon charge misassignment rate is negligible in the p_{T} range relevant to this analysis.

JHEP06(2021)179

Several of the event categories introduced in section 5 were designed to be enriched in specific processes and are used to derive normalisation factors to improve their modelling by the simulation. The 2ℓMatC and 3ℓMatC CRs are enriched in MatC and QMisID backgrounds and only the total event yield is used. There are four CRs enriched in contributions from HF non-prompt leptons in $t\bar{t}$ events, i.e. 2ℓtt(e)+, 2ℓtt(e)-, 2ℓtt(μ)+, and 2ℓtt(μ)-. In these CRs, the $H_{\mathrm{T,\,lep}}$ distribution is used to provide separation from the $t\bar{t}W$ background and thus optimise the sensitivity to the HF non-prompt electron and muon contributions. The simultaneous fit to these regions, split by total charge, provides additional separation due to the charge asymmetry of the $t\bar{t}W$ process. Normalisation factors for three non-prompt-lepton background contributions are estimated from the likelihood fit. The normalisation factor for HF non-prompt leptons is estimated separately for electrons and muons, λ_e^{had} and $\lambda_\mu^{\mathrm{had}}$ respectively. An additional normalisation factor is determined for the sum of MatC and QMisID backgrounds, $\lambda_e^{\mathrm{MatC}}$. The measured normalisation factors are: $\hat{\lambda}_e^{\mathrm{had}} = 1.06 \pm 0.30$, $\hat{\lambda}_\mu^{\mathrm{had}} = 0.81 \pm 0.12$, and $\hat{\lambda}_e^{\mathrm{MatC}} = 1.03 \pm 0.24$, where the uncertainties are dominated by the statistical uncertainty. The systematic uncertainties considered are discussed in the following, although they have a negligible impact on the final result. The background estimation procedure for non-prompt light leptons relies on the simulation to predict the kinematic distributions of the $t\bar{t}$ process, and thus is affected by related modelling uncertainties (see section 3). Additional uncertainties are estimated by relaxing lepton criteria to enrich the samples in the different types of non-prompt leptons, and comparing the data with the simulation. A 25% uncertainty is estimated for material conversions, based on a comparison between data and simulation in a dedicated control sample enhanced in $Z \to \mu^+\mu^-\gamma(\to e^+e^-)$ candidate events, defined by requiring two OS Tight muons and one Tight electron that fails the material conversion veto requirement. This uncertainty is applied to all categories except for 2ℓMatC and 3ℓMatC as thus acts as an extrapolation uncertainty. Figures 9a and 9b display the $H_{\mathrm{T,\,lep}}$ distribution in the 2ℓtt(e)- and 2ℓtt(μ)- CRs after the likelihood fit to data. As shown in the figures, the spectra for the HF non-prompt electron and muon contributions are softer than those for the $t\bar{t}W$ and VV backgrounds. For this comparison, the CRs with negative total charge are selected, as this requirement suppresses the $t\bar{t}W$ and VV contributions, due to their charge asymmetry, thus increasing the fraction of non-prompt-lepton background.

7 Analysis model and results

A maximum-likelihood fit is performed on all bins in the 22 event categories considered, consisting of 15 CRs and 7 SRs (see table 8), to simultaneously determine the background and $\mathrm{LQ}_3^{\mathrm{d}}$ signal yields that are most consistent with the data. The m_{eff} spectrum is used in the SRs to maximise the sensitivity to the $\mathrm{LQ}_3^{\mathrm{d}}$ signal, while the CRs are used to either determine or constrain different backgrounds. In the eight CRs from the 2ℓSS+0τ and 3ℓ+0τ channels that require very tight selection criteria for light leptons including the internal and material conversion vetoes, the $H_{\mathrm{T,\,lep}}$ spectrum is used to discriminate between, and separately normalise, the $t\bar{t}$ (with non-prompt electrons and muons) and $t\bar{t}W$ backgrounds, as well as to constrain the $t\bar{t}(Z/\gamma^*)$, and VV background predictions. In the remaining seven CRs, the

JHEP06(2021)179

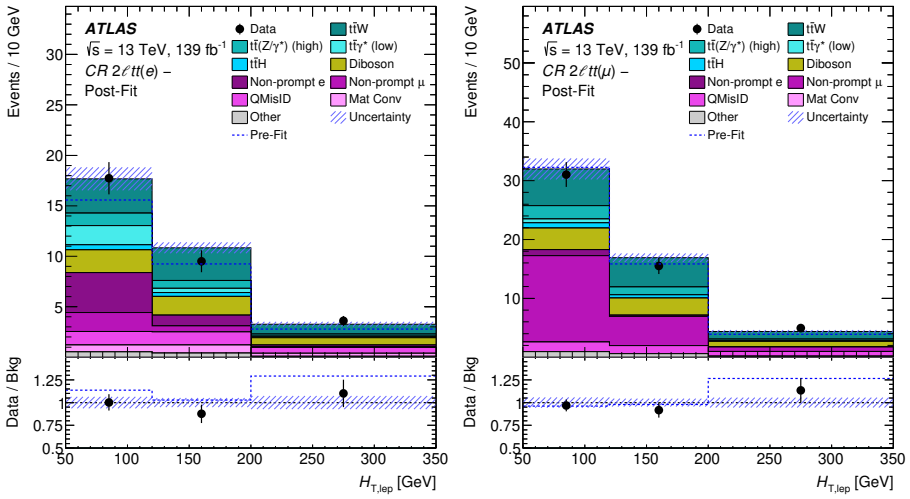

(a) **(b)**

Figure 9. Comparison between data and the background prediction for the distribution of the scalar sum of the lepton p_{T} ($H_{\mathrm{T,\,lep}}$) in (a) the 2ℓtt(e)- CR and (b) the 2ℓtt(μ)- CR. The background contributions after the likelihood fit to data ("Post-Fit") under the background-only hypothesis are shown as filled histograms. The total background prediction before the likelihood fit to data ("Pre-Fit") is shown as a dashed blue histogram in the upper panel. The ratio of the data to the background ("Bkg") prediction is shown in the lower panel, separately for post-fit background (black points) and pre-fit background (dashed blue line). The size of the combined statistical and systematic uncertainty in the background prediction is indicated by the blue hatched band. The last bin in each figure contains the overflow.

	1ℓ+≥1τ	2ℓOS+≥1τ	2ℓSS/3ℓ+≥1τ	2ℓSS+0τ	3ℓ+0τ
Number of event categories	6	2	2	8	4
m_{eff} spectrum	3 SRs	2 SRs	2 SRs	—	—
$H_{\mathrm{T,lep}}$ spectrum	—	—	—	6 CRs	2 CRs
Event yield	3 CRs	—	—	2 CRs	2 CRs
Total number of bins	16	9	6	20	10

Table 8. Summary of the event categories per channel, discriminating variables per event category, and number of bins used in the statistical analysis.

total event yield (i.e. a single bin) is used: three CRs are used to constrain the $t\bar{t}$ background prediction with either real or fake τ_{had} candidates, and four CRs are used to normalise the backgrounds with an internal conversion, and with a material conversion or QMisID.

The likelihood function $\mathcal{L}(\mu, \vec{\lambda}, \vec{\theta})$ is constructed as a product of Poisson probability terms over all bins considered in the search, and depends on the signal-strength parameter, μ, defined as a multiplicative factor applied to the predicted yield for the $\mathrm{LQ}_3^{\mathrm{d}}$ signal (depending on the assumed $\mathrm{LQ}_3^{\mathrm{d}}$ mass and the $\mathrm{LQ}_3^{\mathrm{d}} \to t\tau$ branching fraction), $\vec{\lambda}$, the normalisation factors for several backgrounds (see section 6), and $\vec{\theta}$, a set of nuisance parameters (NP) encoding systematic uncertainties in the signal and background expectations [117]. Systematic

JHEP06(2021)179

Systematic uncertainty	Components
Luminosity	1
Pile-up reweighting	1
Physics objects	
Electron	6
Muon	16
τ-leptons	21
Jet energy scale and resolution	34
Jet vertex fraction	1
Jet flavour tagging	22
$E_{\mathrm{T}}^{\mathrm{miss}}$	3
Total (Experimental)	105
Data-driven reducible background estimates	
$t\bar{t}$ kinematic reweighting	2
Fake-τ_{had} estimates	14
Material conversions modelling	1
Internal conversions modelling	1
Total (Data-driven reducible background)	18

Systematic uncertainty	Components
Signal modelling	
Cross section (N)	1
QCD scale (μ_{f}, μ_{r})	1
PDFs+α_{S}	1
QCD radiation	1
$t\bar{t}$ **modelling**	
Cross section (N)	1
Parton shower and hadronisation model	2
Generator	2
QCD radiation	2
QED radiative top-quark decay (N)	1
$t\bar{t}W$ **modelling**	
QCD scale	1
Generator	1
$t\bar{t}(Z/\gamma^*)$ **(high mass) modelling**	
Cross section (N)	1
Generator	1
$t\bar{t}H$ **modelling**	
Cross section (N)	1
Parton shower and hadronisation model	1
WZ **modelling**	
Cross section (N)	1
Heavy-flavour composition (N)	1
Other background modelling	
Cross section (N)	10
Total (Signal and background modelling)	30
Total (Overall)	153

Table 9. Sources of systematic uncertainty considered in the analysis. "N" means that the uncertainty is taken as normalisation-only for all processes and channels affected. Some of the systematic uncertainties are split into several components, as indicated by the number in the rightmost column.

uncertainties can impact the estimated signal and background rates, the migration of events between categories, and the shape of the fitted distributions; they are summarised in table 9. Both μ and $\vec{\lambda}$ are treated as free parameters in the likelihood fit. The NPs $\vec{\theta}$ allow variations of the expectations for signal and background according to the systematic uncertainties, subject to Gaussian constraints in the likelihood fit. Their fitted values represent the deviations from the nominal expectations that globally provide the best fit to the data. Statistical uncertainties in each bin due to the limited size of the simulated samples are taken into account by dedicated parameters using the Beeston-Barlow technique [118].

The test statistic q_μ is defined as the profile likelihood ratio: $q_\mu = -2\ln\left(\mathcal{L}(\mu, \hat{\vec{\lambda}}_\mu, \hat{\vec{\theta}}_\mu)/\mathcal{L}(\hat{\mu}, \hat{\vec{\lambda}}_{\hat{\mu}}, \hat{\vec{\theta}}_{\hat{\mu}})\right)$, where $\hat{\mu}$, $\hat{\vec{\lambda}}_{\hat{\mu}}$, and $\hat{\vec{\theta}}_{\hat{\mu}}$ are the values of the parameters that maximise the likelihood function, and $\hat{\vec{\lambda}}_\mu$ and $\hat{\vec{\theta}}_\mu$ are the values of the parameters that maximise the likelihood function for a given value of μ. The test statistic q_μ is evaluated with the RooFit package [119]. A related statistic is used to determine the probability that the observed data are compatible with the background-only hypothesis (i.e. the discovery test) by setting $\mu = 0$ in the profile likelihood ratio (q_0). The p-value (referred to as p_0) representing the probability of the data being compatible with the background-only hypothesis is estimated by

JHEP06(2021)179

integrating the distribution of q_0 from background-only pseudo-experiments, approximated using the asymptotic formulae given in ref. [120], above the observed value of q_0. Some model dependence exists in the estimation of the p_0, as a given signal scenario needs to be assumed in the calculation of the denominator of q_0, even if the overall signal normalisation is allowed to float and is fitted to data. The observed p_0 is checked for each explored signal scenario. Upper limits on the signal production cross section for each of the signal scenarios considered are derived by using q_μ in the $\mathrm{CL_s}$ method [121, 122]. For a given signal scenario, values of the production cross section (parameterised by μ) yielding $\mathrm{CL_s} < 0.05$, where $\mathrm{CL_s}$ is computed using the asymptotic approximation [120], are excluded at $\geq 95\%$ confidence level (CL). The upper limits derived with the asymptotic approximation agree very well with those estimated via background-only pseudo-experiments.

A comparison of the distributions of observed and expected yields in the 15 CRs and the 7 SRs after the combined likelihood fit under the background-only hypothesis is shown in figures 10a and 10b, respectively. The corresponding post-fit yields for the SRs can be found in table 10. In general, good agreement between the data and predicted background yields is found across all event categories. As shown in figure 11, good agreement is also obtained between the data and post-fit background prediction in the VRs, which were not used in the fit, giving confidence in the overall procedure.

The comparison between data and the background prediction for the m_{eff} distributions used in the different SRs is shown in figures 12 and 13. The binning used for the m_{eff} distributions in the different SRs represents a compromise between preserving enough discrimination in the fit between the background and the signal for the different values of LQ mass considered, and keeping the statistical uncertainty of the background prediction per bin well below 30%. No significant excess is observed in any of the SRs. The observed p_0 is found to be consistent with the background-only hypothesis for all values of $m_{\mathrm{LQ}_3^{\mathrm{d}}}$ and $\mathcal{B}$ considered. The observed and expected p_0 as a function of $m_{\mathrm{LQ}_3^{\mathrm{d}}}$ are shown in figure 14, assuming values of $\mathcal{B} = 1$ and $\mathcal{B} = 0.5$. This illustrates the significant expected sensitivity of the search, which for $\mathcal{B} = 1$ exceeds 5 standard deviations for $m_{\mathrm{LQ}_3^{\mathrm{d}}} < 1.21\,\mathrm{TeV}$ and 3 standard deviations for $m_{\mathrm{LQ}_3^{\mathrm{d}}} < 1.36\,\mathrm{TeV}$.

In absence of any significant excess above the SM background prediction, 95% CL upper limits are set on the cross section for the $\mathrm{LQ}_3^{\mathrm{d}}$ pair production as a function of the assumed $m_{\mathrm{LQ}_3^{\mathrm{d}}}$ and $\mathcal{B}$. Figure 15a shows the 95% CL upper limits on the $\mathrm{LQ}_3^{\mathrm{d}}$ pair production cross section as a function of $m_{\mathrm{LQ}_3^{\mathrm{d}}}$ resulting from the combination of all analysis channels, assuming $\mathcal{B} = 1$. The sensitivity is dominated by the $1\ell{+}{\geq}1\tau$ channel, although the $2\ell\mathrm{OS}{+}{\geq}1\tau$ and $2\ell\mathrm{SS}/3\ell{+}{\geq}1\tau$ channels bring a significant improvement to the combined limit. The result is completely limited by the statistical uncertainty of the data, with the impact of systematic uncertainties being only to raise the expected cross-section upper limit by 2.3% at $m_{\mathrm{LQ}_3^{\mathrm{d}}} = 1\,\mathrm{TeV}$, and more at lower and higher masses, reaching 4.5% at $m_{\mathrm{LQ}_3^{\mathrm{d}}} = 500\,\mathrm{GeV}$ and $m_{\mathrm{LQ}_3^{\mathrm{d}}} = 1.6\,\mathrm{TeV}$. The leading source of systematic uncertainty arises from τ_{had} identification and energy scale calibration, followed by $t\bar{t}$ modelling. A comparison of the cross-section limits with the theoretical prediction is used to derive 95% CL limits on $\mathcal{B}$ as a function of $m_{\mathrm{LQ}_3^{\mathrm{d}}}$, as shown in figure 15b. Assuming that $\mathcal{B} = 1$, the observed and expected 95% CL lower limits on $m_{\mathrm{LQ}_3^{\mathrm{d}}}$ are 1.43 TeV and 1.41 TeV, respectively. The corresponding limits for $\mathcal{B} = 0.5$ are 1.22 TeV and 1.19 TeV, respectively. The above limits

JHEP06(2021)179

	1ℓ+1τOS	1ℓ+1τSS	1ℓ+$\geq 2\tau$
Data	339	19	6
Total background	340 ± 20	17.1 ± 2.1	5.2 ± 1.2
Fake τ_{had}	10.2 ± 6.5	1.8 ± 1.7	1.9 ± 1.0
$t\bar{t}$	270 ± 21	2.4 ± 1.0	—
Single top	37.4 ± 5.4	0.79 ± 0.56	—
$t\bar{t}W$	6.7 ± 1.0	3.93 ± 0.59	0.66 ± 0.13
$t\bar{t}Z/\gamma^*$ (high mass)	2.38 ± 0.65	1.11 ± 0.30	0.57 ± 0.15
$t\bar{t}\gamma^*$ (low mass)	—	0.03 ± 0.01	—
$t\bar{t}H$	2.38 ± 0.44	0.87 ± 0.21	1.18 ± 0.34
Diboson	5.02 ± 0.66	1.70 ± 0.27	0.31 ± 0.07
QMisID	2.59 ± 0.68	3.38 ± 0.90	0.10 ± 0.08
Other	3.50 ± 0.91	1.14 ± 0.38	0.45 ± 0.13
LQ_3^{d} (0.9 TeV)	80.3 ± 9.2	25.1 ± 2.6	51.9 ± 9.3
LQ_3^{d} (1.1 TeV)	20.9 ± 2.5	6.92 ± 0.74	11.4 ± 2.1
LQ_3^{d} (1.3 TeV)	6.02 ± 0.75	1.93 ± 0.25	2.89 ± 0.57

	2ℓOS+1τ	2ℓOS+$\geq 2\tau$	2ℓSS/3ℓ+$\geq 1\tau$-L	2ℓSS/3ℓ+$\geq 1\tau$-H
Data	13	1	7	3
Total background	14.6 ± 3.3	1.66 ± 0.58	5.38 ± 0.68	0.83 ± 0.14
Fake τ_{had}	8.0 ± 3.4	0.96 ± 0.54	0.33 ± 0.07	0.09 ± 0.04
$t\bar{t}W$	2.68 ± 0.51	—	1.57 ± 0.39	0.13 ± 0.05
$t\bar{t}Z/\gamma^*$ (high mass)	0.86 ± 0.26	0.15 ± 0.06	1.10 ± 0.20	0.20 ± 0.06
$t\bar{t}\gamma^*$ (low mass)	0.02 ± 0.01	—	0.03 ± 0.02	—
$t\bar{t}H$	1.07 ± 0.19	0.51 ± 0.14	1.09 ± 0.27	0.14 ± 0.03
Diboson	0.51 ± 0.08	—	0.53 ± 0.10	0.13 ± 0.03
Non-prompt e	0.14 ± 0.13	—	—	—
Non-prompt μ	0.44 ± 0.28	—	0.06 ± 0.06	—
QMisID	0.19 ± 0.13	—	0.04 ± 0.05	—
Mat Conv	0.18 ± 0.15	—	0.01 ± 0.02	—
Other	0.55 ± 0.22	0.04 ± 0.03	0.61 ± 0.28	0.13 ± 0.06
LQ_3^{d} (0.9 TeV)	26.0 ± 3.9	6.1 ± 1.1	6.02 ± 0.90	13.6 ± 2.1
LQ_3^{d} (1.1 TeV)	6.4 ± 1.0	1.35 ± 0.26	1.09 ± 0.17	3.44 ± 0.57
LQ_3^{d} (1.3 TeV)	1.69 ± 0.31	0.36 ± 0.08	0.20 ± 0.05	1.07 ± 0.19

Table 10. Summary of observed and predicted yields in the seven signal region categories. The background prediction is shown after the combined likelihood fit to data under the background-only hypothesis across all control region and signal region categories. The expected signal yields that are obtained by using their theoretical cross sections are also shown with their pre-fit uncertainties, assuming $\mathcal{B} = 1$. Dashes refer to components that are negligible or not applicable.

JHEP06(2021)179

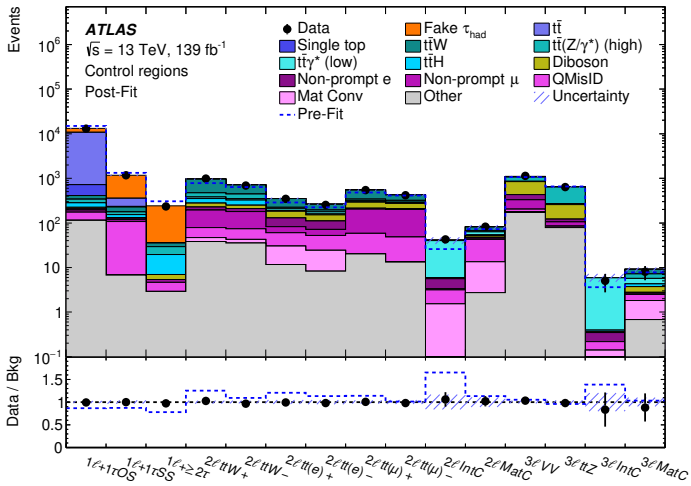

(a)

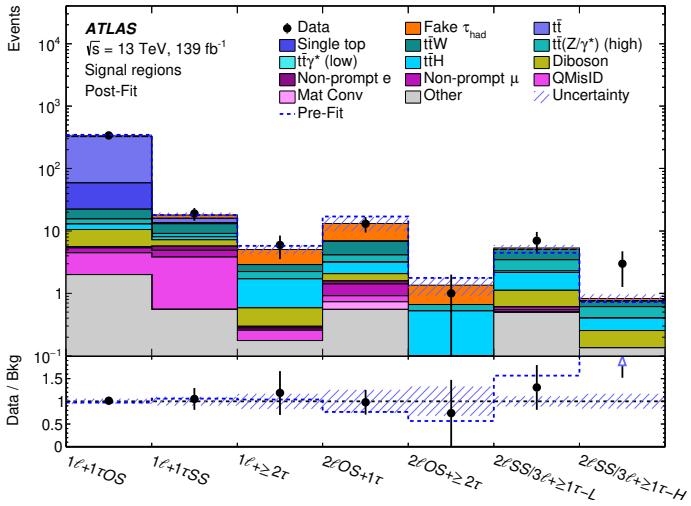

(b)

Figure 10. Comparison between data and the background prediction for the event yields in (a) the 15 control region categories and (b) the 7 signal region categories. The background contributions after the likelihood fit to data ("Post-Fit") under the background-only hypothesis are shown as filled histograms. The total background prediction before the likelihood fit to data ("Pre-Fit") is shown as a dashed blue histogram in the upper panel. The ratio of the data to the background ("Bkg") prediction is shown in the lower panel, separately for post-fit background (black points) and pre-fit background (dashed blue line). The size of the combined statistical and systematic uncertainty in the background prediction is indicated by the blue hatched band. The blue triangles indicate points that are outside the vertical range of the figure.

assume that the only possible decay modes are $\mathrm{LQ} \to t\tau/b\nu$. In the case of a non-negligible contribution from the $\mathrm{LQ} \to q\tau$ ($q = u, c$) decay mode, more stringent limits could be derived for intermediate values of $\mathcal{B}$, since $\mathrm{LQ}\overline{\mathrm{LQ}} \to t\tau q\tau$ final states would be probed by the $1\ell{+}{\geq}2\tau$ SR, which dominates the sensitivity of this search.

JHEP06(2021)179

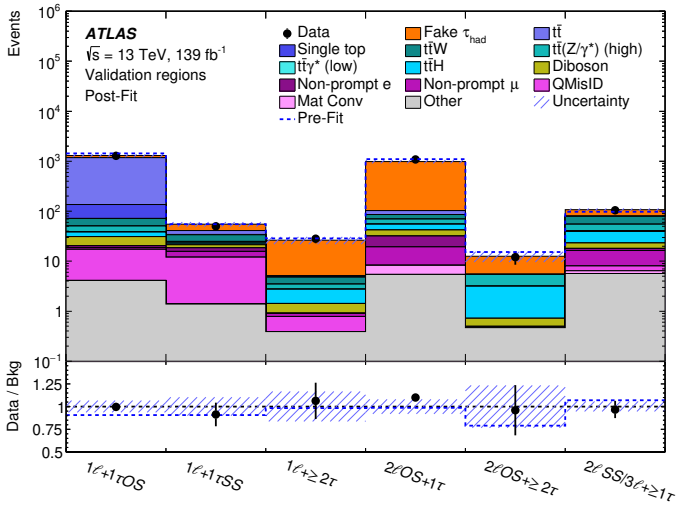

Figure 11. Comparison between data and the background prediction for the event yields in the six validation region categories. The background contributions after the likelihood fit to data ("Post-Fit") under the background-only hypothesis are shown as filled histograms. The ratio of the data to the background ("Bkg") prediction is shown in the lower panel. The total background prediction before the likelihood fit to data ("Pre-Fit") is shown as a dashed blue histogram (line) in the upper (lower) panel. The size of the combined statistical and systematic uncertainty in the background prediction is indicated by the blue hatched band.

JHEP06(2021)179

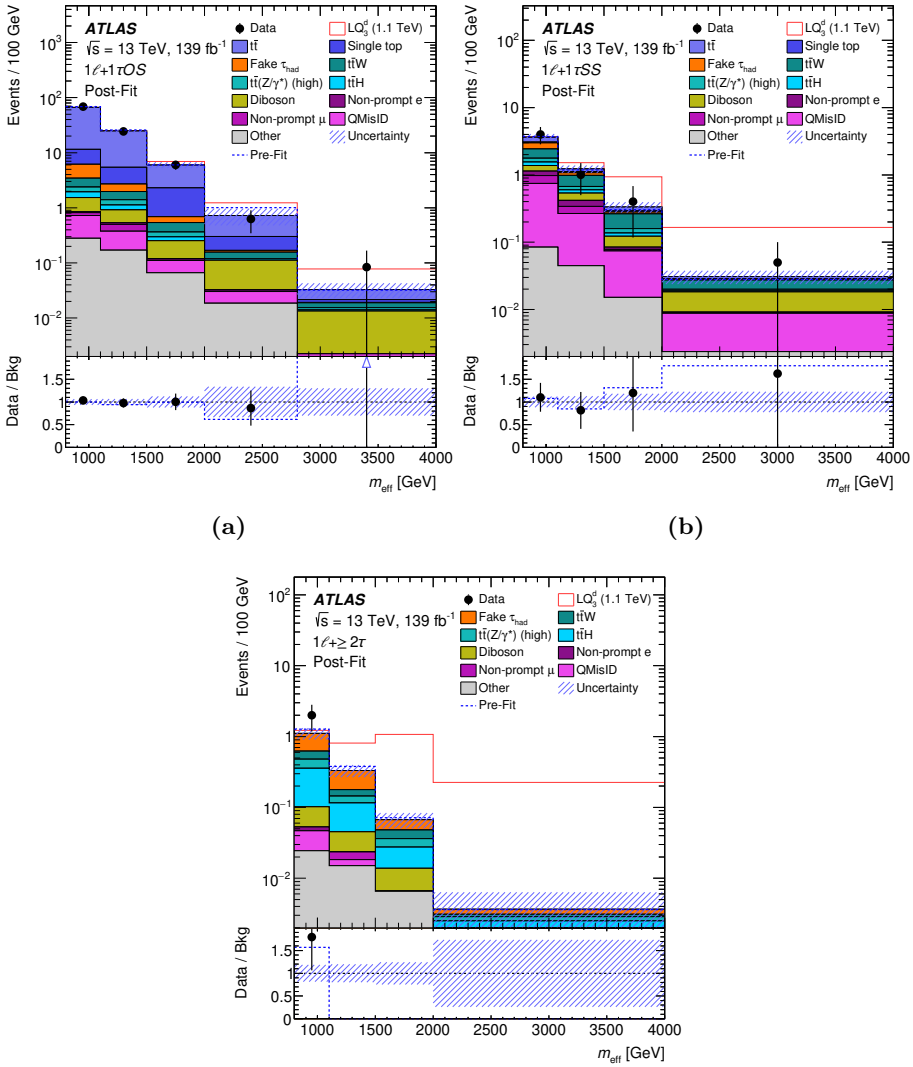

Figure 12. Comparison between data and prediction for the m_{eff} distribution used in different signal region categories of the $1\ell{+}{\geq}1\tau$ channel: (a) $1\ell{+}1\tau$OS, (b) $1\ell{+}1\tau$SS, and (c) $1\ell{+}{\geq}2\tau$. The background contributions after the likelihood fit to data ("Post-Fit") under the background-only hypothesis are shown as filled histograms. For illustrative purposes, the expected signal for $m_{\text{LQ}_3^{\text{d}}} = 1.1\,\text{TeV}$ and $\mathcal{B} = 1$ is shown as a unfilled red histogram added to the post-fit background. The total background prediction before the likelihood fit to data ("Pre-Fit") is shown as a dashed blue histogram in the upper panel. The ratio of the data to the background ("Bkg") prediction is shown in the lower panel, separately for post-fit background (black points) and pre-fit background (dashed blue line). The size of the combined statistical and systematic uncertainty in the background prediction is indicated by the blue hatched band. The blue triangles indicate points that are outside the vertical range of the figure. The last bin in each figure contains the overflow.

JHEP06(2021)179

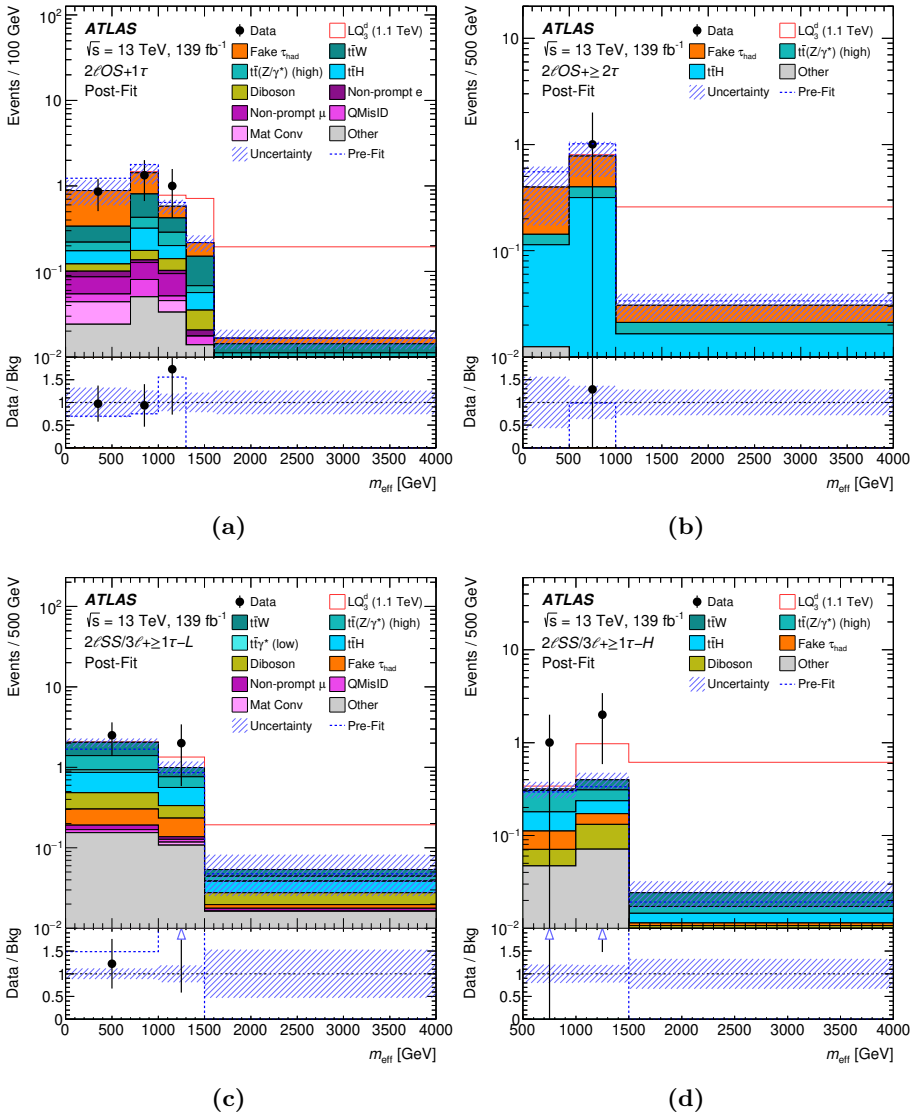

Figure 13. Comparison between data and prediction for the m_{eff} distribution used in different signal region categories of the $2\ell\text{OS}+\geq 1\tau$ and $2\ell\text{SS}/3\ell+\geq 1\tau$ channels: (a) $2\ell\text{OS}+1\tau$, (b) $2\ell\text{OS}+\geq 2\tau$, (c) $2\ell\text{SS}/3\ell+\geq 1\tau$-L, and (d) $2\ell\text{SS}/3\ell+\geq 1\tau$-H. The background contributions after the likelihood fit to data ("Post-Fit") under the background-only hypothesis are shown as filled histograms. For illustrative purposes, the expected signal for $m_{\text{LQ}_3^{\text{d}}} = 1.1\,\text{TeV}$ and $\mathcal{B} = 1$ is shown as unfilled red histogram added to the post-fit background. The total background prediction before the likelihood fit to data ("Pre-Fit") is shown as a dashed blue histogram in the upper panel. The ratio of the data to the background ("Bkg") prediction is shown in the lower panel, separately for post-fit background (black points) and pre-fit background (dashed blue line). The size of the combined statistical and systematic uncertainty in the background prediction is indicated by the blue hatched band. The blue triangles indicate points that are outside the vertical range of the figure. The last bin in each figure contains the overflow.

JHEP06(2021)179

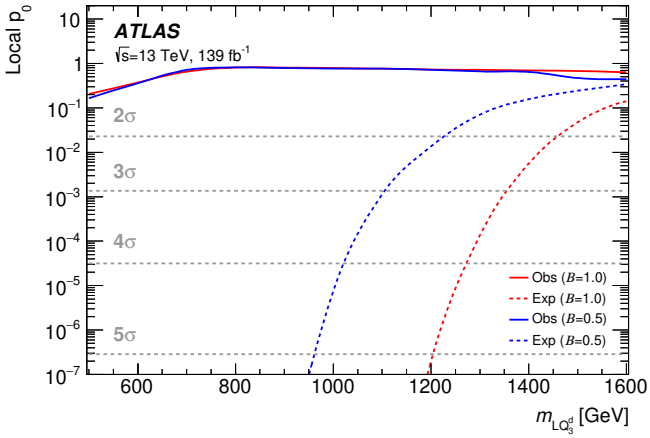

Figure 14. The observed (solid) local p_0 as a function of LQ_3^d mass ($m_{\mathrm{LQ}_3^\mathrm{d}}$) assuming $\mathcal{B} = 0.5$ (blue) and $\mathcal{B} = 1$ (red). The dashed curve shows the expected local p_0 under the hypothesis of a LQ_3^d signal at that mass. The horizontal dashed lines indicate the p-values corresponding to significances of 2 to 5 standard deviations.

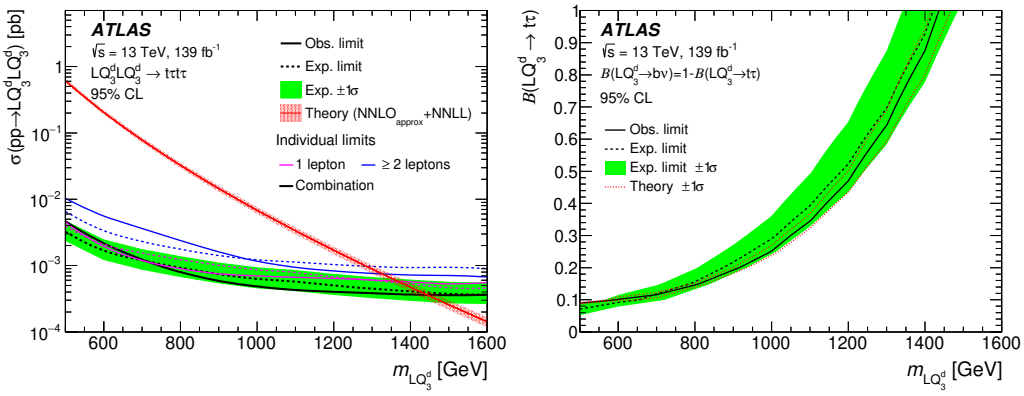

(a) **(b)**

Figure 15. (a) Observed (solid line) and expected (dashed line) 95% CL upper limits on the LQ_3^d pair production cross section as a function of $m_{\mathrm{LQ}_3^\mathrm{d}}$ resulting from the combination of all analysis channels, assuming $\mathcal{B} = 1$. The surrounding shaded band corresponds to the ± 1 standard deviation ($\pm 1\,\sigma$) uncertainty around the combined expected limit, as estimated using the asymptotic approximation (see text). This approximation is found to overestimate the $+1\,\sigma$ ($-1\,\sigma$) uncertainty of the combined expected limit by about 5%–15% (15%–30%), depending on $m_{\mathrm{LQ}_3^\mathrm{d}}$. The red line and band show the theoretical prediction and its $\pm 1\,\sigma$ uncertainty. The individual expected limits for the $1\ell{+}{\geq}1\tau$ channel and the combination of the $2\ell\mathrm{OS}{+}{\geq}1\tau$ and $2\ell\mathrm{SS}/3\ell{+}{\geq}1\tau$ channels are shown as the magenta and blue dashed lines, respectively. (b) Observed (solid line) and expected (dashed line) 95% CL upper limits on $\mathcal{B}$ as a function of $m_{\mathrm{LQ}_3^\mathrm{d}}$ resulting from the combination of all analysis channels. The surrounding shaded band corresponds to the $\pm 1\,\sigma$ uncertainty around the combined expected limit. The same statement regarding the asymptotic approximation given for (a) applies. The dotted red line around the observed limit indicates how the observed limit changes when varying the theoretical prediction for the LQ_3^d pair production cross section by its $\pm 1\,\sigma$ uncertainty.

JHEP06(2021)179

8 Conclusion

A search for pair production of third-generation scalar leptoquarks with a significant branching fraction into a top quark and a τ-lepton has been presented. The search is based on the full Run 2 dataset recorded with the ATLAS detector at Large Hadron Collider, which corresponds to 139 fb^{-1} of pp collisions at $\sqrt{s} = 13$ TeV. Events are selected if they have one light lepton (electron or muon) and at least one hadronically decaying τ-lepton, or at least two light leptons, and additional jets. Six final states, defined by the multiplicity and flavour of lepton candidates, are considered in the analysis. Each of them is split into multiple event categories used to search for the signal and improve the modelling of several leading backgrounds. The signal-rich event categories require at least one hadronically decaying τ-lepton candidate and employ the total effective mass distribution to discriminate between the signal and the background. The search reaches an expected significance of 5 standard deviations for a scalar leptoquark decaying exclusively into $t\tau$ and with mass below about 1.2 TeV, which represents a significant improvement compared to previous searches. This results from a combination of the higher integrated luminosity used, a significantly improved identification of hadronically decaying τ-leptons, and the sophisticated event selection and categorisation employed, which ensures a high signal acceptance and low background yields. No significant excess above the Standard Model expectation is observed in any of the considered event categories, and 95% CL upper limits are set on the production cross section as a function of the leptoquark mass, for different assumptions about the branching fractions into $t\tau$ and $b\nu$. Scalar leptoquarks decaying exclusively into $t\tau$ are excluded up to masses of 1.43 TeV while, for a branching fraction of 50% into $t\tau$, the lower mass limit is 1.22 TeV. The corresponding expected mass exclusions are 1.41 TeV and 1.19 TeV, respectively.

Acknowledgments

We thank CERN for the very successful operation of the LHC, as well as the support staff from our institutions without whom ATLAS could not be operated efficiently.

We acknowledge the support of ANPCyT, Argentina; YerPhI, Armenia; ARC, Australia; BMWFW and FWF, Austria; ANAS, Azerbaijan; SSTC, Belarus; CNPq and FAPESP, Brazil; NSERC, NRC and CFI, Canada; CERN; ANID, Chile; CAS, MOST and NSFC, China; COLCIENCIAS, Colombia; MSMT CR, MPO CR and VSC CR, Czech Republic; DNRF and DNSRC, Denmark; IN2P3-CNRS and CEA-DRF/IRFU, France; SRNSFG, Georgia; BMBF, HGF and MPG, Germany; GSRT, Greece; RGC and Hong Kong SAR, China; ISF and Benoziyo Center, Israel; INFN, Italy; MEXT and JSPS, Japan; CNRST, Morocco; NWO, Netherlands; RCN, Norway; MNiSW and NCN, Poland; FCT, Portugal; MNE/IFA, Romania; JINR; MES of Russia and NRC KI, Russian Federation; MESTD, Serbia; MSSR, Slovakia; ARRS and MIZŠ, Slovenia; DST/NRF, South Africa; MICINN, Spain; SRC and Wallenberg Foundation, Sweden; SERI, SNSF and Cantons of Bern and Geneva, Switzerland; MOST, Taiwan; TAEK, Turkey; STFC, United Kingdom; DOE and NSF, United States of America. In addition, individual groups and members have received

JHEP06(2021)179

support from BCKDF, CANARIE, Compute Canada, CRC and IVADO, Canada; Beijing Municipal Science & Technology Commission, China; COST, ERC, ERDF, Horizon 2020 and Marie Skłodowska-Curie Actions, European Union; Investissements d'Avenir Labex, Investissements d'Avenir Idex and ANR, France; DFG and AvH Foundation, Germany; Herakleitos, Thales and Aristeia programmes co-financed by EU-ESF and the Greek NSRF, Greece; BSF-NSF and GIF, Israel; La Caixa Banking Foundation, CERCA Programme Generalitat de Catalunya and PROMETEO and GenT Programmes Generalitat Valenciana, Spain; Göran Gustafssons Stiftelse, Sweden; The Royal Society and Leverhulme Trust, United Kingdom.

The crucial computing support from all WLCG partners is acknowledged gratefully, in particular from CERN, the ATLAS Tier-1 facilities at TRIUMF (Canada), NDGF (Denmark, Norway, Sweden), CC-IN2P3 (France), KIT/GridKA (Germany), INFN-CNAF (Italy), NL-T1 (Netherlands), PIC (Spain), ASGC (Taiwan), RAL (U.K.) and BNL (U.S.A.), the Tier-2 facilities worldwide and large non-WLCG resource providers. Major contributors of computing resources are listed in ref. [123].

Open Access. This article is distributed under the terms of the Creative Commons Attribution License (CC-BY 4.0), which permits any use, distribution and reproduction in any medium, provided the original author(s) and source are credited.

References

[1] J.C. Pati and A. Salam, *Lepton Number as the Fourth Color*, *Phys. Rev. D* **10** (1974) 275 [*Erratum ibid.* **11** (1975) 703] [INSPIRE].

[2] H. Georgi and S.L. Glashow, *Unity of All Elementary Particle Forces*, *Phys. Rev. Lett.* **32** (1974) 438 [INSPIRE].

[3] S. Dimopoulos and L. Susskind, *Mass Without Scalars*, *Nucl. Phys. B* **155** (1979) 237 [INSPIRE].

[4] S. Dimopoulos, *Technicolored Signatures*, *Nucl. Phys. B* **168** (1980) 69 [INSPIRE].

[5] E. Eichten and K.D. Lane, *Dynamical Breaking of Weak Interaction Symmetries*, *Phys. Lett. B* **90** (1980) 125 [INSPIRE].

[6] V.D. Angelopoulos, J.R. Ellis, H. Kowalski, D.V. Nanopoulos, N.D. Tracas and F. Zwirner, *Search for New Quarks Suggested by the Superstring*, *Nucl. Phys. B* **292** (1987) 59 [INSPIRE].

[7] W. Buchmüller and D. Wyler, *Constraints on* SU(5) *Type Leptoquarks*, *Phys. Lett. B* **177** (1986) 377 [INSPIRE].

[8] G. Hiller and M. Schmaltz, R_K *and future* $b \to s\ell\ell$ *physics beyond the standard model opportunities*, *Phys. Rev. D* **90** (2014) 054014 [arXiv:1408.1627] [INSPIRE].

[9] B. Gripaios, M. Nardecchia and S.A. Renner, *Composite leptoquarks and anomalies in B-meson decays*, *JHEP* **05** (2015) 006 [arXiv:1412.1791] [INSPIRE].

[10] M. Freytsis, Z. Ligeti and J.T. Ruderman, *Flavor models for* $\bar{B} \to D^{(*)}\tau\bar{\nu}$, *Phys. Rev. D* **92** (2015) 054018 [arXiv:1506.08896] [INSPIRE].

[11] M. Bauer and M. Neubert, *Minimal Leptoquark Explanation for the* $R_{D^{(*)}}$, R_K, *and* $(g-2)_\mu$ *Anomalies*, *Phys. Rev. Lett.* **116** (2016) 141802 [arXiv:1511.01900] [INSPIRE].

JHEP06(2021)179

[12] L. Di Luzio and M. Nardecchia, *What is the scale of new physics behind the B-flavour anomalies?*, *Eur. Phys. J. C* **77** (2017) 536 [arXiv:1706.01868] [INSPIRE].

[13] D. Buttazzo, A. Greljo, G. Isidori and D. Marzocca, *B-physics anomalies: a guide to combined explanations*, *JHEP* **11** (2017) 044 [arXiv:1706.07808] [INSPIRE].

[14] J.M. Cline, *B decay anomalies and dark matter from vectorlike confinement*, *Phys. Rev. D* **97** (2018) 015013 [arXiv:1710.02140] [INSPIRE].

[15] W. Buchmüller, R. Ruckl and D. Wyler, *Leptoquarks in lepton-quark collisions*, *Phys. Lett. B* **191** (1987) 442 [*Erratum ibid.* **448** (1999) 320] [INSPIRE].

[16] ATLAS collaboration, *Searches for third-generation scalar leptoquarks in* $\sqrt{s} = 13$ *TeV pp collisions with the ATLAS detector*, *JHEP* **06** (2019) 144 [arXiv:1902.08103] [INSPIRE].

[17] ATLAS collaboration, *Search for pairs of scalar leptoquarks decaying into quarks and electrons or muons in* $\sqrt{s} = 13$ *TeV pp collisions with the ATLAS detector*, *JHEP* **10** (2020) 112 [arXiv:2006.05872] [INSPIRE].

[18] ATLAS collaboration, *Search for pair production of scalar leptoquarks decaying into first- or second-generation leptons and top quarks in proton-proton collisions at* $\sqrt{s} = 13$ *TeV with the ATLAS detector*, *Eur. Phys. J. C* **81** (2021) 313 [arXiv:2010.02098] [INSPIRE].

[19] CMS collaboration, *Constraints on models of scalar and vector leptoquarks decaying to a quark and a neutrino at* $\sqrt{s} = 13$ *TeV*, *Phys. Rev. D* **98** (2018) 032005 [arXiv:1805.10228] [INSPIRE].

[20] CMS collaboration, *Search for third-generation scalar leptoquarks decaying to a top quark and a* τ *lepton at* $\sqrt{s} = 13$ *TeV*, *Eur. Phys. J. C* **78** (2018) 707 [arXiv:1803.02864] [INSPIRE].

[21] CMS collaboration, *Search for leptoquarks coupled to third-generation quarks in proton-proton collisions at* $\sqrt{s} = 13$ *TeV*, *Phys. Rev. Lett.* **121** (2018) 241802 [arXiv:1809.05558] [INSPIRE].

[22] CMS collaboration, *Search for heavy neutrinos and third-generation leptoquarks in hadronic states of two* τ *leptons and two jets in proton-proton collisions at* $\sqrt{s} = 13$ *TeV*, *JHEP* **03** (2019) 170 [arXiv:1811.00806] [INSPIRE].

[23] CMS collaboration, *Search for a singly produced third-generation scalar leptoquark decaying to a* τ *lepton and a bottom quark in proton-proton collisions at* $\sqrt{s} = 13$ *TeV*, *JHEP* **07** (2018) 115 [arXiv:1806.03472] [INSPIRE].

[24] ATLAS collaboration, *The ATLAS Experiment at the CERN Large Hadron Collider*, 2008 *JINST* **3** S08003 [INSPIRE].

[25] ATLAS collaboration, *ATLAS Insertable B-Layer Technical Design Report*, ATLAS-TDR-19, CERN-LHCC-2010-013 (2010).

[26] ATLAS IBL collaboration, *Production and Integration of the ATLAS Insertable B-Layer*, 2018 *JINST* **13** T05008 [arXiv:1803.00844] [INSPIRE].

[27] ATLAS collaboration, *Performance of the ATLAS Trigger System in 2015*, *Eur. Phys. J. C* **77** (2017) 317 [arXiv:1611.09661] [INSPIRE].

[28] ATLAS collaboration, *Luminosity determination in pp collisions at* $\sqrt{s} = 13$ *TeV using the ATLAS detector at the LHC*, ATLAS-CONF-2019-021 (2019).

[29] G. Avoni et al., *The new LUCID-2 detector for luminosity measurement and monitoring in ATLAS*, 2018 *JINST* **13** P07017 [INSPIRE].

JHEP06(2021)179

[30] T. Gleisberg et al., *Event generation with SHERPA 1.1*, *JHEP* **02** (2009) 007 [arXiv:0811.4622] [INSPIRE].

[31] D.J. Lange, *The EvtGen particle decay simulation package*, *Nucl. Instrum. Meth. A* **462** (2001) 152 [INSPIRE].

[32] T. Sjöstrand, S. Mrenna and P.Z. Skands, *A Brief Introduction to PYTHIA 8.1*, *Comput. Phys. Commun.* **178** (2008) 852 [arXiv:0710.3820] [INSPIRE].

[33] ATLAS collaboration, *Further ATLAS tunes of PYTHIA6 and PYTHIA 8*, ATL-PHYS-PUB-2011-014 (2011).

[34] ATLAS collaboration, *The ATLAS Simulation Infrastructure*, *Eur. Phys. J. C* **70** (2010) 823 [arXiv:1005.4568] [INSPIRE].

[35] GEANT4 collaboration, *GEANT4: a simulation toolkit*, *Nucl. Instrum. Meth. A* **506** (2003) 250 [INSPIRE].

[36] J. Alwall et al., *The automated computation of tree-level and next-to-leading order differential cross sections, and their matching to parton shower simulations*, *JHEP* **07** (2014) 079 [arXiv:1405.0301] [INSPIRE].

[37] T. Mandal, S. Mitra and S. Seth, *Pair Production of Scalar Leptoquarks at the LHC to NLO Parton Shower Accuracy*, *Phys. Rev. D* **93** (2016) 035018 [arXiv:1506.07369] [INSPIRE].

[38] M. Krämer, T. Plehn, M. Spira and P.M. Zerwas, *Pair production of scalar leptoquarks at the CERN LHC*, *Phys. Rev. D* **71** (2005) 057503 [hep-ph/0411038] [INSPIRE].

[39] M. Krämer, T. Plehn, M. Spira and P.M. Zerwas, *Pair production of scalar leptoquarks at the Tevatron*, *Phys. Rev. Lett.* **79** (1997) 341 [hep-ph/9704322] [INSPIRE].

[40] NNPDF collaboration, *Parton distributions for the LHC Run II*, *JHEP* **04** (2015) 040 [arXiv:1410.8849] [INSPIRE].

[41] ATLAS collaboration, *ATLAS Pythia 8 tunes to 7 TeV data*, ATL-PHYS-PUB-2014-021 (2014).

[42] P. Artoisenet, R. Frederix, O. Mattelaer and R. Rietkerk, *Automatic spin-entangled decays of heavy resonances in Monte Carlo simulations*, *JHEP* **03** (2013) 015 [arXiv:1212.3460] [INSPIRE].

[43] A. Belyaev, C. Leroy, R. Mehdiyev and A. Pukhov, *Leptoquark single and pair production at LHC with CalcHEP/CompHEP in the complete model*, *JHEP* **09** (2005) 005 [hep-ph/0502067] [INSPIRE].

[44] W. Beenakker, C. Borschensky, M. Krämer, A. Kulesza and E. Laenen, *NNLL-fast: predictions for coloured supersymmetric particle production at the LHC with threshold and Coulomb resummation*, *JHEP* **12** (2016) 133 [arXiv:1607.07741] [INSPIRE].

[45] W. Beenakker, M. Krämer, T. Plehn, M. Spira and P.M. Zerwas, *Stop production at hadron colliders*, *Nucl. Phys. B* **515** (1998) 3 [hep-ph/9710451] [INSPIRE].

[46] W. Beenakker, S. Brensing, M. Krämer, A. Kulesza, E. Laenen and I. Niessen, *Supersymmetric top and bottom squark production at hadron colliders*, *JHEP* **08** (2010) 098 [arXiv:1006.4771] [INSPIRE].

[47] W. Beenakker, C. Borschensky, R. Heger, M. Krämer, A. Kulesza and E. Laenen, *NNLL resummation for stop pair-production at the LHC*, *JHEP* **05** (2016) 153 [arXiv:1601.02954] [INSPIRE].

JHEP06(2021)179

[48] C. Borschensky, B. Fuks, A. Kulesza and D. Schwartländer, *Scalar leptoquark pair production at hadron colliders*, *Phys. Rev. D* **101** (2020) 115017 [arXiv:2002.08971] [INSPIRE].

[49] J. Butterworth et al., *PDF4LHC recommendations for LHC Run II*, *J. Phys. G* **43** (2016) 023001 [arXiv:1510.03865] [INSPIRE].

[50] ATLAS collaboration, *Simulation of top quark production for the ATLAS experiment at* $\sqrt{s} = 13$ *TeV*, ATL-PHYS-PUB-2016-004 (2016).

[51] S. Frixione, P. Nason and G. Ridolfi, *A Positive-weight next-to-leading-order Monte Carlo for heavy flavour hadroproduction*, *JHEP* **09** (2007) 126 [arXiv:0707.3088] [INSPIRE].

[52] P. Nason, *A New method for combining NLO QCD with shower Monte Carlo algorithms*, *JHEP* **11** (2004) 040 [hep-ph/0409146] [INSPIRE].

[53] S. Frixione, P. Nason and C. Oleari, *Matching NLO QCD computations with Parton Shower simulations: the POWHEG method*, *JHEP* **11** (2007) 070 [arXiv:0709.2092] [INSPIRE].

[54] S. Alioli, P. Nason, C. Oleari and E. Re, *A general framework for implementing NLO calculations in shower Monte Carlo programs: the POWHEG BOX*, *JHEP* **06** (2010) 043 [arXiv:1002.2581] [INSPIRE].

[55] S. Alioli, P. Nason, C. Oleari and E. Re, *NLO single-top production matched with shower in POWHEG: s- and t-channel contributions*, *JHEP* **09** (2009) 111 [*Erratum ibid.* **02** (2010) 011] [arXiv:0907.4076] [INSPIRE].

[56] E. Re, *Single-top Wt-channel production matched with parton showers using the POWHEG method*, *Eur. Phys. J. C* **71** (2011) 1547 [arXiv:1009.2450] [INSPIRE].

[57] S. Frixione, E. Laenen, P. Motylinski and B.R. Webber, *Single-top production in MC@NLO*, *JHEP* **03** (2006) 092 [hep-ph/0512250] [INSPIRE].

[58] R.D. Ball et al., *Parton distributions with LHC data*, *Nucl. Phys. B* **867** (2013) 244 [arXiv:1207.1303] [INSPIRE].

[59] ATLAS collaboration, *Studies on top-quark Monte Carlo modelling for Top2016*, ATL-PHYS-PUB-2016-020 (2016).

[60] M. Czakon and A. Mitov, *Top++: A Program for the Calculation of the Top-Pair Cross-Section at Hadron Colliders*, *Comput. Phys. Commun.* **185** (2014) 2930 [arXiv:1112.5675] [INSPIRE].

[61] N. Kidonakis, *Next-to-next-to-leading-order collinear and soft gluon corrections for t-channel single top quark production*, *Phys. Rev. D* **83** (2011) 091503 [arXiv:1103.2792] [INSPIRE].

[62] N. Kidonakis, *Two-loop soft anomalous dimensions for single top quark associated production with a* W^- *or* H^-, *Phys. Rev. D* **82** (2010) 054018 [arXiv:1005.4451] [INSPIRE].

[63] N. Kidonakis, *NNLL resummation for s-channel single top quark production*, *Phys. Rev. D* **81** (2010) 054028 [arXiv:1001.5034] [INSPIRE].

[64] H.B. Hartanto, B. Jager, L. Reina and D. Wackeroth, *Higgs boson production in association with top quarks in the POWHEG BOX*, *Phys. Rev. D* **91** (2015) 094003 [arXiv:1501.04498] [INSPIRE].

[65] T. Gleisberg and S. Hoeche, *Comix, a new matrix element generator*, *JHEP* **12** (2008) 039 [arXiv:0808.3674] [INSPIRE].

[66] F. Cascioli, P. Maierhofer and S. Pozzorini, *Scattering Amplitudes with Open Loops*, *Phys. Rev. Lett.* **108** (2012) 111601 [arXiv:1111.5206] [INSPIRE].

JHEP06(2021)179

[67] S. Schumann and F. Krauss, *A Parton shower algorithm based on Catani-Seymour dipole factorisation*, *JHEP* **03** (2008) 038 [arXiv:0709.1027] [INSPIRE].

[68] S. Hoeche, F. Krauss, M. Schonherr and F. Siegert, *QCD matrix elements + parton showers: The NLO case*, *JHEP* **04** (2013) 027 [arXiv:1207.5030] [INSPIRE].

[69] LHC Higgs Cross Section Working Group collaboration, *Handbook of LHC Higgs Cross Sections: 4. Deciphering the Nature of the Higgs Sector*, arXiv:1610.07922 [INSPIRE].

[70] A. Djouadi, J. Kalinowski and M. Spira, *HDECAY: A Program for Higgs boson decays in the standard model and its supersymmetric extension*, *Comput. Phys. Commun.* **108** (1998) 56 [hep-ph/9704448] [INSPIRE].

[71] W. Beenakker, S. Dittmaier, M. Krämer, B. Plumper, M. Spira and P.M. Zerwas, *Higgs radiation off top quarks at the Tevatron and the LHC*, *Phys. Rev. Lett.* **87** (2001) 201805 [hep-ph/0107081] [INSPIRE].

[72] W. Beenakker, S. Dittmaier, M. Krämer, B. Plumper, M. Spira and P.M. Zerwas, *NLO QCD corrections to $t\bar{t}H$ production in hadron collisions*, *Nucl. Phys. B* **653** (2003) 151 [hep-ph/0211352] [INSPIRE].

[73] S. Dawson, L.H. Orr, L. Reina and D. Wackeroth, *Associated top quark Higgs boson production at the LHC*, *Phys. Rev. D* **67** (2003) 071503 [hep-ph/0211438] [INSPIRE].

[74] S. Dawson, C. Jackson, L.H. Orr, L. Reina and D. Wackeroth, *Associated Higgs production with top quarks at the large hadron collider: NLO QCD corrections*, *Phys. Rev. D* **68** (2003) 034022 [hep-ph/0305087] [INSPIRE].

[75] Y. Zhang, W.-G. Ma, R.-Y. Zhang, C. Chen and L. Guo, *QCD NLO and EW NLO corrections to $t\bar{t}H$ production with top quark decays at hadron collider*, *Phys. Lett. B* **738** (2014) 1 [arXiv:1407.1110] [INSPIRE].

[76] S. Frixione, V. Hirschi, D. Pagani, H.S. Shao and M. Zaro, *Weak corrections to Higgs hadroproduction in association with a top-quark pair*, *JHEP* **09** (2014) 065 [arXiv:1407.0823] [INSPIRE].

[77] S. Frixione, V. Hirschi, D. Pagani, H.S. Shao and M. Zaro, *Electroweak and QCD corrections to top-pair hadroproduction in association with heavy bosons*, *JHEP* **06** (2015) 184 [arXiv:1504.03446] [INSPIRE].

[78] T. Sjöstrand et al., *High-energy physics event generation with PYTHIA 6.1*, *Comput. Phys. Commun.* **135** (2001) 238 [hep-ph/0010017] [INSPIRE].

[79] M. Bahr et al., *HERWIG++ Physics and Manual*, *Eur. Phys. J. C* **58** (2008) 639 [arXiv:0803.0883] [INSPIRE].

[80] J. Bellm et al., *HERWIG 7.0/HERWIG++ 3.0 release note*, *Eur. Phys. J. C* **76** (2016) 196 [arXiv:1512.01178] [INSPIRE].

[81] P. Golonka and Z. Was, *PHOTOS Monte Carlo: A Precision tool for QED corrections in Z and W decays*, *Eur. Phys. J. C* **45** (2006) 97 [hep-ph/0506026] [INSPIRE].

[82] L.A. Harland-Lang, A.D. Martin, P. Motylinski and R.S. Thorne, *Parton distributions in the LHC era: MMHT 2014 PDFs*, *Eur. Phys. J. C* **75** (2015) 204 [arXiv:1412.3989] [INSPIRE].

[83] P.Z. Skands, *Tuning Monte Carlo Generators: The Perugia Tunes*, *Phys. Rev. D* **82** (2010) 074018 [arXiv:1005.3457] [INSPIRE].

JHEP06(2021)179

[84] ATLAS collaboration, *Multi-Boson Simulation for 13 TeV ATLAS Analyses*, ATL-PHYS-PUB-2016-002 (2016).

[85] M. Cacciari, M. Czakon, M. Mangano, A. Mitov and P. Nason, *Top-pair production at hadron colliders with next-to-next-to-leading logarithmic soft-gluon resummation*, *Phys. Lett. B* **710** (2012) 612 [arXiv:1111.5869] [INSPIRE].

[86] P. Bärnreuther, M. Czakon and A. Mitov, *Percent Level Precision Physics at the Tevatron: First Genuine NNLO QCD Corrections to $q\bar{q} \to t\bar{t} + X$*, *Phys. Rev. Lett.* **109** (2012) 132001 [arXiv:1204.5201] [INSPIRE].

[87] M. Czakon and A. Mitov, *NNLO corrections to top-pair production at hadron colliders: the all-fermionic scattering channels*, *JHEP* **12** (2012) 054 [arXiv:1207.0236] [INSPIRE].

[88] M. Czakon and A. Mitov, *NNLO corrections to top pair production at hadron colliders: the quark-gluon reaction*, *JHEP* **01** (2013) 080 [arXiv:1210.6832] [INSPIRE].

[89] M. Czakon, P. Fiedler and A. Mitov, *Total Top-Quark Pair-Production Cross Section at Hadron Colliders Through $O(\alpha_S^4)$*, *Phys. Rev. Lett.* **110** (2013) 252004 [arXiv:1303.6254] [INSPIRE].

[90] ATLAS collaboration, *Vertex Reconstruction Performance of the ATLAS Detector at $\sqrt{s} = 13$ TeV*, ATL-PHYS-PUB-2015-026 (2015).

[91] ATLAS collaboration, *Electron reconstruction and identification in the ATLAS experiment using the 2015 and 2016 LHC proton-proton collision data at $\sqrt{s} = 13$ TeV*, *Eur. Phys. J. C* **79** (2019) 639 [arXiv:1902.04655] [INSPIRE].

[92] ATLAS collaboration, *Electron and photon performance measurements with the ATLAS detector using the 2015–2017 LHC proton-proton collision data*, 2019 *JINST* **14** P12006 [arXiv:1908.00005] [INSPIRE].

[93] ATLAS collaboration, *Measurement of the photon identification efficiencies with the ATLAS detector using LHC Run 2 data collected in 2015 and 2016*, *Eur. Phys. J. C* **79** (2019) 205 [arXiv:1810.05087] [INSPIRE].

[94] ATLAS collaboration, *Muon reconstruction performance of the ATLAS detector in proton-proton collision data at $\sqrt{s} = 13$ TeV*, *Eur. Phys. J. C* **76** (2016) 292 [arXiv:1603.05598] [INSPIRE].

[95] ATLAS collaboration, *Evidence for the associated production of the Higgs boson and a top quark pair with the ATLAS detector*, *Phys. Rev. D* **97** (2018) 072003 [arXiv:1712.08891] [INSPIRE].

[96] ATLAS collaboration, *Identification and energy calibration of hadronically decaying tau leptons with the ATLAS experiment in pp collisions at $\sqrt{s} = 8$ TeV*, *Eur. Phys. J. C* **75** (2015) 303 [arXiv:1412.7086] [INSPIRE].

[97] ATLAS collaboration, *Reconstruction, Energy Calibration, and Identification of Hadronically Decaying Tau Leptons in the ATLAS Experiment for Run-2 of the LHC*, ATL-PHYS-PUB-2015-045 (2015).

[98] ATLAS collaboration, *Identification of hadronic tau lepton decays using neural networks in the ATLAS experiment*, ATL-PHYS-PUB-2019-033 (2019).

[99] ATLAS collaboration, *Measurement of the tau lepton reconstruction and identification performance in the ATLAS experiment using pp collisions at $\sqrt{s} = 13$ TeV*, ATLAS-CONF-2017-029 (2017).

JHEP06(2021)179

[100] ATLAS collaboration, *Jet reconstruction and performance using particle flow with the ATLAS Detector*, *Eur. Phys. J. C* **77** (2017) 466 [arXiv:1703.10485] [INSPIRE].

[101] ATLAS collaboration, *Jet energy scale and resolution measured in proton-proton collisions at $\sqrt{s} = 13$ TeV with the ATLAS detector*, arXiv:2007.02645 [INSPIRE].

[102] M. Cacciari, G.P. Salam and G. Soyez, *The anti-k_t jet clustering algorithm*, *JHEP* **04** (2008) 063 [arXiv:0802.1189] [INSPIRE].

[103] M. Cacciari, G.P. Salam and G. Soyez, *FastJet User Manual*, *Eur. Phys. J. C* **72** (2012) 1896 [arXiv:1111.6097] [INSPIRE].

[104] M. Cacciari, G.P. Salam and G. Soyez, *The Catchment Area of Jets*, *JHEP* **04** (2008) 005 [arXiv:0802.1188] [INSPIRE].

[105] ATLAS collaboration, *Performance of pile-up mitigation techniques for jets in pp collisions at $\sqrt{s} = 8$ TeV using the ATLAS detector*, *Eur. Phys. J. C* **76** (2016) 581 [arXiv:1510.03823] [INSPIRE].

[106] ATLAS collaboration, *ATLAS b-jet identification performance and efficiency measurement with $t\bar{t}$ events in pp collisions at $\sqrt{s} = 13$ TeV*, *Eur. Phys. J. C* **79** (2019) 970 [arXiv:1907.05120] [INSPIRE].

[107] ATLAS collaboration, *Optimisation and performance studies of the ATLAS b-tagging algorithms for the 2017-18 LHC run*, ATL-PHYS-PUB-2017-013 (2017).

[108] ATLAS collaboration, *Measurement of b-tagging Efficiency of c-jets in $t\bar{t}$ Events Using a Likelihood Approach with the ATLAS Detector*, ATLAS-CONF-2018-001 (2018).

[109] ATLAS collaboration, *Calibration of light-flavour b-jet mistagging rates using ATLAS proton-proton collision data at $\sqrt{s} = 13$ TeV*, ATLAS-CONF-2018-006 (2018).

[110] ATLAS collaboration, *Performance of missing transverse momentum reconstruction with the ATLAS detector using proton-proton collisions at $\sqrt{s} = 13$ TeV*, *Eur. Phys. J. C* **78** (2018) 903 [arXiv:1802.08168] [INSPIRE].

[111] ATLAS collaboration, *Performance of electron and photon triggers in ATLAS during LHC Run 2*, *Eur. Phys. J. C* **80** (2020) 47 [arXiv:1909.00761] [INSPIRE].

[112] ATLAS collaboration, *Performance of the ATLAS muon triggers in Run 2*, 2020 *JINST* **15** P09015 [arXiv:2004.13447] [INSPIRE].

[113] ATLAS collaboration, *Measurement of the $t\bar{t}$ production cross-section and lepton differential distributions in $e\mu$ dilepton events from pp collisions at $\sqrt{s} = 13$ TeV with the ATLAS detector*, *Eur. Phys. J. C* **80** (2020) 528 [arXiv:1910.08819] [INSPIRE].

[114] ATLAS collaboration, *Measurements of top-quark pair differential and double-differential cross-sections in the ℓ+jets channel with pp collisions at $\sqrt{s} = 13$ TeV using the ATLAS detector*, *Eur. Phys. J. C* **79** (2019) 1028 [*Erratum ibid.* **80** (2020) 1092] [arXiv:1908.07305] [INSPIRE].

[115] ATLAS collaboration, *Evidence for $t\bar{t}t\bar{t}$ production in the multilepton final state in proton-proton collisions at $\sqrt{s} = 13$ TeV with the ATLAS detector*, *Eur. Phys. J. C* **80** (2020) 1085 [arXiv:2007.14858] [INSPIRE].

[116] ATLAS collaboration, *Measurement of the $t\bar{t}Z$ and $t\bar{t}W$ cross sections in proton-proton collisions at $\sqrt{s} = 13$ TeV with the ATLAS detector*, *Phys. Rev. D* **99** (2019) 072009 [arXiv:1901.03584] [INSPIRE].

JHEP06(2021)179

[117] ROOT collaboration, *HistFactory: A tool for creating statistical models for use with RooFit and RooStats*, CERN-OPEN-2012-016 (2012).

[118] R.J. Barlow and C. Beeston, *Fitting using finite Monte Carlo samples*, *Comput. Phys. Commun.* **77** (1993) 219 [INSPIRE].

[119] W. Verkerke and D.P. Kirkby, *The RooFit toolkit for data modeling*, *eConf* **C 0303241** (2003) MOLT007 [physics/0306116] [INSPIRE].

[120] G. Cowan, K. Cranmer, E. Gross and O. Vitells, *Asymptotic formulae for likelihood-based tests of new physics*, *Eur. Phys. J. C* **71** (2011) 1554 [*Erratum ibid.* **73** (2013) 2501] [arXiv:1007.1727] [INSPIRE].

[121] T. Junk, *Confidence level computation for combining searches with small statistics*, *Nucl. Instrum. Meth. A* **434** (1999) 435 [hep-ex/9902006] [INSPIRE].

[122] A.L. Read, *Presentation of search results: the CL_s technique*, *J. Phys. G* **28** (2002) 2693 [INSPIRE].

[123] ATLAS collaboration, *ATLAS Computing Acknowledgements*, ATL-SOFT-PUB-2020-001 (2020).

JHEP06(2021)179

The ATLAS collaboration

G. Aad[102], B. Abbott[128], D.C. Abbott[103], A. Abed Abud[36], K. Abeling[53], D.K. Abhayasinghe[94], S.H. Abidi[167], O.S. AbouZeid[40], N.L. Abraham[156], H. Abramowicz[161], H. Abreu[160], Y. Abulaiti[6], B.S. Acharya[67a,67b,n], B. Achkar[53], C. Adam Bourdarios[5], L. Adamczyk[84a], L. Adamek[167], J. Adelman[121], A. Adiguzel[12c,ac], S. Adorni[54], T. Adye[143], A.A. Affolder[145], Y. Afik[160], C. Agapopoulou[65], M.N. Agaras[38], A. Aggarwal[119], C. Agheorghiesei[27c], J.A. Aguilar-Saavedra[139f,139a,ab], A. Ahmad[36], F. Ahmadov[80], W.S. Ahmed[104], X. Ai[18], G. Aielli[74a,74b], S. Akatsuka[86], M. Akbiyik[100], T.P.A. Åkesson[97], E. Akilli[54], A.V. Akimov[111], K. Al Khoury[65], G.L. Alberghi[23b,23a], J. Albert[176], M.J. Alconada Verzini[161], S. Alderweireldt[36], M. Aleksa[36], I.N. Aleksandrov[80], C. Alexa[27b], T. Alexopoulos[10], A. Alfonsi[120], F. Alfonsi[23b,23a], M. Alhroob[128], B. Ali[141], S. Ali[158], M. Aliev[166], G. Alimonti[69a], C. Allaire[36], B.M.M. Allbrooke[156], B.W. Allen[131], P.P. Allport[21], A. Aloisio[70a,70b], F. Alonso[89], C. Alpigiani[148], E. Alunno Camelia[74a,74b], M. Alvarez Estevez[99], M.G. Alviggi[70a,70b], Y. Amaral Coutinho[81b], A. Ambler[104], L. Ambroz[134], C. Amelung[36], D. Amidei[106], S.P. Amor Dos Santos[139a], S. Amoroso[46], F. An[79], C. Anastopoulos[149], T. Andeen[11], J.K. Anders[20], S.Y. Andrean[45a,45b], A. Andreazza[69a,69b], V. Andrei[61a], C.R. Anelli[176], S. Angelidakis[9], A. Angerami[39], A.V. Anisenkov[122b,122a], A. Annovi[72a], C. Antel[54], M.T. Anthony[149], E. Antipov[129], M. Antonelli[51], D.J.A. Antrim[18], F. Anulli[73a], M. Aoki[82], J.A. Aparisi Pozo[174], M.A. Aparo[156], L. Aperio Bella[46], N. Aranzabal[36], V. Araujo Ferraz[81a], R. Araujo Pereira[81b], C. Arcangeletti[51], A.T.H. Arce[49], J-F. Arguin[110], S. Argyropoulos[52], J.-H. Arling[46], A.J. Armbruster[36], O. Arnaez[167], H. Arnold[120], Z.P. Arrubarrena Tame[114], G. Artoni[134], H. Asada[117], K. Asai[126], S. Asai[163], T. Asawatavonvanich[165], N.A. Asbah[59], L. Asquith[156], J. Assahsah[35e], K. Assamagan[29], R. Astalos[28a], R.J. Atkin[33a], M. Atkinson[173], N.B. Atlay[19], H. Atmani[65], P.A. Atmasiddha[106], K. Augsten[141], V.A. Austrup[182], G. Avolio[36], M.K. Ayoub[15a], G. Azuelos[110,aj], D. Babal[28a], H. Bachacou[144], K. Bachas[162], F. Backman[45a,45b], P. Bagnaia[73a,73b], H. Bahrasemani[152], A.J. Bailey[174], V.R. Bailey[173], J.T. Baines[143], C. Bakalis[10], O.K. Baker[183], P.J. Bakker[120], E. Bakos[16], D. Bakshi Gupta[8], S. Balaji[157], R. Balasubramanian[120], E.M. Baldin[122b,122a], P. Balek[180], F. Balli[144], W.K. Balunas[134], J. Balz[100], E. Banas[85], M. Bandieramonte[138], A. Bandyopadhyay[19], Sw. Banerjee[181,i], L. Barak[161], W.M. Barbe[38], E.L. Barberio[105], D. Barberis[55b,55a], M. Barbero[102], G. Barbour[95], T. Barillari[115], M-S. Barisits[36], T. Barklow[153], R. Barnea[160], B.M. Barnett[143], R.M. Barnett[18], Z. Barnovska-Blenessy[60a], A. Baroncelli[60a], G. Barone[29], A.J. Barr[134], L. Barranco Navarro[45a,45b], F. Barreiro[99], J. Barreiro Guimarães da Costa[15a], U. Barron[161], S. Barsov[137], F. Bartels[61a], R. Bartoldus[153], G. Bartolini[102], A.E. Barton[90], P. Bartos[28a], A. Basalaev[46], A. Basan[100], A. Bassalat[65,ag], M.J. Basso[167], R.L. Bates[57], S. Batlamous[35f], J.R. Batley[32], B. Batool[151], M. Battaglia[145], M. Bauce[73a,73b], F. Bauer[144,*], P. Bauer[24], H.S. Bawa[31], A. Bayirli[12c], J.B. Beacham[49], T. Beau[135], P.H. Beauchemin[170], F. Becherer[52], P. Bechtle[24], H.C. Beck[53], H.P. Beck[20,p], K. Becker[178], A. Beddall[12d], A.J. Beddall[12a], V.A. Bednyakov[80], M. Bedognetti[120], C.P. Bee[155], T.A. Beermann[182], M. Begalli[81b], M. Begel[29], A. Behera[155], J.K. Behr[46], F. Beisiegel[24], M. Belfkir[5], A.S. Bell[95], G. Bella[161], L. Bellagamba[23b], A. Bellerive[34], P. Bellos[9], K. Beloborodov[122b,122a], K. Belotskiy[112], N.L. Belyaev[112], D. Benchekroun[35a], N. Benekos[10], Y. Benhammou[161], D.P. Benjamin[6], M. Benoit[29], J.R. Bensinger[26], S. Bentvelsen[120], L. Beresford[134], M. Beretta[51], D. Berge[19], E. Bergeaas Kuutmann[172], N. Berger[5], B. Bergmann[141], L.J. Bergsten[26], J. Beringer[18], S. Berlendis[7], G. Bernardi[135], C. Bernius[153], F.U. Bernlochner[24], T. Berry[94], P. Berta[100], A. Berthold[48], I.A. Bertram[90], N. Besson[144], S. Bethke[115], A. Betti[42], A.J. Bevan[93], J. Beyer[115], S. Bhatta[155], D.S. Bhattacharya[177], P. Bhattarai[26], V.S. Bhopatkar[6], R.M. Bianchi[138], O. Biebel[114], D. Biedermann[19], R. Bielski[36], K. Bierwagen[100], M. Biglietti[75a],

JHEP06(2021)179

T.R.V. Billoud[141], M. Bindi[53], A. Bingul[12d], C. Bini[73a,73b], S. Biondi[23b,23a], C.J. Birch-sykes[101], M. Birman[180], T. Bisanz[36], J.P. Biswal[3], D. Biswas[181,i], A. Bitadze[101], C. Bittrich[48], K. Bjørke[133], T. Blazek[28a], I. Bloch[46], C. Blocker[26], A. Blue[57], U. Blumenschein[93], G.J. Bobbink[120], V.S. Bobrovnikov[122b,122a], S.S. Bocchetta[97], D. Bogavac[14], A.G. Bogdanchikov[122b,122a], C. Bohm[45a], V. Boisvert[94], P. Bokan[172,53], T. Bold[84a], A.E. Bolz[61b], M. Bomben[135], M. Bona[93], J.S. Bonilla[131], M. Boonekamp[144], C.D. Booth[94], A.G. Borbély[57], H.M. Borecka-Bielska[91], L.S. Borgna[95], A. Borisov[123], G. Borissov[90], D. Bortoletto[134], D. Boscherini[23b], M. Bosman[14], J.D. Bossio Sola[104], K. Bouaouda[35a], J. Boudreau[138], E.V. Bouhova-Thacker[90], D. Boumediene[38], A. Boveia[127], J. Boyd[36], D. Boye[33c], I.R. Boyko[80], A.J. Bozson[94], J. Bracinik[21], N. Brahimi[60d,60c], G. Brandt[182], O. Brandt[32], F. Braren[46], B. Brau[103], J.E. Brau[131], K. Brendlinger[46], R. Brener[160], L. Brenner[36], R. Brenner[172], S. Bressler[180], B. Brickwedde[100], D.L. Briglin[21], D. Britton[57], D. Britzger[115], I. Brock[24], R. Brock[107], G. Brooijmans[39], W.K. Brooks[146d], E. Brost[29], P.A. Bruckman de Renstrom[85], B. Brüers[46], D. Bruncko[28b], A. Bruni[23b], G. Bruni[23b], M. Bruschi[23b], N. Bruscino[73a,73b], L. Bryngemark[153], T. Buanes[17], Q. Buat[155], P. Buchholz[151], A.G. Buckley[57], I.A. Budagov[80], M.K. Bugge[133], O. Bulekov[112], B.A. Bullard[59], T.J. Burch[121], S. Burdin[91], C.D. Burgard[120], A.M. Burger[129], B. Burghgrave[8], J.T.P. Burr[46], C.D. Burton[11], J.C. Burzynski[103], V. Büscher[100], E. Buschmann[53], P.J. Bussey[57], J.M. Butler[25], C.M. Buttar[57], J.M. Butterworth[95], P. Butti[36], W. Buttinger[143], C.J. Buxo Vazquez[107], A. Buzatu[158], A.R. Buzykaev[122b,122a], G. Cabras[23b,23a], S. Cabrera Urbán[174], D. Caforio[56], H. Cai[138], V.M.M. Cairo[153], O. Cakir[4a], N. Calace[36], P. Calafiura[18], G. Calderini[135], P. Calfayan[66], G. Callea[57], L.P. Caloba[81b], A. Caltabiano[74a,74b], S. Calvente Lopez[99], D. Calvet[38], S. Calvet[38], T.P. Calvet[102], M. Calvetti[72a,72b], R. Camacho Toro[135], S. Camarda[36], D. Camarero Munoz[99], P. Camarri[74a,74b], M.T. Camerlingo[75a,75b], D. Cameron[133], C. Camincher[36], S. Campana[36], M. Campanelli[95], A. Camplani[40], V. Canale[70a,70b], A. Canesse[104], M. Cano Bret[78], J. Cantero[129], T. Cao[161], Y. Cao[173], M.D.M. Capeans Garrido[36], M. Capua[41b,41a], R. Cardarelli[74a], F. Cardillo[174], G. Carducci[41b,41a], I. Carli[142], T. Carli[36], G. Carlino[70a], B.T. Carlson[138], E.M. Carlson[176,168a], L. Carminati[69a,69b], R.M.D. Carney[153], S. Caron[119], E. Carquin[146d], S. Carrá[46], G. Carratta[23b,23a], J.W.S. Carter[167], T.M. Carter[50], M.P. Casado[14,f], A.F. Casha[167], E.G. Castiglia[183], F.L. Castillo[174], L. Castillo Garcia[14], V. Castillo Gimenez[174], N.F. Castro[139a,139e], A. Catinaccio[36], J.R. Catmore[133], A. Cattai[36], V. Cavaliere[29], V. Cavasinni[72a,72b], E. Celebi[12b], F. Celli[134], K. Cerny[130], A.S. Cerqueira[81a], A. Cerri[156], L. Cerrito[74a,74b], F. Cerutti[18], A. Cervelli[23b,23a], S.A. Cetin[12b], Z. Chadi[35a], D. Chakraborty[121], J. Chan[181], W.Y. Chan[91], J.D. Chapman[32], B. Chargeishvili[159b], D.G. Charlton[21], T.P. Charman[93], M. Chatterjee[20], C.C. Chau[34], S. Che[127], S. Chekanov[6], S.V. Chekulaev[168a], G.A. Chelkov[80,ae], B. Chen[79], C. Chen[60a], C.H. Chen[79], H. Chen[15c], H. Chen[29], J. Chen[60a], J. Chen[39], J. Chen[26], S. Chen[136], S.J. Chen[15c], X. Chen[15b], Y. Chen[60a], Y-H. Chen[46], H.C. Cheng[63a], H.J. Cheng[15a], A. Cheplakov[80], E. Cheremushkina[123], R. Cherkaoui El Moursli[35f], E. Cheu[7], K. Cheung[64], T.J.A. Chevalérias[144], L. Chevalier[144], V. Chiarella[51], G. Chiarelli[72a], G. Chiodini[68a], A.S. Chisholm[21], A. Chitan[27b], I. Chiu[163], Y.H. Chiu[176], M.V. Chizhov[80], K. Choi[11], A.R. Chomont[73a,73b], Y. Chou[103], Y.S. Chow[120], L.D. Christopher[33f], M.C. Chu[63a], X. Chu[15a,15d], J. Chudoba[140], J.J. Chwastowski[85], L. Chytka[130], D. Cieri[115], K.M. Ciesla[85], V. Cindro[92], I.A. Cioară[27b], A. Ciocio[18], F. Cirotto[70a,70b], Z.H. Citron[180,j], M. Citterio[69a], D.A. Ciubotaru[27b], B.M. Ciungu[167], A. Clark[54], P.J. Clark[50], S.E. Clawson[101], C. Clement[45a,45b], Y. Coadou[102], M. Cobal[67a,67c], A. Coccaro[55b], J. Cochran[79], R. Coelho Lopes De Sa[103], H. Cohen[161], A.E.C. Coimbra[36], B. Cole[39], A.P. Colijn[120], J. Collot[58], P. Conde Muiño[139a,139h], S.H. Connell[33c], I.A. Connelly[57], S. Constantinescu[27b], F. Conventi[70a,ak], A.M. Cooper-Sarkar[134], F. Cormier[175], K.J.R. Cormier[167], L.D. Corpe[95], M. Corradi[73a,73b], E.E. Corrigan[97], F. Corriveau[104,z], M.J. Costa[174], F. Costanza[5], D. Costanzo[149], G. Cowan[94], J.W. Cowley[32],

JHEP06(2021)179

J. Crane[101], K. Cranmer[125], R.A. Creager[136], S. Crépé-Renaudin[58], F. Crescioli[135], M. Cristinziani[24], V. Croft[170], G. Crosetti[41b,41a], A. Cueto[5], T. Cuhadar Donszelmann[171], H. Cui[15a,15d], A.R. Cukierman[153], W.R. Cunningham[57], S. Czekierda[85], P. Czodrowski[36], M.M. Czurylo[61b], M.J. Da Cunha Sargedas De Sousa[60b], J.V. Da Fonseca Pinto[81b], C. Da Via[101], W. Dabrowski[84a], F. Dachs[36], T. Dado[47], S. Dahbi[33f], T. Dai[106], C. Dallapiccola[103], M. Dam[40], G. D'amen[29], V. D'Amico[75a,75b], J. Damp[100], J.R. Dandoy[136], M.F. Daneri[30], M. Danninger[152], V. Dao[36], G. Darbo[55b], O. Dartsi[5], T. Daubney[46], S. D'Auria[69a,69b], C. David[168b], T. Davidek[142], D.R. Davis[49], I. Dawson[149], K. De[8], R. De Asmundis[70a], M. De Beurs[120], S. De Castro[23b,23a], N. De Groot[119], P. de Jong[120], H. De la Torre[107], A. De Maria[15c], D. De Pedis[73a], A. De Salvo[73a], U. De Sanctis[74a,74b], A. De Santo[156], J.B. De Vivie De Regie[65], D.V. Dedovich[80], A.M. Deiana[42], J. Del Peso[99], Y. Delabat Diaz[46], D. Delgove[65], F. Deliot[144], C.M. Delitzsch[7], M. Della Pietra[70a,70b], D. Della Volpe[54], A. Dell'Acqua[36], L. Dell'Asta[74a,74b], M. Delmastro[5], C. Delporte[65], P.A. Delsart[58], S. Demers[183], M. Demichev[80], G. Demontigny[110], S.P. Denisov[123], L. D'Eramo[121], D. Derendarz[85], J.E. Derkaoui[35e], F. Derue[135], P. Dervan[91], K. Desch[24], K. Dette[167], C. Deutsch[24], M.R. Devesa[30], P.O. Deviveiros[36], F.A. Di Bello[73a,73b], A. Di Ciaccio[74a,74b], L. Di Ciaccio[5], W.K. Di Clemente[136], C. Di Donato[70a,70b], A. Di Girolamo[36], G. Di Gregorio[72a,72b], A. Di Luca[76a,76b], B. Di Micco[75a,75b], R. Di Nardo[75a,75b], K.F. Di Petrillo[59], R. Di Sipio[167], C. Diaconu[102], F.A. Dias[120], T. Dias Do Vale[139a], M.A. Diaz[146a], F.G. Diaz Capriles[24], J. Dickinson[18], M. Didenko[166], E.B. Diehl[106], J. Dietrich[19], S. Díez Cornell[46], C. Diez Pardos[151], A. Dimitrievska[18], W. Ding[15b], J. Dingfelder[24], S.J. Dittmeier[61b], F. Dittus[36], F. Djama[102], T. Djobava[159b], J.I. Djuvsland[17], M.A.B. Do Vale[147], M. Dobre[27b], C. Doglioni[97], J. Dolejsi[142], Z. Dolezal[142], M. Donadelli[81c], B. Dong[60c], J. Donini[38], A. D'onofrio[15c], M. D'Onofrio[91], J. Dopke[143], A. Doria[70a], M.T. Dova[89], A.T. Doyle[57], E. Drechsler[152], E. Dreyer[152], T. Dreyer[53], A.S. Drobac[170], D. Du[60b], T.A. du Pree[120], Y. Duan[60d], F. Dubinin[111], M. Dubovsky[28a], A. Dubreuil[54], E. Duchovni[180], G. Duckeck[114], O.A. Ducu[36,27b], D. Duda[115], A. Dudarev[36], A.C. Dudder[100], E.M. Duffield[18], M. D'uffizi[101], L. Duflot[65], M. Dührssen[36], C. Dülsen[182], M. Dumancic[180], A.E. Dumitriu[27b], M. Dunford[61a], S. Dungs[47], A. Duperrin[102], H. Duran Yildiz[4a], M. Düren[56], A. Durglishvili[159b], D. Duschinger[48], B. Dutta[46], D. Duvnjak[1], G.I. Dyckes[136], M. Dyndal[36], S. Dysch[101], B.S. Dziedzic[85], M.G. Eggleston[49], T. Eifert[8], G. Eigen[17], K. Einsweiler[18], T. Ekelof[172], H. El Jarrari[35f], V. Ellajosyula[172], M. Ellert[172], F. Ellinghaus[182], A.A. Elliot[93], N. Ellis[36], J. Elmsheuser[29], M. Elsing[36], D. Emeliyanov[143], A. Emerman[39], Y. Enari[163], M.B. Epland[49], J. Erdmann[47], A. Ereditato[20], P.A. Erland[85], M. Errenst[182], M. Escalier[65], C. Escobar[174], O. Estrada Pastor[174], E. Etzion[161], G. Evans[139a], H. Evans[66], M.O. Evans[156], A. Ezhilov[137], F. Fabbri[57], L. Fabbri[23b,23a], V. Fabiani[119], G. Facini[178], R.M. Fakhrutdinov[123], S. Falciano[73a], P.J. Falke[24], S. Falke[36], J. Faltova[142], Y. Fang[15a], Y. Fang[15a], G. Fanourakis[44], M. Fanti[69a,69b], M. Faraj[67a,67c], A. Farbin[8], A. Farilla[75a], E.M. Farina[71a,71b], T. Farooque[107], S.M. Farrington[50], P. Farthouat[36], F. Fassi[35f], P. Fassnacht[36], D. Fassouliotis[9], M. Faucci Giannelli[50], W.J. Fawcett[32], L. Fayard[65], O.L. Fedin[137,o], W. Fedorko[175], A. Fehr[20], M. Feickert[173], L. Feligioni[102], A. Fell[149], C. Feng[60b], M. Feng[49], M.J. Fenton[171], A.B. Fenyuk[123], S.W. Ferguson[43], J. Ferrando[46], A. Ferrari[172], P. Ferrari[120], R. Ferrari[71a], D.E. Ferreira de Lima[61b], A. Ferrer[174], D. Ferrere[54], C. Ferretti[106], F. Fiedler[100], A. Filipčič[92], F. Filthaut[119], K.D. Finelli[25], M.C.N. Fiolhais[139a,139c,a], L. Fiorini[174], F. Fischer[114], J. Fischer[100], W.C. Fisher[107], T. Fitschen[21], I. Fleck[151], P. Fleischmann[106], T. Flick[182], B.M. Flierl[114], L. Flores[136], L.R. Flores Castillo[63a], F.M. Follega[76a,76b], N. Fomin[17], J.H. Foo[167], G.T. Forcolin[76a,76b], B.C. Forland[66], A. Formica[144], F.A. Förster[14], A.C. Forti[101], E. Fortin[102], M.G. Foti[134], D. Fournier[65], H. Fox[90], P. Francavilla[72a,72b], S. Francescato[73a,73b], M. Franchini[23b,23a], S. Franchino[61a], D. Francis[36], L. Franco[5], L. Franconi[20], M. Franklin[59], G. Frattari[73a,73b], A.N. Fray[93], P.M. Freeman[21], B. Freund[110], W.S. Freund[81b], E.M. Freundlich[47],

JHEP06(2021)179

D.C. Frizzell[128], D. Froidevaux[36], J.A. Frost[134], M. Fujimoto[126], C. Fukunaga[164], E. Fullana Torregrosa[174], T. Fusayasu[116], J. Fuster[174], A. Gabrielli[23b,23a], A. Gabrielli[36], S. Gadatsch[54], P. Gadow[115], G. Gagliardi[55b,55a], L.G. Gagnon[110], G.E. Gallardo[134], E.J. Gallas[134], B.J. Gallop[143], R. Gamboa Goni[93], K.K. Gan[127], S. Ganguly[180], J. Gao[60a], Y. Gao[50], Y.S. Gao[31,l], F.M. Garay Walls[146a], C. García[174], J.E. García Navarro[174], J.A. García Pascual[15a], C. Garcia-Argos[52], M. Garcia-Sciveres[18], R.W. Gardner[37], N. Garelli[153], S. Gargiulo[52], C.A. Garner[167], V. Garonne[133], S.J. Gasiorowski[148], P. Gaspar[81b], A. Gaudiello[55b,55a], G. Gaudio[71a], P. Gauzzi[73a,73b], I.L. Gavrilenko[111], A. Gavrilyuk[124], C. Gay[175], G. Gaycken[46], E.N. Gazis[10], A.A. Geanta[27b], C.M. Gee[145], C.N.P. Gee[143], J. Geisen[97], M. Geisen[100], C. Gemme[55b], M.H. Genest[58], C. Geng[106], S. Gentile[73a,73b], S. George[94], T. Geralis[44], L.O. Gerlach[53], P. Gessinger-Befurt[100], G. Gessner[47], M. Ghasemi Bostanabad[176], M. Ghneimat[151], A. Ghosh[65], A. Ghosh[78], B. Giacobbe[23b], S. Giagu[73a,73b], N. Giangiacomi[167], P. Giannetti[72a], A. Giannini[70a,70b], G. Giannini[14], S.M. Gibson[94], M. Gignac[145], D.T. Gil[84b], B.J. Gilbert[39], D. Gillberg[34], G. Gilles[182], N.E.K. Gillwald[46], D.M. Gingrich[3,aj], M.P. Giordani[67a,67c], P.F. Giraud[144], G. Giugliarelli[67a,67c], D. Giugni[69a], F. Giuli[74a,74b], S. Gkaitatzis[162], I. Gkialas[9,g], E.L. Gkougkousis[14], P. Gkountoumis[10], L.K. Gladilin[113], C. Glasman[99], J. Glatzer[14], P.C.F. Glaysher[46], A. Glazov[46], G.R. Gledhill[131], I. Gnesi[41b,b], M. Goblirsch-Kolb[26], D. Godin[110], S. Goldfarb[105], T. Golling[54], D. Golubkov[123], A. Gomes[139a,139b], R. Goncalves Gama[53], R. Gonçalo[139a,139c], G. Gonella[131], L. Gonella[21], A. Gongadze[80], F. Gonnella[21], J.L. Gonski[39], S. González de la Hoz[174], S. Gonzalez Fernandez[14], R. Gonzalez Lopez[91], C. Gonzalez Renteria[18], R. Gonzalez Suarez[172], S. Gonzalez-Sevilla[54], G.R. Gonzalvo Rodriguez[174], L. Goossens[36], N.A. Gorasia[21], P.A. Gorbounov[124], H.A. Gordon[29], B. Gorini[36], E. Gorini[68a,68b], A. Gorišek[92], A.T. Goshaw[49], M.I. Gostkin[80], C.A. Gottardo[119], M. Gouighri[35b], A.G. Goussiou[148], N. Govender[33c], C. Goy[5], I. Grabowska-Bold[84a], E.C. Graham[91], J. Gramling[171], E. Gramstad[133], S. Grancagnolo[19], M. Grandi[156], V. Gratchev[137], P.M. Gravila[27f], F.G. Gravili[68a,68b], C. Gray[57], H.M. Gray[18], C. Grefe[24], K. Gregersen[97], I.M. Gregor[46], P. Grenier[153], K. Grevtsov[46], C. Grieco[14], N.A. Grieser[128], A.A. Grillo[145], K. Grimm[31,k], S. Grinstein[14,v], J.-F. Grivaz[65], S. Groh[100], E. Gross[180], J. Grosse-Knetter[53], Z.J. Grout[95], C. Grud[106], A. Grummer[118], J.C. Grundy[134], L. Guan[106], W. Guan[181], C. Gubbels[175], J. Guenther[77], A. Guerguichon[65], J.G.R. Guerrero Rojas[174], F. Guescini[115], D. Guest[77], R. Gugel[100], A. Guida[46], T. Guillemin[5], S. Guindon[36], J. Guo[60c], W. Guo[106], Y. Guo[60a], Z. Guo[102], R. Gupta[46], S. Gurbuz[12c], G. Gustavino[128], M. Guth[52], P. Gutierrez[128], C. Gutschow[95], C. Guyot[144], C. Gwenlan[134], C.B. Gwilliam[91], E.S. Haaland[133], A. Haas[125], C. Haber[18], H.K. Hadavand[8], A. Hadef[100], M. Haleem[177], J. Haley[129], J.J. Hall[149], G. Halladjian[107], G.D. Hallewell[102], K. Hamano[176], H. Hamdaoui[35f], M. Hamer[24], G.N. Hamity[50], K. Han[60a], L. Han[15c], L. Han[60a], S. Han[18], Y.F. Han[167], K. Hanagaki[82,t], M. Hance[145], D.M. Handl[114], M.D. Hank[37], R. Hankache[135], E. Hansen[97], J.B. Hansen[40], J.D. Hansen[40], M.C. Hansen[24], P.H. Hansen[40], E.C. Hanson[101], K. Hara[169], T. Harenberg[182], S. Harkusha[108], P.F. Harrison[178], N.M. Hartman[153], N.M. Hartmann[114], Y. Hasegawa[150], A. Hasib[50], S. Hassani[144], S. Haug[20], R. Hauser[107], M. Havranek[141], C.M. Hawkes[21], R.J. Hawkings[36], S. Hayashida[117], D. Hayden[107], C. Hayes[106], R.L. Hayes[175], C.P. Hays[134], J.M. Hays[93], H.S. Hayward[91], S.J. Haywood[143], F. He[60a], Y. He[165], M.P. Heath[50], V. Hedberg[97], A.L. Heggelund[133], N.D. Hehir[93], C. Heidegger[52], K.K. Heidegger[52], W.D. Heidorn[79], J. Heilman[34], S. Heim[46], T. Heim[18], B. Heinemann[46,ah], J.G. Heinlein[136], J.J. Heinrich[131], L. Heinrich[36], J. Hejbal[140], L. Helary[46], A. Held[125], S. Hellesund[133], C.M. Helling[145], S. Hellman[45a,45b], C. Helsens[36], R.C.W. Henderson[90], L. Henkelmann[32], A.M. Henriques Correia[36], H. Herde[26], Y. Hernández Jiménez[33f], M.G. Herrmann[114], T. Herrmann[48], G. Herten[52], R. Hertenberger[114], L. Hervas[36], G.G. Hesketh[95], N.P. Hessey[168a], H. Hibi[83], S. Higashino[82], E. Higón-Rodriguez[174], K. Hildebrand[37], J.C. Hill[32], K.K. Hill[29],

JHEP06(2021)179

K.H. Hiller[46], S.J. Hillier[21], M. Hils[48], I. Hinchliffe[18], F. Hinterkeuser[24], M. Hirose[132], S. Hirose[169], D. Hirschbuehl[182], B. Hiti[92], O. Hladik[140], J. Hobbs[155], R. Hobincu[27e], N. Hod[180], M.C. Hodgkinson[149], A. Hoecker[36], D. Hohn[52], D. Hohov[65], T. Holm[24], T.R. Holmes[37], M. Holzbock[115], L.B.A.H. Hommels[32], T.M. Hong[138], J.C. Honig[52], A. Hönle[115], B.H. Hooberman[173], W.H. Hopkins[6], Y. Horii[117], P. Horn[48], L.A. Horyn[37], S. Hou[158], A. Hoummada[35a], J. Howarth[57], J. Hoya[89], M. Hrabovsky[130], J. Hrivnac[65], A. Hrynevich[109], T. Hryn'ova[5], P.J. Hsu[64], S.-C. Hsu[148], Q. Hu[39], S. Hu[60c], Y.F. Hu[15a,15d,al], D.P. Huang[95], X. Huang[15c], Y. Huang[60a], Y. Huang[15a], Z. Hubacek[141], F. Hubaut[102], M. Huebner[24], F. Huegging[24], T.B. Huffman[134], M. Huhtinen[36], R. Hulsken[58], R.F.H. Hunter[34], N. Huseynov[80,aa], J. Huston[107], J. Huth[59], R. Hyneman[153], S. Hyrych[28a], G. Iacobucci[54], G. Iakovidis[29], I. Ibragimov[151], L. Iconomidou-Fayard[65], P. Iengo[36], R. Ignazzi[40], R. Iguchi[163], T. Iizawa[54], Y. Ikegami[82], M. Ikeno[82], N. Ilic[119,167,z], F. Iltzsche[48], H. Imam[35a], G. Introzzi[71a,71b], M. Iodice[75a], K. Iordanidou[168a], V. Ippolito[73a,73b], M.F. Isacson[172], M. Ishino[163], W. Islam[129], C. Issever[19,46], S. Istin[160], J.M. Iturbe Ponce[63a], R. Iuppa[76a,76b], A. Ivina[180], J.M. Izen[43], V. Izzo[70a], P. Jacka[140], P. Jackson[1], R.M. Jacobs[46], B.P. Jaeger[152], V. Jain[2], G. Jäkel[182], K.B. Jakobi[100], K. Jakobs[52], T. Jakoubek[180], J. Jamieson[57], K.W. Janas[84a], R. Jansky[54], M. Janus[53], P.A. Janus[84a], G. Jarlskog[97], A.E. Jaspan[91], N. Javadov[80,aa], M. Javurkova[103], F. Jeanneau[144], L. Jeanty[131], J. Jejelava[159a], P. Jenni[52,c], N. Jeong[46], S. Jézéquel[5], J. Jia[155], Z. Jia[15c], H. Jiang[79], Y. Jiang[60a], Z. Jiang[153], S. Jiggins[52], F.A. Jimenez Morales[38], J. Jimenez Pena[115], S. Jin[15c], A. Jinaru[27b], O. Jinnouchi[165], P. Johansson[149], K.A. Johns[7], E. Jones[178], R.W.L. Jones[90], S.D. Jones[156], T.J. Jones[91], J. Jovicevic[36], X. Ju[18], J.J. Junggeburth[115], A. Juste Rozas[14,v], A. Kaczmarska[85], M. Kado[73a,73b], H. Kagan[127], M. Kagan[153], A. Kahn[39], C. Kahra[100], T. Kaji[179], E. Kajomovitz[160], C.W. Kalderon[29], A. Kaluza[100], M. Kaneda[163], N.J. Kang[145], S. Kang[79], Y. Kano[117], J. Kanzaki[82], L.S. Kaplan[181], D. Kar[33f], K. Karava[134], M.J. Kareem[168b], I. Karkanias[162], S.N. Karpov[80], Z.M. Karpova[80], V. Kartvelishvili[90], A.N. Karyukhin[123], E. Kasimi[162], A. Kastanas[45a,45b], C. Kato[60d], J. Katzy[46], K. Kawade[150], K. Kawagoe[88], T. Kawamoto[144], G. Kawamura[53], E.F. Kay[176], F.I. Kaya[170], S. Kazakos[14], V.F. Kazanin[122b,122a], J.M. Keaveney[33a], R. Keeler[176], J.S. Keller[34], E. Kellermann[97], D. Kelsey[156], J.J. Kempster[21], K.E. Kennedy[39], O. Kepka[140], S. Kersten[182], B.P. Kerševan[92], S. Ketabchi Haghighat[167], F. Khalil-Zada[13], M. Khandoga[144], A. Khanov[129], A.G. Kharlamov[122b,122a], T. Kharlamova[122b,122a], E.E. Khoda[175], T.J. Khoo[77], G. Khoriauli[177], E. Khramov[80], J. Khubua[159b], S. Kido[83], M. Kiehn[36], E. Kim[165], Y.K. Kim[37], N. Kimura[95], A. Kirchhoff[53], D. Kirchmeier[48], J. Kirk[143], A.E. Kiryunin[115], T. Kishimoto[163], D.P. Kisliuk[167], V. Kitali[46], C. Kitsaki[10], O. Kivernyk[24], T. Klapdor-Kleingrothaus[52], M. Klassen[61a], C. Klein[34], M.H. Klein[106], M. Klein[91], U. Klein[91], K. Kleinknecht[100], P. Klimek[36], A. Klimentov[29], F. Klimpel[36], T. Klingl[24], T. Klioutchnikova[36], F.F. Klitzner[114], P. Kluit[120], S. Kluth[115], E. Kneringer[77], E.B.F.G. Knoops[102], A. Knue[52], D. Kobayashi[88], M. Kobel[48], M. Kocian[153], P. Kodys[142], D.M. Koeck[156], P.T. Koenig[24], T. Koffas[34], N.M. Köhler[36], M. Kolb[144], I. Koletsou[5], T. Komarek[130], T. Kondo[82], K. Köneke[52], A.X.Y. Kong[1], A.C. König[119], T. Kono[126], V. Konstantinides[95], N. Konstantinidis[95], B. Konya[97], R. Kopeliansky[66], S. Koperny[84a], K. Korcyl[85], K. Kordas[162], G. Koren[161], A. Korn[95], I. Korolkov[14], E.V. Korolkova[149], N. Korotkova[113], O. Kortner[115], S. Kortner[115], V.V. Kostyukhin[149,166], A. Kotsokechagia[65], A. Kotwal[49], A. Koulouris[10], A. Kourkoumeli-Charalampidi[71a,71b], C. Kourkoumelis[9], E. Kourlitis[6], V. Kouskoura[29], R. Kowalewski[176], W. Kozanecki[101], A.S. Kozhin[123], V.A. Kramarenko[113], G. Kramberger[92], D. Krasnopevtsev[60a], M.W. Krasny[135], A. Krasznahorkay[36], D. Krauss[115], J.A. Kremer[100], J. Kretzschmar[91], K. Kreul[19], P. Krieger[167], F. Krieter[114], S. Krishnamurthy[103], A. Krishnan[61b], M. Krivos[142], K. Krizka[18], K. Kroeninger[47], H. Kroha[115], J. Kroll[140], J. Kroll[136], K.S. Krowpman[107], U. Kruchonak[80], H. Krüger[24], N. Krumnack[79], M.C. Kruse[49], J.A. Krzysiak[85],

JHEP06(2021)179

A. Kubota[165], O. Kuchinskaia[166], S. Kuday[4b], D. Kuechler[46], J.T. Kuechler[46], S. Kuehn[36], T. Kuhl[46], V. Kukhtin[80], Y. Kulchitsky[108,ad], S. Kuleshov[146b], Y.P. Kulinich[173], A. Kupco[140], T. Kupfer[47], O. Kuprash[52], H. Kurashige[83], L.L. Kurchaninov[168a], Y.A. Kurochkin[108], A. Kurova[112], M.G. Kurth[15a,15d], M. Kuze[165], A.K. Kvam[148], J. Kvita[130], T. Kwan[104], C. Lacasta[174], F. Lacava[73a,73b], D.P.J. Lack[101], H. Lacker[19], D. Lacour[135], E. Ladygin[80], R. Lafaye[5], B. Laforge[135], T. Lagouri[146c], S. Lai[53], I.K. Lakomiec[84a], J.E. Lambert[128], S. Lammers[66], W. Lampl[7], C. Lampoudis[162], E. Lançon[29], U. Landgraf[52], M.P.J. Landon[93], V.S. Lang[52], J.C. Lange[53], R.J. Langenberg[103], A.J. Lankford[171], F. Lanni[29], K. Lantzsch[24], A. Lanza[71a], A. Lapertosa[55b,55a], J.F. Laporte[144], T. Lari[69a], F. Lasagni Manghi[23b,23a], M. Lassnig[36], V. Latonova[140], T.S. Lau[63a], A. Laudrain[100], A. Laurier[34], M. Lavorgna[70a,70b], S.D. Lawlor[94], M. Lazzaroni[69a,69b], B. Le[101], E. Le Guirriec[102], A. Lebedev[79], M. LeBlanc[7], T. LeCompte[6], F. Ledroit-Guillon[58], A.C.A. Lee[95], C.A. Lee[29], G.R. Lee[17], L. Lee[59], S.C. Lee[158], S. Lee[79], B. Lefebvre[168a], H.P. Lefebvre[94], M. Lefebvre[176], C. Leggett[18], K. Lehmann[152], N. Lehmann[20], G. Lehmann Miotto[36], W.A. Leight[46], A. Leisos[162,u], M.A.L. Leite[81c], C.E. Leitgeb[114], R. Leitner[142], K.J.C. Leney[42], T. Lenz[24], S. Leone[72a], C. Leonidopoulos[50], A. Leopold[135], C. Leroy[110], R. Les[107], C.G. Lester[32], M. Levchenko[137], J. Levêque[5], D. Levin[106], L.J. Levinson[180], D.J. Lewis[21], B. Li[15b], B. Li[106], C-Q. Li[60c,60d], F. Li[60c], H. Li[60a], H. Li[60b], J. Li[60c], K. Li[148], L. Li[60c], M. Li[15a,15d], Q.Y. Li[60a], S. Li[60d,60c], X. Li[46], Y. Li[46], Z. Li[60b], Z. Li[134], Z. Li[104], Z. Li[91], Z. Liang[15a], M. Liberatore[46], B. Liberti[74a], K. Lie[63c], S. Lim[29], C.Y. Lin[32], K. Lin[107], R.A. Linck[66], R.E. Lindley[7], J.H. Lindon[21], A. Linss[46], A.L. Lionti[54], E. Lipeles[136], A. Lipniacka[17], T.M. Liss[173,ai], A. Lister[175], J.D. Little[8], B. Liu[79], B.X. Liu[152], H.B. Liu[29], J.B. Liu[60a], J.K.K. Liu[37], K. Liu[60d,60c], M. Liu[60a], M.Y. Liu[60a], P. Liu[15a], X. Liu[60a], Y. Liu[46], Y. Liu[15a,15d], Y.L. Liu[106], Y.W. Liu[60a], M. Livan[71a,71b], A. Lleres[58], J. Llorente Merino[152], S.L. Lloyd[93], C.Y. Lo[63b], E.M. Lobodzinska[46], P. Loch[7], S. Loffredo[74a,74b], T. Lohse[19], K. Lohwasser[149], M. Lokajicek[140], J.D. Long[173], R.E. Long[90], I. Longarini[73a,73b], L. Longo[36], I. Lopez Paz[101], A. Lopez Solis[149], J. Lorenz[114], N. Lorenzo Martinez[5], A.M. Lory[114], A. Lösle[52], X. Lou[45a,45b], X. Lou[15a], A. Lounis[65], J. Love[6], P.A. Love[90], J.J. Lozano Bahilo[174], M. Lu[60a], Y.J. Lu[64], H.J. Lubatti[148], C. Luci[73a,73b], F.L. Lucio Alves[15c], A. Lucotte[58], F. Luehring[66], I. Luise[155], L. Luminari[73a], B. Lund-Jensen[154], N.A. Luongo[131], M.S. Lutz[161], D. Lynn[29], H. Lyons[91], R. Lysak[140], E. Lytken[97], F. Lyu[15a], V. Lyubushkin[80], T. Lyubushkina[80], H. Ma[29], L.L. Ma[60b], Y. Ma[95], D.M. Mac Donell[176], G. Maccarrone[51], C.M. Macdonald[149], J.C. MacDonald[149], J. Machado Miguens[136], R. Madar[38], W.F. Mader[48], M. Madugoda Ralalage Don[129], N. Madysa[48], J. Maeda[83], T. Maeno[29], M. Maerker[48], V. Magerl[52], N. Magini[79], J. Magro[67a,67c,q], D.J. Mahon[39], C. Maidantchik[81b], A. Maio[139a,139b,139d], K. Maj[84a], O. Majersky[28a], S. Majewski[131], Y. Makida[82], N. Makovec[65], B. Malaescu[135], Pa. Malecki[85], V.P. Maleev[137], F. Malek[58], D. Malito[41b,41a], U. Mallik[78], C. Malone[32], S. Maltezos[10], S. Malyukov[80], J. Mamuzic[174], G. Mancini[51], J.P. Mandalia[93], I. Mandić[92], L. Manhaes de Andrade Filho[81a], I.M. Maniatis[162], J. Manjarres Ramos[48], A. Mann[114], B. Mansoulie[144], I. Manthos[162], S. Manzoni[120], A. Marantis[162,u], G. Marceca[30], L. Marchese[134], G. Marchiori[135], M. Marcisovsky[140], L. Marcoccia[74a,74b], C. Marcon[97], M. Marjanovic[128], Z. Marshall[18], M.U.F. Martensson[172], S. Marti-Garcia[174], C.B. Martin[127], T.A. Martin[178], V.J. Martin[50], B. Martin dit Latour[17], L. Martinelli[75a,75b], M. Martinez[14,v], P. Martinez Agullo[174], V.I. Martinez Outschoorn[103], S. Martin-Haugh[143], V.S. Martoiu[27b], A.C. Martyniuk[95], A. Marzin[36], S.R. Maschek[115], L. Masetti[100], T. Mashimo[163], R. Mashinistov[111], J. Masik[101], A.L. Maslennikov[122b,122a], L. Massa[23b,23a], P. Massarotti[70a,70b], P. Mastrandrea[72a,72b], A. Mastroberardino[41b,41a], T. Masubuchi[163], D. Matakias[29], N. Matsuzawa[163], P. Mättig[24], J. Maurer[27b], B. Maček[92], D.A. Maximov[122b,122a], R. Mazini[158], I. Maznas[162], S.M. Mazza[145], J.P. Mc Gowan[104], S.P. Mc Kee[106], W.P. McCormack[18],

JHEP06(2021)179

E.F. McDonald[105], A.E. McDougall[120], J.A. Mcfayden[18], G. Mchedlidze[159b], M.A. McKay[42], K.D. McLean[176], S.J. McMahon[143], P.C. McNamara[105], C.J. McNicol[178], R.A. McPherson[176,z], Z.A. Meadows[103], T. Megy[38], S. Mehlhase[114], A. Mehta[91], B. Meirose[43], D. Melini[160], B.R. Mellado Garcia[33f], J.D. Mellenthin[53], M. Melo[28a], F. Meloni[46], A. Melzer[24], E.D. Mendes Gouveia[139a,139e], A.M. Mendes Jacques Da Costa[21], H.Y. Meng[167], L. Meng[36], X.T. Meng[106], S. Menke[115], E. Meoni[41b,41a], S. Mergelmeyer[19], S.A.M. Merkt[138], C. Merlassino[134], P. Mermod[54,*], L. Merola[70a,70b], C. Meroni[69a], G. Merz[106], O. Meshkov[113,111], J.K.R. Meshreki[151], J. Metcalfe[6], A.S. Mete[6], C. Meyer[66], J-P. Meyer[144], M. Michetti[19], R.P. Middleton[143], L. Mijović[50], G. Mikenberg[180], M. Mikestikova[140], M. Mikuž[92], H. Mildner[149], A. Milic[167], C.D. Milke[42], D.W. Miller[37], L.S. Miller[34], A. Milov[180], D.A. Milstead[45a,45b], A.A. Minaenko[123], I.A. Minashvili[159b], L. Mince[57], A.I. Mincer[125], B. Mindur[84a], M. Mineev[80], Y. Mino[86], L.M. Mir[14], M. Mironova[134], T. Mitani[179], J. Mitrevski[114], V.A. Mitsou[174], M. Mittal[60c], O. Miu[167], A. Miucci[20], P.S. Miyagawa[93], A. Mizukami[82], J.U. Mjörnmark[97], T. Mkrtchyan[61a], M. Mlynarikova[121], T. Moa[45a,45b], S. Mobius[53], K. Mochizuki[110], P. Moder[46], P. Mogg[114], S. Mohapatra[39], R. Moles-Valls[24], K. Mönig[46], E. Monnier[102], A. Montalbano[152], J. Montejo Berlingen[36], M. Montella[95], F. Monticelli[89], S. Monzani[69a], N. Morange[65], A.L. Moreira De Carvalho[139a], D. Moreno[22a], M. Moreno Llácer[174], C. Moreno Martinez[14], P. Morettini[55b], M. Morgenstern[160], S. Morgenstern[48], D. Mori[152], M. Morii[59], M. Morinaga[179], V. Morisbak[133], A.K. Morley[36], G. Mornacchi[36], A.P. Morris[95], L. Morvaj[36], P. Moschovakos[36], B. Moser[120], M. Mosidze[159b], T. Moskalets[144], P. Moskvitina[119], J. Moss[31,m], E.J.W. Moyse[103], S. Muanza[102], J. Mueller[138], R.S.P. Mueller[114], D. Muenstermann[90], G.A. Mullier[97], D.P. Mungo[69a,69b], J.L. Munoz Martinez[14], F.J. Munoz Sanchez[101], P. Murin[28b], W.J. Murray[178,143], A. Murrone[69a,69b], J.M. Muse[128], M. Muškinja[18], C. Mwewa[33a], A.G. Myagkov[123,ae], A.A. Myers[138], G. Myers[66], J. Myers[131], M. Myska[141], B.P. Nachman[18], O. Nackenhorst[47], A.Nag Nag[48], K. Nagai[134], K. Nagano[82], Y. Nagasaka[62], J.L. Nagle[29], E. Nagy[102], A.M. Nairz[36], Y. Nakahama[117], K. Nakamura[82], T. Nakamura[163], H. Nanjo[132], F. Napolitano[61a], R.F. Naranjo Garcia[46], R. Narayan[42], I. Naryshkin[137], M. Naseri[34], T. Naumann[46], G. Navarro[22a], P.Y. Nechaeva[111], F. Nechansky[46], T.J. Neep[21], A. Negri[71a,71b], M. Negrini[23b], C. Nellist[119], C. Nelson[104], M.E. Nelson[45a,45b], S. Nemecek[140], M. Nessi[36,e], M.S. Neubauer[173], F. Neuhaus[100], M. Neumann[182], R. Newhouse[175], P.R. Newman[21], C.W. Ng[138], Y.S. Ng[19], Y.W.Y. Ng[171], B. Ngair[35f], H.D.N. Nguyen[102], T. Nguyen Manh[110], E. Nibigira[38], R.B. Nickerson[134], R. Nicolaidou[144], D.S. Nielsen[40], J. Nielsen[145], M. Niemeyer[53], N. Nikiforou[11], V. Nikolaenko[123,ae], I. Nikolic-Audit[135], K. Nikolopoulos[21], P. Nilsson[29], H.R. Nindhito[54], A. Nisati[73a], N. Nishu[60c], R. Nisius[115], I. Nitsche[47], T. Nitta[179], T. Nobe[163], D.L. Noel[32], Y. Noguchi[86], I. Nomidis[135], M.A. Nomura[29], M. Nordberg[36], J. Novak[92], T. Novak[92], O. Novgorodova[48], R. Novotny[118], L. Nozka[130], K. Ntekas[171], E. Nurse[95], F.G. Oakham[34,aj], J. Ocariz[135], A. Ochi[83], I. Ochoa[139a], J.P. Ochoa-Ricoux[146a], K. O'Connor[26], S. Oda[88], S. Odaka[82], S. Oerdek[53], A. Ogrodnik[84a], A. Oh[101], C.C. Ohm[154], H. Oide[165], R. Oishi[163], M.L. Ojeda[167], H. Okawa[169], Y. Okazaki[86], M.W. O'Keefe[91], Y. Okumura[163], A. Olariu[27b], L.F. Oleiro Seabra[139a], S.A. Olivares Pino[146a], D. Oliveira Damazio[29], J.L. Oliver[1], M.J.R. Olsson[171], A. Olszewski[85], J. Olszowska[85], Ö.O. Öncel[24], D.C. O'Neil[152], A.P. O'neill[134], A. Onofre[139a,139e], P.U.E. Onyisi[11], H. Oppen[133], R.G. Oreamuno Madriz[121], M.J. Oreglia[37], G.E. Orellana[89], D. Orestano[75a,75b], N. Orlando[14], R.S. Orr[167], V. O'Shea[57], R. Ospanov[60a], G. Otero y Garzon[30], H. Otono[88], P.S. Ott[61a], G.J. Ottino[18], M. Ouchrif[35e], J. Ouellette[29], F. Ould-Saada[133], A. Ouraou[144,*], Q. Ouyang[15a], M. Owen[57], R.E. Owen[143], V.E. Ozcan[12c], N. Ozturk[8], J. Pacalt[130], H.A. Pacey[32], K. Pachal[49], A. Pacheco Pages[14], C. Padilla Aranda[14], S. Pagan Griso[18], G. Palacino[66], S. Palazzo[50], S. Palestini[36], M. Palka[84b], P. Palni[84a], C.E. Pandini[54], J.G. Panduro Vazquez[94], P. Pani[46], G. Panizzo[67a,67c], L. Paolozzi[54],

JHEP06(2021)179

C. Papadatos[110], K. Papageorgiou[9,g], S. Parajuli[42], A. Paramonov[6], C. Paraskevopoulos[10], D. Paredes Hernandez[63b], S.R. Paredes Saenz[134], B. Parida[180], T.H. Park[167], A.J. Parker[31], M.A. Parker[32], F. Parodi[55b,55a], E.W. Parrish[121], J.A. Parsons[39], U. Parzefall[52], L. Pascual Dominguez[135], V.R. Pascuzzi[18], J.M.P. Pasner[145], F. Pasquali[120], E. Pasqualucci[73a], S. Passaggio[55b], F. Pastore[94], P. Pasuwan[45a,45b], S. Pataraia[100], J.R. Pater[101], A. Pathak[181,i], J. Patton[91], T. Pauly[36], J. Pearkes[153], M. Pedersen[133], L. Pedraza Diaz[119], R. Pedro[139a], T. Peiffer[53], S.V. Peleganchuk[122b,122a], O. Penc[140], C. Peng[63b], H. Peng[60a], B.S. Peralva[81a], M.M. Perego[65], A.P. Pereira Peixoto[139a], L. Pereira Sanchez[45a,45b], D.V. Perepelitsa[29], E. Perez Codina[168a], L. Perini[69a,69b], H. Pernegger[36], S. Perrella[36], A. Perrevoort[120], K. Peters[46], R.F.Y. Peters[101], B.A. Petersen[36], T.C. Petersen[40], E. Petit[102], V. Petousis[141], C. Petridou[162], F. Petrucci[75a,75b], M. Pettee[183], N.E. Pettersson[103], K. Petukhova[142], A. Peyaud[144], R. Pezoa[146d], L. Pezzotti[71a,71b], T. Pham[105], P.W. Phillips[143], M.W. Phipps[173], G. Piacquadio[155], E. Pianori[18], A. Picazio[103], R.H. Pickles[101], R. Piegaia[30], D. Pietreanu[27b], J.E. Pilcher[37], A.D. Pilkington[101], M. Pinamonti[67a,67c], J.L. Pinfold[3], C. Pitman Donaldson[95], M. Pitt[161], L. Pizzimento[74a,74b], A. Pizzini[120], M.-A. Pleier[29], V. Plesanovs[52], V. Pleskot[142], E. Plotnikova[80], P. Podberezko[122b,122a], R. Poettgen[97], R. Poggi[54], L. Poggioli[135], I. Pogrebnyak[107], D. Pohl[24], I. Pokharel[53], G. Polesello[71a], A. Poley[152,168a], A. Policicchio[73a,73b], R. Polifka[142], A. Polini[23b], C.S. Pollard[46], V. Polychronakos[29], D. Ponomarenko[112], L. Pontecorvo[36], S. Popa[27a], G.A. Popeneciu[27d], L. Portales[5], D.M. Portillo Quintero[58], S. Pospisil[141], K. Potamianos[46], I.N. Potrap[80], C.J. Potter[32], H. Potti[11], T. Poulsen[97], J. Poveda[174], T.D. Powell[149], M.E. Pozo Astigarraga[36], A. Prades Ibanez[174], P. Pralavorio[102], M.M. Prapa[44], S. Prell[79], D. Price[101], M. Primavera[68a], M.L. Proffitt[148], N. Proklova[112], K. Prokofiev[63c], F. Prokoshin[80], S. Protopopescu[29], J. Proudfoot[6], M. Przybycien[84a], D. Pudzha[137], A. Puri[173], P. Puzo[65], D. Pyatiizbyantseva[112], J. Qian[106], Y. Qin[101], A. Quadt[53], M. Queitsch-Maitland[36], G. Rabanal Bolanos[59], M. Racko[28a], F. Ragusa[69a,69b], G. Rahal[98], J.A. Raine[54], S. Rajagopalan[29], A. Ramirez Morales[93], K. Ran[15a,15d], D.F. Rassloff[61a], D.M. Rauch[46], F. Rauscher[114], S. Rave[100], B. Ravina[57], I. Ravinovich[180], J.H. Rawling[101], M. Raymond[36], A.L. Read[133], N.P. Readioff[149], M. Reale[68a,68b], D.M. Rebuzzi[71a,71b], G. Redlinger[29], K. Reeves[43], D. Reikher[161], A. Reiss[100], A. Rej[151], C. Rembser[36], A. Renardi[46], M. Renda[27b], M.B. Rendel[115], A.G. Rennie[57], S. Resconi[69a], E.D. Resseguie[18], S. Rettie[95], B. Reynolds[127], E. Reynolds[21], O.L. Rezanova[122b,122a], P. Reznicek[142], E. Ricci[76a,76b], R. Richter[115], S. Richter[46], E. Richter-Was[84b], M. Ridel[135], P. Rieck[115], O. Rifki[46], M. Rijssenbeek[155], A. Rimoldi[71a,71b], M. Rimoldi[46], L. Rinaldi[23b], T.T. Rinn[173], G. Ripellino[154], I. Riu[14], P. Rivadeneira[46], J.C. Rivera Vergara[176], F. Rizatdinova[129], E. Rizvi[93], C. Rizzi[36], S.H. Robertson[104,z], M. Robin[46], D. Robinson[32], C.M. Robles Gajardo[146d], M. Robles Manzano[100], A. Robson[57], A. Rocchi[74a,74b], C. Roda[72a,72b], S. Rodriguez Bosca[174], A. Rodriguez Rodriguez[52], A.M. Rodríguez Vera[168b], S. Roe[36], J. Roggel[182], O. Røhne[133], R. Röhrig[115], R.A. Rojas[146d], B. Roland[52], C.P.A. Roland[66], J. Roloff[29], A. Romaniouk[112], M. Romano[23b,23a], N. Rompotis[91], M. Ronzani[125], L. Roos[135], S. Rosati[73a], G. Rosin[103], B.J. Rosser[136], E. Rossi[46], E. Rossi[75a,75b], E. Rossi[70a,70b], L.P. Rossi[55b], L. Rossini[46], R. Rosten[14], M. Rotaru[27b], B. Rottler[52], D. Rousseau[65], G. Rovelli[71a,71b], A. Roy[11], D. Roy[33f], A. Rozanov[102], Y. Rozen[160], X. Ruan[33f], T.A. Ruggeri[1], F. Rühr[52], A. Ruiz-Martinez[174], A. Rummler[36], Z. Rurikova[52], N.A. Rusakovich[80], H.L. Russell[104], L. Rustige[38,47], J.P. Rutherfoord[7], M. Rybar[142], G. Rybkin[65], E.B. Rye[133], A. Ryzhov[123], J.A. Sabater Iglesias[46], P. Sabatini[174], L. Sabetta[73a,73b], S. Sacerdoti[65], H.F-W. Sadrozinski[145], R. Sadykov[80], F. Safai Tehrani[73a], B. Safarzadeh Samani[156], M. Safdari[153], P. Saha[121], S. Saha[104], M. Sahinsoy[115], A. Sahu[182], M. Saimpert[36], M. Saito[163], T. Saito[163], H. Sakamoto[163], D. Salamani[54], G. Salamanna[75a,75b], A. Salnikov[153], J. Salt[174], A. Salvador Salas[14], D. Salvatore[41b,41a], F. Salvatore[156], A. Salvucci[63a], A. Salzburger[36], J. Samarati[36], D. Sammel[52],

JHEP06(2021)179

D. Sampsonidis[162], D. Sampsonidou[60d,60c], J. Sánchez[174], A. Sanchez Pineda[67a,36,67c], H. Sandaker[133], C.O. Sander[46], I.G. Sanderswood[90], M. Sandhoff[182], C. Sandoval[22b], D.P.C. Sankey[143], M. Sannino[55b,55a], Y. Sano[117], A. Sansoni[51], C. Santoni[38], H. Santos[139a,139b], S.N. Santpur[18], A. Santra[174], K.A. Saoucha[149], A. Sapronov[80], J.G. Saraiva[139a,139d], O. Sasaki[82], K. Sato[169], F. Sauerburger[52], E. Sauvan[5], P. Savard[167,aj], R. Sawada[163], C. Sawyer[143], L. Sawyer[96], I. Sayago Galvan[174], C. Sbarra[23b], A. Sbrizzi[67a,67c], T. Scanlon[95], J. Schaarschmidt[148], P. Schacht[115], D. Schaefer[37], L. Schaefer[136], U. Schäfer[100], A.C. Schaffer[65], D. Schaile[114], R.D. Schamberger[155], E. Schanet[114], C. Scharf[19], N. Scharmberg[101], V.A. Schegelsky[137], D. Scheirich[142], F. Schenck[19], M. Schernau[171], C. Schiavi[55b,55a], L.K. Schildgen[24], Z.M. Schillaci[26], E.J. Schioppa[68a,68b], M. Schioppa[41b,41a], K.E. Schleicher[52], S. Schlenker[36], K.R. Schmidt-Sommerfeld[115], K. Schmieden[100], C. Schmitt[100], S. Schmitt[46], L. Schoeffel[144], A. Schoening[61b], P.G. Scholer[52], E. Schopf[134], M. Schott[100], J.F.P. Schouwenberg[119], J. Schovancova[36], S. Schramm[54], F. Schroeder[182], A. Schulte[100], H-C. Schultz-Coulon[61a], M. Schumacher[52], B.A. Schumm[145], Ph. Schune[144], A. Schwartzman[153], T.A. Schwarz[106], Ph. Schwemling[144], R. Schwienhorst[107], A. Sciandra[145], G. Sciolla[26], F. Scuri[72a], F. Scutti[105], L.M. Scyboz[115], C.D. Sebastiani[91], K. Sedlaczek[47], P. Seema[19], S.C. Seidel[118], A. Seiden[145], B.D. Seidlitz[29], T. Seiss[37], C. Seitz[46], J.M. Seixas[81b], G. Sekhniaidze[70a], S.J. Sekula[42], N. Semprini-Cesari[23b,23a], S. Sen[49], C. Serfon[29], L. Serin[65], L. Serkin[67a,67b], M. Sessa[60a], H. Severini[128], S. Sevova[153], F. Sforza[55b,55a], A. Sfyrla[54], E. Shabalina[53], J.D. Shahinian[136], N.W. Shaikh[45a,45b], D. Shaked Renous[180], L.Y. Shan[15a], M. Shapiro[18], A. Sharma[36], A.S. Sharma[1], P.B. Shatalov[124], K. Shaw[156], S.M. Shaw[101], M. Shehade[180], Y. Shen[128], A.D. Sherman[25], P. Sherwood[95], L. Shi[95], C.O. Shimmin[183], Y. Shimogama[179], M. Shimojima[116], J.D. Shinner[94], I.P.J. Shipsey[134], S. Shirabe[165], M. Shiyakova[80,x], J. Shlomi[180], A. Shmeleva[111], M.J. Shochet[37], J. Shojaii[105], D.R. Shope[154], S. Shrestha[127], E.M. Shrif[33f], M.J. Shroff[176], E. Shulga[180], P. Sicho[140], A.M. Sickles[173], E. Sideras Haddad[33f], A. Sidoti[23b,23a], F. Siegert[48], Dj. Sijacki[16], M.Jr. Silva[181], M.V. Silva Oliveira[36], S.B. Silverstein[45a], S. Simion[65], R. Simoniello[100], C.J. Simpson-allsop[21], S. Simsek[12b], P. Sinervo[167], V. Sinetckii[113], S. Singh[152], S. Sinha[33f], M. Sioli[23b,23a], I. Siral[131], S.Yu. Sivoklokov[113], J. Sjölin[45a,45b], A. Skaf[53], E. Skorda[97], P. Skubic[128], M. Slawinska[85], K. Sliwa[170], V. Smakhtin[180], B.H. Smart[143], J. Smiesko[28b], N. Smirnov[112], S.Yu. Smirnov[112], Y. Smirnov[112], L.N. Smirnova[113,r], O. Smirnova[97], E.A. Smith[37], H.A. Smith[134], M. Smizanska[90], K. Smolek[141], A. Smykiewicz[85], A.A. Snesarev[111], H.L. Snoek[120], I.M. Snyder[131], S. Snyder[29], R. Sobie[176,z], A. Soffer[161], A. Søgaard[50], F. Sohns[53], C.A. Solans Sanchez[36], E.Yu. Soldatov[112], U. Soldevila[174], A.A. Solodkov[123], A. Soloshenko[80], O.V. Solovyanov[123], V. Solovyev[137], P. Sommer[149], H. Son[170], A. Sonay[14], W. Song[143], W.Y. Song[168b], A. Sopczak[141], A.L. Sopio[95], F. Sopkova[28b], S. Sottocornola[71a,71b], R. Soualah[67a,67c], A.M. Soukharev[122b,122a], D. South[46], S. Spagnolo[68a,68b], M. Spalla[115], M. Spangenberg[178], F. Spanò[94], D. Sperlich[52], T.M. Spieker[61a], G. Spigo[36], M. Spina[156], M. Spousta[142], A. Stabile[69a,69b], B.L. Stamas[121], R. Stamen[61a], M. Stamenkovic[120], A. Stampekis[21], E. Stanecka[85], B. Stanislaus[134], M.M. Stanitzki[46], M. Stankaityte[134], B. Stapf[120], E.A. Starchenko[123], G.H. Stark[145], J. Stark[58], P. Staroba[140], P. Starovoitov[61a], S. Stärz[104], R. Staszewski[85], G. Stavropoulos[44], M. Stegler[46], P. Steinberg[29], A.L. Steinhebel[131], B. Stelzer[152,168a], H.J. Stelzer[138], O. Stelzer-Chilton[168a], H. Stenzel[56], T.J. Stevenson[156], G.A. Stewart[36], M.C. Stockton[36], G. Stoicea[27b], M. Stolarski[139a], S. Stonjek[115], A. Straessner[48], J. Strandberg[154], S. Strandberg[45a,45b], M. Strauss[128], T. Strebler[102], P. Strizenec[28b], R. Ströhmer[177], D.M. Strom[131], R. Stroynowski[42], A. Strubig[45a,45b], S.A. Stucci[29], B. Stugu[17], J. Stupak[128], N.A. Styles[46], D. Su[153], W. Su[60d,148,60c], X. Su[60a], N.B. Suarez[138], V.V. Sulin[111], M.J. Sullivan[91], D.M.S. Sultan[54], S. Sultansoy[4c], T. Sumida[86], S. Sun[106], X. Sun[101], C.J.E. Suster[157], M.R. Sutton[156], S. Suzuki[82], M. Svatos[140], M. Swiatlowski[168a], S.P. Swift[2],

JHEP06(2021)179

T. Swirski[177], A. Sydorenko[100], I. Sykora[28a], M. Sykora[142], T. Sykora[142], D. Ta[100], K. Tackmann[46,w], J. Taenzer[161], A. Taffard[171], R. Tafirout[168a], E. Tagiev[123], R.H.M. Taibah[135], R. Takashima[87], K. Takeda[83], T. Takeshita[150], E.P. Takeva[50], Y. Takubo[82], M. Talby[102], A.A. Talyshev[122b,122a], K.C. Tam[63b], N.M. Tamir[161], J. Tanaka[163], R. Tanaka[65], S. Tapia Araya[173], S. Tapprogge[100], A. Tarek Abouelfadl Mohamed[107], S. Tarem[160], K. Tariq[60b], G. Tarna[27b,d], G.F. Tartarelli[69a], P. Tas[142], M. Tasevsky[140], E. Tassi[41b,41a], G. Tateno[163], A. Tavares Delgado[139a], Y. Tayalati[35f], A.J. Taylor[50], G.N. Taylor[105], W. Taylor[168b], H. Teagle[91], A.S. Tee[90], R. Teixeira De Lima[153], P. Teixeira-Dias[94], H. Ten Kate[36], J.J. Teoh[120], K. Terashi[163], J. Terron[99], S. Terzo[14], M. Testa[51], R.J. Teuscher[167,z], N. Themistokleous[50], T. Theveneaux-Pelzer[19], D.W. Thomas[94], J.P. Thomas[21], E.A. Thompson[46], P.D. Thompson[21], E. Thomson[136], E.J. Thorpe[93], V.O. Tikhomirov[111,af], Yu.A. Tikhonov[122b,122a], S. Timoshenko[112], P. Tipton[183], S. Tisserant[102], K. Todome[23b,23a], S. Todorova-Nova[142], S. Todt[48], J. Tojo[88], S. Tokár[28a], K. Tokushuku[82], E. Tolley[127], R. Tombs[32], K.G. Tomiwa[33f], M. Tomoto[82,117], L. Tompkins[153], P. Tornambe[103], E. Torrence[131], H. Torres[48], E. Torró Pastor[174], M. Toscani[30], C. Tosciri[134], J. Toth[102,y], D.R. Tovey[149], A. Traeet[17], C.J. Treado[125], T. Trefzger[177], F. Tresoldi[156], A. Tricoli[29], I.M. Trigger[168a], S. Trincaz-Duvoid[135], D.A. Trischuk[175], W. Trischuk[167], B. Trocmé[58], A. Trofymov[65], C. Troncon[69a], F. Trovato[156], L. Truong[33c], M. Trzebinski[85], A. Trzupek[85], F. Tsai[46], P.V. Tsiareshka[108,ad], A. Tsirigotis[162,u], V. Tsiskaridze[155], E.G. Tskhadadze[159a], M. Tsopoulou[162], I.I. Tsukerman[124], V. Tsulaia[18], S. Tsuno[82], D. Tsybychev[155], Y. Tu[63b], A. Tudorache[27b], V. Tudorache[27b], A.N. Tuna[36], S. Turchikhin[80], D. Turgeman[180], I. Turk Cakir[4b,s], R.J. Turner[21], R. Turra[69a], P.M. Tuts[39], S. Tzamarias[162], E. Tzovara[100], K. Uchida[163], F. Ukegawa[169], G. Unal[36], M. Unal[11], A. Undrus[29], G. Unel[171], F.C. Ungaro[105], Y. Unno[82], J. Urban[28b], P. Urquijo[105], G. Usai[8], Z. Uysal[12d], V. Vacek[141], B. Vachon[104], K.O.H. Vadla[133], T. Vafeiadis[36], A. Vaidya[95], C. Valderanis[114], E. Valdes Santurio[45a,45b], M. Valente[168a], S. Valentinetti[23b,23a], A. Valero[174], L. Valéry[46], R.A. Vallance[21], A. Vallier[36], J.A. Valls Ferrer[174], T.R. Van Daalen[14], P. Van Gemmeren[6], S. Van Stroud[95], I. Van Vulpen[120], M. Vanadia[74a,74b], W. Vandelli[36], M. Vandenbroucke[144], E.R. Vandewall[129], D. Vannicola[73a,73b], R. Vari[73a], E.W. Varnes[7], C. Varni[55b,55a], T. Varol[158], D. Varouchas[65], K.E. Varvell[157], M.E. Vasile[27b], G.A. Vasquez[176], F. Vazeille[38], D. Vazquez Furelos[14], T. Vazquez Schroeder[36], J. Veatch[53], V. Vecchio[101], M.J. Veen[120], L.M. Veloce[167], F. Veloso[139a,139c], S. Veneziano[73a], A. Ventura[68a,68b], A. Verbytskyi[115], V. Vercesi[71a], M. Verducci[72a,72b], C.M. Vergel Infante[79], C. Vergis[24], W. Verkerke[120], A.T. Vermeulen[120], J.C. Vermeulen[120], C. Vernieri[153], P.J. Verschuuren[94], M.C. Vetterli[152,aj], N. Viaux Maira[146d], T. Vickey[149], O.E. Vickey Boeriu[149], G.H.A. Viehhauser[134], L. Vigani[61b], M. Villa[23b,23a], M. Villaplana Perez[174], E.M. Villhauer[50], E. Vilucchi[51], M.G. Vincter[34], G.S. Virdee[21], A. Vishwakarma[50], C. Vittori[23b,23a], I. Vivarelli[156], M. Vogel[182], P. Vokac[141], J. Von Ahnen[46], S.E. von Buddenbrock[33f], E. Von Toerne[24], V. Vorobel[142], K. Vorobev[112], M. Vos[174], J.H. Vossebeld[91], M. Vozak[101], N. Vranjes[16], M. Vranjes Milosavljevic[16], V. Vrba[141,*], M. Vreeswijk[120], N.K. Vu[102], R. Vuillermet[36], I. Vukotic[37], S. Wada[169], P. Wagner[24], W. Wagner[182], J. Wagner-Kuhr[114], S. Wahdan[182], H. Wahlberg[89], R. Wakasa[169], V.M. Walbrecht[115], J. Walder[143], R. Walker[114], S.D. Walker[94], W. Walkowiak[151], V. Wallangen[45a,45b], A.M. Wang[59], A.Z. Wang[181], C. Wang[60a], C. Wang[60c], H. Wang[18], H. Wang[3], J. Wang[63a], P. Wang[42], Q. Wang[128], R.-J. Wang[100], R. Wang[60a], R. Wang[6], S.M. Wang[158], W.T. Wang[60a], W. Wang[15c], W.X. Wang[60a], Y. Wang[60a], Z. Wang[106], C. Wanotayaroj[46], A. Warburton[104], C.P. Ward[32], R.J. Ward[21], N. Warrack[57], A.T. Watson[21], M.F. Watson[21], G. Watts[148], B.M. Waugh[95], A.F. Webb[11], C. Weber[29], M.S. Weber[20], S.M. Weber[61a], Y. Wei[134], A.R. Weidberg[134], J. Weingarten[47], M. Weirich[100], C. Weiser[52], P.S. Wells[36], T. Wenaus[29], B. Wendland[47], T. Wengler[36], S. Wenig[36], N. Wermes[24], M. Wessels[61a],

JHEP06(2021)179

T.D. Weston[20], K. Whalen[131], A.M. Wharton[90], A.S. White[106], A. White[8], M.J. White[1], D. Whiteson[171], B.W. Whitmore[90], W. Wiedenmann[181], C. Wiel[48], M. Wielers[143], N. Wieseotte[100], C. Wiglesworth[40], L.A.M. Wiik-Fuchs[52], H.G. Wilkens[36], L.J. Wilkins[94], D.M. Williams[39], H.H. Williams[136], S. Williams[32], S. Willocq[103], P.J. Windischhofer[134], I. Wingerter-Seez[5], E. Winkels[156], F. Winklmeier[131], B.T. Winter[52], M. Wittgen[153], M. Wobisch[96], R. Wölker[134], J. Wollrath[52], M.W. Wolter[85], H. Wolters[139a,139c], V.W.S. Wong[175], A.F. Wongel[46], N.L. Woods[145], S.D. Worm[46], B.K. Wosiek[85], K.W. Woźniak[85], K. Wraight[57], S.L. Wu[181], X. Wu[54], Y. Wu[60a], J. Wuerzinger[134], T.R. Wyatt[101], B.M. Wynne[50], S. Xella[40], J. Xiang[63c], X. Xiao[106], X. Xie[60a], I. Xiotidis[156], D. Xu[15a], H. Xu[60a], H. Xu[60a], L. Xu[29], R. Xu[136], T. Xu[144], W. Xu[106], Y. Xu[15b], Z. Xu[60b], Z. Xu[153], B. Yabsley[157], S. Yacoob[33a], D.P. Yallup[95], N. Yamaguchi[88], Y. Yamaguchi[165], A. Yamamoto[82], M. Yamatani[163], T. Yamazaki[163], Y. Yamazaki[83], J. Yan[60c], Z. Yan[25], H.J. Yang[60c,60d], H.T. Yang[18], S. Yang[60a], T. Yang[63c], X. Yang[60a], X. Yang[60b,58], Y. Yang[163], Z. Yang[106,60a], W-M. Yao[18], Y.C. Yap[46], H. Ye[15c], J. Ye[42], S. Ye[29], I. Yeletskikh[80], M.R. Yexley[90], E. Yigitbasi[25], P. Yin[39], K. Yorita[179], K. Yoshihara[79], C.J.S. Young[36], C. Young[153], J. Yu[79], R. Yuan[60b,h], X. Yue[61a], M. Zaazoua[35f], B. Zabinski[85], G. Zacharis[10], E. Zaffaroni[54], J. Zahreddine[135], A.M. Zaitsev[123,ae], T. Zakareishvili[159b], N. Zakharchuk[34], S. Zambito[36], D. Zanzi[36], S.V. Zeißner[47], C. Zeitnitz[182], G. Zemaityte[134], J.C. Zeng[173], O. Zenin[123], T. Ženiš[28a], D. Zerwas[65], M. Zgubič[134], B. Zhang[15c], D.F. Zhang[15b], G. Zhang[15b], J. Zhang[6], K. Zhang[15a], L. Zhang[15c], L. Zhang[60a], M. Zhang[173], R. Zhang[181], S. Zhang[106], X. Zhang[60c], X. Zhang[60b], Y. Zhang[15a,15d], Z. Zhang[63a], Z. Zhang[65], P. Zhao[49], Y. Zhao[145], Z. Zhao[60a], A. Zhemchugov[80], Z. Zheng[106], D. Zhong[173], B. Zhou[106], C. Zhou[181], H. Zhou[7], M. Zhou[155], N. Zhou[60c], Y. Zhou[7], C.G. Zhu[60b], C. Zhu[15a,15d], H.L. Zhu[60a], H. Zhu[15a], J. Zhu[106], Y. Zhu[60a], X. Zhuang[15a], K. Zhukov[111], V. Zhulanov[122b,122a], D. Zieminska[66], N.I. Zimine[80], S. Zimmermann[52,*], Z. Zinonos[115], M. Ziolkowski[151], L. Živković[16], G. Zobernig[181], A. Zoccoli[23b,23a], K. Zoch[53], T.G. Zorbas[149], R. Zou[37], L. Zwalinski[36]

[1] *Department of Physics, University of Adelaide, Adelaide; Australia*
[2] *Physics Department, SUNY Albany, Albany NY; United States of America*
[3] *Department of Physics, University of Alberta, Edmonton AB; Canada*
[4] [(a)] *Department of Physics, Ankara University, Ankara;* [(b)] *Istanbul Aydin University, Application and Research Center for Advanced Studies, Istanbul;* [(c)] *Division of Physics, TOBB University of Economics and Technology, Ankara; Turkey*
[5] *LAPP, Univ. Savoie Mont Blanc, CNRS/IN2P3, Annecy; France*
[6] *High Energy Physics Division, Argonne National Laboratory, Argonne IL; United States of America*
[7] *Department of Physics, University of Arizona, Tucson AZ; United States of America*
[8] *Department of Physics, University of Texas at Arlington, Arlington TX; United States of America*
[9] *Physics Department, National and Kapodistrian University of Athens, Athens; Greece*
[10] *Physics Department, National Technical University of Athens, Zografou; Greece*
[11] *Department of Physics, University of Texas at Austin, Austin TX; United States of America*
[12] [(a)] *Bahcesehir University, Faculty of Engineering and Natural Sciences, Istanbul;* [(b)] *Istanbul Bilgi University, Faculty of Engineering and Natural Sciences, Istanbul;* [(c)] *Department of Physics, Bogazici University, Istanbul;* [(d)] *Department of Physics Engineering, Gaziantep University, Gaziantep; Turkey*
[13] *Institute of Physics, Azerbaijan Academy of Sciences, Baku; Azerbaijan*
[14] *Institut de Física d'Altes Energies (IFAE), Barcelona Institute of Science and Technology, Barcelona; Spain*
[15] [(a)] *Institute of High Energy Physics, Chinese Academy of Sciences, Beijing;* [(b)] *Physics Department, Tsinghua University, Beijing;* [(c)] *Department of Physics, Nanjing University, Nanjing;* [(d)] *University of Chinese Academy of Science (UCAS), Beijing; China*
[16] *Institute of Physics, University of Belgrade, Belgrade; Serbia*
[17] *Department for Physics and Technology, University of Bergen, Bergen; Norway*

JHEP06(2021)179

[18] *Physics Division, Lawrence Berkeley National Laboratory and University of California, Berkeley CA; United States of America*
[19] *Institut für Physik, Humboldt Universität zu Berlin, Berlin; Germany*
[20] *Albert Einstein Center for Fundamental Physics and Laboratory for High Energy Physics, University of Bern, Bern; Switzerland*
[21] *School of Physics and Astronomy, University of Birmingham, Birmingham; United Kingdom*
[22] [(a)] *Facultad de Ciencias y Centro de Investigaciónes, Universidad Antonio Nariño, Bogotá;* [(b)] *Departamento de Física, Universidad Nacional de Colombia, Bogotá, Colombia; Colombia*
[23] [(a)] *INFN Bologna and Universita' di Bologna, Dipartimento di Fisica;* [(b)] *INFN Sezione di Bologna; Italy*
[24] *Physikalisches Institut, Universität Bonn, Bonn; Germany*
[25] *Department of Physics, Boston University, Boston MA; United States of America*
[26] *Department of Physics, Brandeis University, Waltham MA; United States of America*
[27] [(a)] *Transilvania University of Brasov, Brasov;* [(b)] *Horia Hulubei National Institute of Physics and Nuclear Engineering, Bucharest;* [(c)] *Department of Physics, Alexandru Ioan Cuza University of Iasi, Iasi;* [(d)] *National Institute for Research and Development of Isotopic and Molecular Technologies, Physics Department, Cluj-Napoca;* [(e)] *University Politehnica Bucharest, Bucharest;* [(f)] *West University in Timisoara, Timisoara; Romania*
[28] [(a)] *Faculty of Mathematics, Physics and Informatics, Comenius University, Bratislava;* [(b)] *Department of Subnuclear Physics, Institute of Experimental Physics of the Slovak Academy of Sciences, Kosice; Slovak Republic*
[29] *Physics Department, Brookhaven National Laboratory, Upton NY; United States of America*
[30] *Departamento de Física, Universidad de Buenos Aires, Buenos Aires; Argentina*
[31] *California State University, CA; United States of America*
[32] *Cavendish Laboratory, University of Cambridge, Cambridge; United Kingdom*
[33] [(a)] *Department of Physics, University of Cape Town, Cape Town;* [(b)] *iThemba Labs, Western Cape;* [(c)] *Department of Mechanical Engineering Science, University of Johannesburg, Johannesburg;* [(d)] *National Institute of Physics, University of the Philippines Diliman;* [(e)] *University of South Africa, Department of Physics, Pretoria;* [(f)] *School of Physics, University of the Witwatersrand, Johannesburg; South Africa*
[34] *Department of Physics, Carleton University, Ottawa ON; Canada*
[35] [(a)] *Faculté des Sciences Ain Chock, Réseau Universitaire de Physique des Hautes Energies - Université Hassan II, Casablanca;* [(b)] *Faculté des Sciences, Université Ibn-Tofail, Kénitra;* [(c)] *Faculté des Sciences Semlalia, Université Cadi Ayyad, LPHEA-Marrakech;* [(d)] *Moroccan Foundation for Advanced Science Innovation and Research (MAScIR), Rabat;* [(e)] *LPMR, Faculté des Sciences, Université Mohamed Premier, Oujda;* [(f)] *Faculté des sciences, Université Mohammed V, Rabat; Morocco*
[36] *CERN, Geneva; Switzerland*
[37] *Enrico Fermi Institute, University of Chicago, Chicago IL; United States of America*
[38] *LPC, Université Clermont Auvergne, CNRS/IN2P3, Clermont-Ferrand; France*
[39] *Nevis Laboratory, Columbia University, Irvington NY; United States of America*
[40] *Niels Bohr Institute, University of Copenhagen, Copenhagen; Denmark*
[41] [(a)] *Dipartimento di Fisica, Università della Calabria, Rende;* [(b)] *INFN Gruppo Collegato di Cosenza, Laboratori Nazionali di Frascati; Italy*
[42] *Physics Department, Southern Methodist University, Dallas TX; United States of America*
[43] *Physics Department, University of Texas at Dallas, Richardson TX; United States of America*
[44] *National Centre for Scientific Research "Demokritos", Agia Paraskevi; Greece*
[45] [(a)] *Department of Physics, Stockholm University;* [(b)] *Oskar Klein Centre, Stockholm; Sweden*
[46] *Deutsches Elektronen-Synchrotron DESY, Hamburg and Zeuthen; Germany*
[47] *Lehrstuhl für Experimentelle Physik IV, Technische Universität Dortmund, Dortmund; Germany*
[48] *Institut für Kern- und Teilchenphysik, Technische Universität Dresden, Dresden; Germany*
[49] *Department of Physics, Duke University, Durham NC; United States of America*
[50] *SUPA - School of Physics and Astronomy, University of Edinburgh, Edinburgh; United Kingdom*

JHEP06(2021)179

[51] INFN e Laboratori Nazionali di Frascati, Frascati; Italy
[52] Physikalisches Institut, Albert-Ludwigs-Universität Freiburg, Freiburg; Germany
[53] II. Physikalisches Institut, Georg-August-Universität Göttingen, Göttingen; Germany
[54] Département de Physique Nucléaire et Corpusculaire, Université de Genève, Genève; Switzerland
[55] [(a)] Dipartimento di Fisica, Università di Genova, Genova;[(b)] INFN Sezione di Genova; Italy
[56] II. Physikalisches Institut, Justus-Liebig-Universität Giessen, Giessen; Germany
[57] SUPA - School of Physics and Astronomy, University of Glasgow, Glasgow; United Kingdom
[58] LPSC, Université Grenoble Alpes, CNRS/IN2P3, Grenoble INP, Grenoble; France
[59] Laboratory for Particle Physics and Cosmology, Harvard University, Cambridge MA; United States of America
[60] [(a)] Department of Modern Physics and State Key Laboratory of Particle Detection and Electronics, University of Science and Technology of China, Hefei;[(b)] Institute of Frontier and Interdisciplinary Science and Key Laboratory of Particle Physics and Particle Irradiation (MOE), Shandong University, Qingdao;[(c)] School of Physics and Astronomy, Shanghai Jiao Tong University, Key Laboratory for Particle Astrophysics and Cosmology (MOE), SKLPPC, Shanghai;[(d)] Tsung-Dao Lee Institute, Shanghai; China
[61] [(a)] Kirchhoff-Institut für Physik, Ruprecht-Karls-Universität Heidelberg, Heidelberg;[(b)] Physikalisches Institut, Ruprecht-Karls-Universität Heidelberg, Heidelberg; Germany
[62] Faculty of Applied Information Science, Hiroshima Institute of Technology, Hiroshima; Japan
[63] [(a)] Department of Physics, Chinese University of Hong Kong, Shatin, N.T., Hong Kong;[(b)] Department of Physics, University of Hong Kong, Hong Kong;[(c)] Department of Physics and Institute for Advanced Study, Hong Kong University of Science and Technology, Clear Water Bay, Kowloon, Hong Kong; China
[64] Department of Physics, National Tsing Hua University, Hsinchu; Taiwan
[65] IJCLab, Université Paris-Saclay, CNRS/IN2P3, 91405, Orsay; France
[66] Department of Physics, Indiana University, Bloomington IN; United States of America
[67] [(a)] INFN Gruppo Collegato di Udine, Sezione di Trieste, Udine;[(b)] ICTP, Trieste;[(c)] Dipartimento Politecnico di Ingegneria e Architettura, Università di Udine, Udine; Italy
[68] [(a)] INFN Sezione di Lecce;[(b)] Dipartimento di Matematica e Fisica, Università del Salento, Lecce; Italy
[69] [(a)] INFN Sezione di Milano;[(b)] Dipartimento di Fisica, Università di Milano, Milano; Italy
[70] [(a)] INFN Sezione di Napoli;[(b)] Dipartimento di Fisica, Università di Napoli, Napoli; Italy
[71] [(a)] INFN Sezione di Pavia;[(b)] Dipartimento di Fisica, Università di Pavia, Pavia; Italy
[72] [(a)] INFN Sezione di Pisa;[(b)] Dipartimento di Fisica E. Fermi, Università di Pisa, Pisa; Italy
[73] [(a)] INFN Sezione di Roma;[(b)] Dipartimento di Fisica, Sapienza Università di Roma, Roma; Italy
[74] [(a)] INFN Sezione di Roma Tor Vergata;[(b)] Dipartimento di Fisica, Università di Roma Tor Vergata, Roma; Italy
[75] [(a)] INFN Sezione di Roma Tre;[(b)] Dipartimento di Matematica e Fisica, Università Roma Tre, Roma; Italy
[76] [(a)] INFN-TIFPA;[(b)] Università degli Studi di Trento, Trento; Italy
[77] Institut für Astro- und Teilchenphysik, Leopold-Franzens-Universität, Innsbruck; Austria
[78] University of Iowa, Iowa City IA; United States of America
[79] Department of Physics and Astronomy, Iowa State University, Ames IA; United States of America
[80] Joint Institute for Nuclear Research, Dubna; Russia
[81] [(a)] Departamento de Engenharia Elétrica, Universidade Federal de Juiz de Fora (UFJF), Juiz de Fora;[(b)] Universidade Federal do Rio De Janeiro COPPE/EE/IF, Rio de Janeiro;[(c)] Instituto de Física, Universidade de São Paulo, São Paulo; Brazil
[82] KEK, High Energy Accelerator Research Organization, Tsukuba; Japan
[83] Graduate School of Science, Kobe University, Kobe; Japan
[84] [(a)] AGH University of Science and Technology, Faculty of Physics and Applied Computer Science, Krakow;[(b)] Marian Smoluchowski Institute of Physics, Jagiellonian University, Krakow; Poland
[85] Institute of Nuclear Physics Polish Academy of Sciences, Krakow; Poland
[86] Faculty of Science, Kyoto University, Kyoto; Japan

JHEP06(2021)179

[87] Kyoto University of Education, Kyoto; Japan
[88] Research Center for Advanced Particle Physics and Department of Physics, Kyushu University, Fukuoka; Japan
[89] Instituto de Física La Plata, Universidad Nacional de La Plata and CONICET, La Plata; Argentina
[90] Physics Department, Lancaster University, Lancaster; United Kingdom
[91] Oliver Lodge Laboratory, University of Liverpool, Liverpool; United Kingdom
[92] Department of Experimental Particle Physics, Jožef Stefan Institute and Department of Physics, University of Ljubljana, Ljubljana; Slovenia
[93] School of Physics and Astronomy, Queen Mary University of London, London; United Kingdom
[94] Department of Physics, Royal Holloway University of London, Egham; United Kingdom
[95] Department of Physics and Astronomy, University College London, London; United Kingdom
[96] Louisiana Tech University, Ruston LA; United States of America
[97] Fysiska institutionen, Lunds universitet, Lund; Sweden
[98] Centre de Calcul de l'Institut National de Physique Nucléaire et de Physique des Particules (IN2P3), Villeurbanne; France
[99] Departamento de Física Teorica C-15 and CIAFF, Universidad Autónoma de Madrid, Madrid; Spain
[100] Institut für Physik, Universität Mainz, Mainz; Germany
[101] School of Physics and Astronomy, University of Manchester, Manchester; United Kingdom
[102] CPPM, Aix-Marseille Université, CNRS/IN2P3, Marseille; France
[103] Department of Physics, University of Massachusetts, Amherst MA; United States of America
[104] Department of Physics, McGill University, Montreal QC; Canada
[105] School of Physics, University of Melbourne, Victoria; Australia
[106] Department of Physics, University of Michigan, Ann Arbor MI; United States of America
[107] Department of Physics and Astronomy, Michigan State University, East Lansing MI; United States of America
[108] B.I. Stepanov Institute of Physics, National Academy of Sciences of Belarus, Minsk; Belarus
[109] Research Institute for Nuclear Problems of Byelorussian State University, Minsk; Belarus
[110] Group of Particle Physics, University of Montreal, Montreal QC; Canada
[111] P.N. Lebedev Physical Institute of the Russian Academy of Sciences, Moscow; Russia
[112] National Research Nuclear University MEPhI, Moscow; Russia
[113] D.V. Skobeltsyn Institute of Nuclear Physics, M.V. Lomonosov Moscow State University, Moscow; Russia
[114] Fakultät für Physik, Ludwig-Maximilians-Universität München, München; Germany
[115] Max-Planck-Institut für Physik (Werner-Heisenberg-Institut), München; Germany
[116] Nagasaki Institute of Applied Science, Nagasaki; Japan
[117] Graduate School of Science and Kobayashi-Maskawa Institute, Nagoya University, Nagoya; Japan
[118] Department of Physics and Astronomy, University of New Mexico, Albuquerque NM; United States of America
[119] Institute for Mathematics, Astrophysics and Particle Physics, Radboud University/Nikhef, Nijmegen; Netherlands
[120] Nikhef National Institute for Subatomic Physics and University of Amsterdam, Amsterdam; Netherlands
[121] Department of Physics, Northern Illinois University, DeKalb IL; United States of America
[122] [(a)] Budker Institute of Nuclear Physics and NSU, SB RAS, Novosibirsk;[(b)] Novosibirsk State University Novosibirsk; Russia
[123] Institute for High Energy Physics of the National Research Centre Kurchatov Institute, Protvino; Russia
[124] Institute for Theoretical and Experimental Physics named by A.I. Alikhanov of National Research Centre "Kurchatov Institute", Moscow; Russia
[125] Department of Physics, New York University, New York NY; United States of America
[126] Ochanomizu University, Otsuka, Bunkyo-ku, Tokyo; Japan
[127] Ohio State University, Columbus OH; United States of America

JHEP06(2021)179

[128] Homer L. Dodge Department of Physics and Astronomy, University of Oklahoma, Norman OK; United States of America
[129] Department of Physics, Oklahoma State University, Stillwater OK; United States of America
[130] Palacký University, Joint Laboratory of Optics, Olomouc; Czech Republic
[131] Institute for Fundamental Science, University of Oregon, Eugene, OR; United States of America
[132] Graduate School of Science, Osaka University, Osaka; Japan
[133] Department of Physics, University of Oslo, Oslo; Norway
[134] Department of Physics, Oxford University, Oxford; United Kingdom
[135] LPNHE, Sorbonne Université, Université de Paris, CNRS/IN2P3, Paris; France
[136] Department of Physics, University of Pennsylvania, Philadelphia PA; United States of America
[137] Konstantinov Nuclear Physics Institute of National Research Centre "Kurchatov Institute", PNPI, St. Petersburg; Russia
[138] Department of Physics and Astronomy, University of Pittsburgh, Pittsburgh PA; United States of America
[139] [(a)] Laboratório de Instrumentação e Física Experimental de Partículas - LIP, Lisboa;[(b)] Departamento de Física, Faculdade de Ciências, Universidade de Lisboa, Lisboa;[(c)] Departamento de Física, Universidade de Coimbra, Coimbra;[(d)] Centro de Física Nuclear da Universidade de Lisboa, Lisboa;[(e)] Departamento de Física, Universidade do Minho, Braga;[(f)] Departamento de Física Teórica y del Cosmos, Universidad de Granada, Granada (Spain);[(g)] Dep Física and CEFITEC of Faculdade de Ciências e Tecnologia, Universidade Nova de Lisboa, Caparica;[(h)] Instituto Superior Técnico, Universidade de Lisboa, Lisboa; Portugal
[140] Institute of Physics of the Czech Academy of Sciences, Prague; Czech Republic
[141] Czech Technical University in Prague, Prague; Czech Republic
[142] Charles University, Faculty of Mathematics and Physics, Prague; Czech Republic
[143] Particle Physics Department, Rutherford Appleton Laboratory, Didcot; United Kingdom
[144] IRFU, CEA, Université Paris-Saclay, Gif-sur-Yvette; France
[145] Santa Cruz Institute for Particle Physics, University of California Santa Cruz, Santa Cruz CA; United States of America
[146] [(a)] Departamento de Física, Pontificia Universidad Católica de Chile, Santiago;[(b)] Universidad Andres Bello, Department of Physics, Santiago;[(c)] Instituto de Alta Investigación, Universidad de Tarapacá, Arica;[(d)] Departamento de Física, Universidad Técnica Federico Santa María, Valparaíso; Chile
[147] Universidade Federal de São João del Rei (UFSJ), São João del Rei; Brazil
[148] Department of Physics, University of Washington, Seattle WA; United States of America
[149] Department of Physics and Astronomy, University of Sheffield, Sheffield; United Kingdom
[150] Department of Physics, Shinshu University, Nagano; Japan
[151] Department Physik, Universität Siegen, Siegen; Germany
[152] Department of Physics, Simon Fraser University, Burnaby BC; Canada
[153] SLAC National Accelerator Laboratory, Stanford CA; United States of America
[154] Department of Physics, Royal Institute of Technology, Stockholm; Sweden
[155] Departments of Physics and Astronomy, Stony Brook University, Stony Brook NY; United States of America
[156] Department of Physics and Astronomy, University of Sussex, Brighton; United Kingdom
[157] School of Physics, University of Sydney, Sydney; Australia
[158] Institute of Physics, Academia Sinica, Taipei; Taiwan
[159] [(a)] E. Andronikashvili Institute of Physics, Iv. Javakhishvili Tbilisi State University, Tbilisi;[(b)] High Energy Physics Institute, Tbilisi State University, Tbilisi; Georgia
[160] Department of Physics, Technion, Israel Institute of Technology, Haifa; Israel
[161] Raymond and Beverly Sackler School of Physics and Astronomy, Tel Aviv University, Tel Aviv; Israel
[162] Department of Physics, Aristotle University of Thessaloniki, Thessaloniki; Greece
[163] International Center for Elementary Particle Physics and Department of Physics, University of Tokyo, Tokyo; Japan
[164] Graduate School of Science and Technology, Tokyo Metropolitan University, Tokyo; Japan

JHEP06(2021)179

[165] Department of Physics, Tokyo Institute of Technology, Tokyo; Japan
[166] Tomsk State University, Tomsk; Russia
[167] Department of Physics, University of Toronto, Toronto ON; Canada
[168] [(a)] TRIUMF, Vancouver BC; [(b)] Department of Physics and Astronomy, York University, Toronto ON; Canada
[169] Division of Physics and Tomonaga Center for the History of the Universe, Faculty of Pure and Applied Sciences, University of Tsukuba, Tsukuba; Japan
[170] Department of Physics and Astronomy, Tufts University, Medford MA; United States of America
[171] Department of Physics and Astronomy, University of California Irvine, Irvine CA; United States of America
[172] Department of Physics and Astronomy, University of Uppsala, Uppsala; Sweden
[173] Department of Physics, University of Illinois, Urbana IL; United States of America
[174] Instituto de Física Corpuscular (IFIC), Centro Mixto Universidad de Valencia - CSIC, Valencia; Spain
[175] Department of Physics, University of British Columbia, Vancouver BC; Canada
[176] Department of Physics and Astronomy, University of Victoria, Victoria BC; Canada
[177] Fakultät für Physik und Astronomie, Julius-Maximilians-Universität Würzburg, Würzburg; Germany
[178] Department of Physics, University of Warwick, Coventry; United Kingdom
[179] Waseda University, Tokyo; Japan
[180] Department of Particle Physics and Astrophysics, Weizmann Institute of Science, Rehovot; Israel
[181] Department of Physics, University of Wisconsin, Madison WI; United States of America
[182] Fakultät für Mathematik und Naturwissenschaften, Fachgruppe Physik, Bergische Universität Wuppertal, Wuppertal; Germany
[183] Department of Physics, Yale University, New Haven CT; United States of America

[a] Also at Borough of Manhattan Community College, City University of New York, New York NY; United States of America
[b] Also at Centro Studi e Ricerche Enrico Fermi; Italy
[c] Also at CERN, Geneva; Switzerland
[d] Also at CPPM, Aix-Marseille Université, CNRS/IN2P3, Marseille; France
[e] Also at Département de Physique Nucléaire et Corpusculaire, Université de Genève, Genève; Switzerland
[f] Also at Departament de Fisica de la Universitat Autonoma de Barcelona, Barcelona; Spain
[g] Also at Department of Financial and Management Engineering, University of the Aegean, Chios; Greece
[h] Also at Department of Physics and Astronomy, Michigan State University, East Lansing MI; United States of America
[i] Also at Department of Physics and Astronomy, University of Louisville, Louisville, KY; United States of America
[j] Also at Department of Physics, Ben Gurion University of the Negev, Beer Sheva; Israel
[k] Also at Department of Physics, California State University, East Bay; United States of America
[l] Also at Department of Physics, California State University, Fresno; United States of America
[m] Also at Department of Physics, California State University, Sacramento; United States of America
[n] Also at Department of Physics, King's College London, London; United Kingdom
[o] Also at Department of Physics, St. Petersburg State Polytechnical University, St. Petersburg; Russia
[p] Also at Department of Physics, University of Fribourg, Fribourg; Switzerland
[q] Also at Dipartimento di Matematica, Informatica e Fisica, Università di Udine, Udine; Italy
[r] Also at Faculty of Physics, M.V. Lomonosov Moscow State University, Moscow; Russia
[s] Also at Giresun University, Faculty of Engineering, Giresun; Turkey
[t] Also at Graduate School of Science, Osaka University, Osaka; Japan
[u] Also at Hellenic Open University, Patras; Greece
[v] Also at Institucio Catalana de Recerca i Estudis Avancats, ICREA, Barcelona; Spain

JHEP06(2021)179

[w] Also at Institut für Experimentalphysik, Universität Hamburg, Hamburg; Germany
[x] Also at Institute for Nuclear Research and Nuclear Energy (INRNE) of the Bulgarian Academy of Sciences, Sofia; Bulgaria
[y] Also at Institute for Particle and Nuclear Physics, Wigner Research Centre for Physics, Budapest; Hungary
[z] Also at Institute of Particle Physics (IPP); Canada
[aa] Also at Institute of Physics, Azerbaijan Academy of Sciences, Baku; Azerbaijan
[ab] Also at Instituto de Fisica Teorica, IFT-UAM/CSIC, Madrid; Spain
[ac] Also at Istanbul University, Dept. of Physics, Istanbul; Turkey
[ad] Also at Joint Institute for Nuclear Research, Dubna; Russia
[ae] Also at Moscow Institute of Physics and Technology State University, Dolgoprudny; Russia
[af] Also at National Research Nuclear University MEPhI, Moscow; Russia
[ag] Also at Physics Department, An-Najah National University, Nablus; Palestine
[ah] Also at Physikalisches Institut, Albert-Ludwigs-Universität Freiburg, Freiburg; Germany
[ai] Also at The City College of New York, New York NY; United States of America
[aj] Also at TRIUMF, Vancouver BC; Canada
[ak] Also at Universita di Napoli Parthenope, Napoli; Italy
[al] Also at University of Chinese Academy of Sciences (UCAS), Beijing; China
[*] Deceased

JHEP06(2021)179